Distribution Agreement

In presenting this thesis or dissertation as a partial fulfillment of the requirements for an advanced degree from Emory University, I hereby grant to Emory University and its agents the non-exclusive license to archive, make accessible, and display my thesis or dissertation in whole or in part in all forms of media, now or hereafter known, including display on the world wide web. I understand that I may select some access restrictions as part of the online submission of this thesis or dissertation. I retain all ownership rights to the copyright of the thesis or dissertation. I also retain the right to use in future works (such as articles or books) all or part of this thesis or dissertation.

Signature:

_____ _____

Kelly Kluge Date

Ligand Design Strategies for Regulating Small Molecule Binding and Reactivity at Transition Metal Centers

By

Kelly A. Kluge
Doctor of Philosophy

Chemistry

_____

Cora E. MacBeth
Advisor

_____

Justin P. Gallivan
Committee Member

_____

Craig L. Hill
Committee Member

Accepted:

_____

Lisa A. Tedesco, Ph.D.
Dean of the James T. Laney School of Graduate Studies

_____

Date

Ligand Design Strategies for Regulating Small Molecule Binding and Reactivity at Transition Metal Centers

By

Kelly A. Kluge
B.S., University of Wisconsin – Milwaukee, 2007

Cora E. MacBeth, Ph.D.

An abstract of
A dissertation submitted to the Faculty of the
James T. Laney School of Graduate Studies of Emory University
in partial fulfillment of the requirements for the degree of
Doctor of Philosophy
in Chemistry
2012

Abstract

Ligand design is an area of great interest to chemists. With respect to coordination chemistry, ligands may be tailored sterically, electronically, and through installation of functionalities that make up the secondary coordination sphere of the transition metal ion.

In Chapter 2 of this dissertation, the synthesis of a series of tetradentate ligands that vary in the electronic character of the aromatic acyl substituent is described. Cobalt(II) complexes of these ligands were prepared, and their synthesis and characterization will also be discussed. The cyanide binding properties of these complexes were explored, and it was found that the complexes with the most electron-withdrawing substituents not only effect the most electron-poor cobalt center, but they also appear to effect a type of secondary interaction between the bound cyanide and the aromatic rings that has not yet been described in the literature.

In Chapter 3, the synthesis, characterization, and reactivity of iron(II) complexes that utilize similar ligands will be explored. Several of the complexes with electron-rich aromatic acyl substituents have proven to be effective catalysts for *N*-methyl C-H bond activation. The catalytic activity and proposed mechanism of action will be discussed. A byproduct of this reaction, a rare, terminal Fe(II)-hemiaminate species was isolated, and its characterization will also be discussed.

In Chapter 4, the synthesis, characterization, and reactivity of cobalt(II), copper(I), and zinc(II) complexes of a neutral, tridentate ligand will be described. These complexes have the potential to be useful as low coordinate, reactive transition metal complexes.

Ligand Design Strategies for Regulating Small Molecule Binding and Reactivity at Transition Metal Centers

By

Kelly A. Kluge
B.S., University of Wisconsin – Milwaukee, 2007

Cora E. MacBeth, Ph.D.

A dissertation submitted to the Faculty of the
James T. Laney School of Graduate Studies of Emory University
in partial fulfillment of the requirements for the degree of
Doctor of Philosophy
in Chemistry
2012

Acknowledgements

S.D.G.

I would first like to thank Dr. Cora MacBeth. She has been my advisor in chemistry and career development, and she has also been a good friend. In chemistry she has guided me knowledgeably. She was always excited about my results, even when I wasn't, and often helped me to see the big picture. She gave me confidence in my career search, helping me in any way that she could, and spoke kindly of me to prospective employers. As a friend, she has always been available to listen and give advice. She loves all of her students, and offered to fight many battles on my behalf. It has truly been an honor to be her student.

I would also like to thank my committee members, Dr. Justin Gallivan and Dr. Craig Hill, for taking time out of their busy schedules to attend my talks and seminars, read my papers, think about and offer advice regarding my work. It was a privilege to have Dr. Gallivan on my committee, as he performed seminal research in my area of study. It was also a privilege to have Dr. Hill on my committee, given his prominence in and many contributions to the field of inorganic chemistry. I learned so much from both gentlemen.

Dr. Kenneth Hardcastle, Dr. John Bacsa, and Dr. Karl Hagen have also been great teaching influences with regard to X-ray crystallography. Dr. Hardcastle has always been so kind to and patient with me, even as I was breaking things left and right in the lab. He was always there to lend a kind word or give me good life advice. Dr. Bacsa and I learned how to perform our duties in the X-ray facility at the same time, and he was patient with me as I settled into that role. Lastly, Dr. Hagen introduced me to

crystallography, solved one of the difficult structures described herein, and was always willing to take a fresh look at my data and give me a different perspective. He also has the unfortunate office location directly across from mine, and, therefore, had to be very patient with my outbursts and unprofessional conversations.

Many thanks go to my lab mates, both past and present. They have all been so kind, patient, willing to listen and offer advice. They have been my confidants and dearest friends throughout graduate school. Theirs are some of the most brilliant minds I have encountered, and it is an honor to be called their peer.

There are many other people in the chemistry department that have my gratitude—the people on the fifth floor (they know who they are) with whom there have been many good times, my step-lab mates (the Blakey lab), the labs that allowed me to use their instruments (Liotta, Scarborough, Hill, Liebeskind, Ryan), those who run the facilities and stockroom (especially Steve and Patti—what would anyone do without them?), and the administrators (especially Ann Dasher—chemistry mom, lifesaver, and mastermind of B.F.s). All of these people have been generous with their time and efforts on my behalf.

Lastly, I would like to thank my family and friends, who understood when I didn't call for months and rarely visited. Specifically, my parents, Dave and Dianne Kluge have always been my number one supporters. Though the acquisition of this degree has taken me cross-country, and I only visit home once or twice a year, they have urged me on and are very proud.

Finally, I thank my fiancée, Rob Smith, who has been my rock. He moved across the country once to be by my side and is about to do it again. He has patiently listened to

me and given me advice. He has been so supportive and loving everyday, and I look forward to being the same for him for the rest of our lives together.

Table of Contents

List of Figures

Chapter 1

Chapter 2

List of Tables

Chapter 1

Chapter 2

Chapter 3

Chapter 4

List of Schemes

Chapter 1

Chapter 2

Chapter 3

Chapter 4

Chapter 1: Ligand Design Strategies for Regulating Small Molecule Binding and Reactivity at Transition Metal Centers

Section 1-1. Introduction

"Ligand design" is a phrase that is frequently used with regard to both pharmacology and coordination chemistry. When this phrase is used in pharmacology, it typically refers to the design of a small molecule (the ligand) that will bind a receptor to induce an increase or decrease in a desired response.[1] In coordination chemistry, this phrase refers to the design of molecules that will bind a transition metal and confer desirable properties onto the resulting complexes. These ligands/complexes may be used for a broad range of transformations—from metal sequestration and selective anion binding to catalysis, the preparation of novel materials for devices to environmental sustainability causes.[2] As the range of applications is broad, so is the range of ligands—from small molecules to supramolecular arrays. Therefore, the focus of this introduction will be on small molecule ligands and their use to stabilize unique bonding and effect unique transformations by transition metal complexes.

The design of small molecule ligands typically involves tailoring of the following:[2]

1. The steric bulk of the ligand—Addition of sterically encumbering groups can block off the transition metal ion, limiting its binding and reactivity to that which is desired.
2. The electronic character of the ligand—The σ and π donation or acceptance by a ligand can affect the geometry of the complex as well as its spin state, which can

be used to tailor the binding and reactivity at the metal center. Also, electron-withdrawing or donating ligands impact the electronic character of the transition metal ion, making it electron-rich or electron-poor, respectively. This can impact the affinity for exogenous ligands and the stability of the resulting complexes and/or intermediates in catalysis, thereby making it more or less likely to bind/react.

3. The secondary coordination sphere of the transition metal ion—Incorporating functionality into the ligand that can interact with the transition metal complex or intermediates in a stabilizing or destabilizing manner.

Section 1-2. Utility of Ligand Design in Tetradentate Triamidoamine Ligands

Tripodal, tetradentate, triamidoamine ligands (Figure 1-1) have proven to be versatile and useful motifs in coordination chemistry.[3,4]

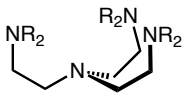

Figure 1-1. General tripodal, tetradentate, triamidoamine ligand platform. The ligand may be altered by changing R or the alkyl, backbone linkers.

The amido substituents are σ- and π-donors that can be tuned electronically to best suit the hardness of the transition metal. The easily modifiable nature of these ligands makes them excellent candidates for studies involving ligand design. Not only can the amido substituents be modified, but the ethylene backbone can be replaced with pyridyl, *N*-heterocyclic carbenes, or phenylene linkages.[5-11] Studies describing the replacement of

the amido substituents with phosphines, hydroxides, and thiols as well as replacement of the central amine have also been undertaken.[6,12-29]

The modularity of the triamidoamine ligand platform was exemplified by Schrock et al. For twenty years, one of the primary goals in their group was to mimic the nitrogen reduction activity of nitrogenase enzymes.[30,31] To do so, they synthesized a number of Rtren ligands [Rtren = tris(2-R-aminoethyl)amine, where R is an alkyl or aromatic substituent] and the Mo(III) complexes thereof.[30] They then explored the N_2 chemistry of these species. What they believed was preventing the reduction complete of dinitrogen when bound to their complex was the formation of a stable, unreactive dimeric species, RtrenMo-N=N-MoRtren. To prevent formation of this species, they incorporated the substituent HIPT (*h*exa*i*so*p*ropyl*t*erphenyl = 3,5-(2,4,6-$^{i}Pr_3C_6H_2)_2C_6H_3$), as shown in Figure 1-2.

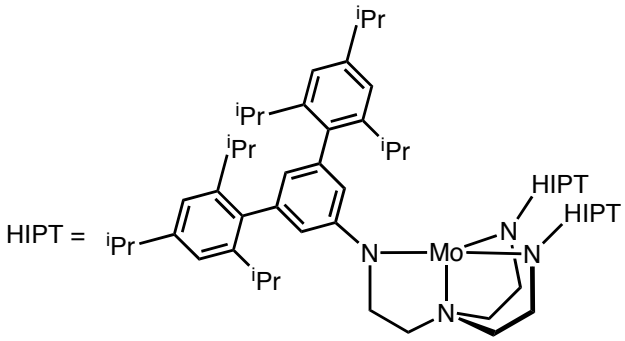

Figure 1-2. Complex employed by the Schrock group to effect the complete reduction of N_2 to NH_3, [Mo(III)(HIPTtren)].[32]

As expected, the steric bulk of this substituent prevented dimerization, allowing for the complete, catalytic reduction of N_2 to NH_3 mediated by [MoHIPTtren].[30,32,33] Not only was the reduced species, $[HIPTtrenMo(NH_3)]^+$ characterized, but five more proposed

intermediates in the catalytic cycle were prepared and characterized.[34] The solid-state structures of $[HIPTtrenMo(NH_3)]^+$, $[HIPTtrenMo{=}NH]^+$, $[HIPTtrenMo{\equiv}N{+}NH_3)]$, $[HIPTtrenMo{=}N\text{-}NH_2]^+$, [HIPTtrenMo-N=NH], and $[HIPTtrenMo(N_2)]^+$ and reveal significant protection by the bulky HIPT substituent about the nitrogen intermediates.[34]

An example of how tripodal, tetradentate ligand systems can be tailored electronically to impact reactivity at the transition metal center is drawn from copper-dioxygen chemistry. The addition of dioxygen to several Cu(I) complexes of neutral ligands results in the formation of either a dicopper(II) μ-1,2-peroxo, dicopper(III) μ-η^2:η^2-peroxo, or an equilibrium between the two species.[35] Studies undertaken by Zhang et al. indicated that the electronic character of the ligand has a significant effect on the rate of formation and stability of the resulting dicopper-peroxo.[36] Specifically, they found that the more electron-donating the ligand is, the higher the rate of association and the stability of the resulting copper-peroxo complex. This can be explained by the fact that this transformation involves oxidation of the copper ion, which is stablilized in higher oxidation states by more electron-releasing ligands. Subsequent studies on these systems led to the discovery that the copper-peroxo complexes mediated toluene oxidation to benzaldehyde and that the yield of benzaldehyde from the reaction is dependent upon the ligand used.[37-40] Some of the ligands studied are shown in Figure 1-3.

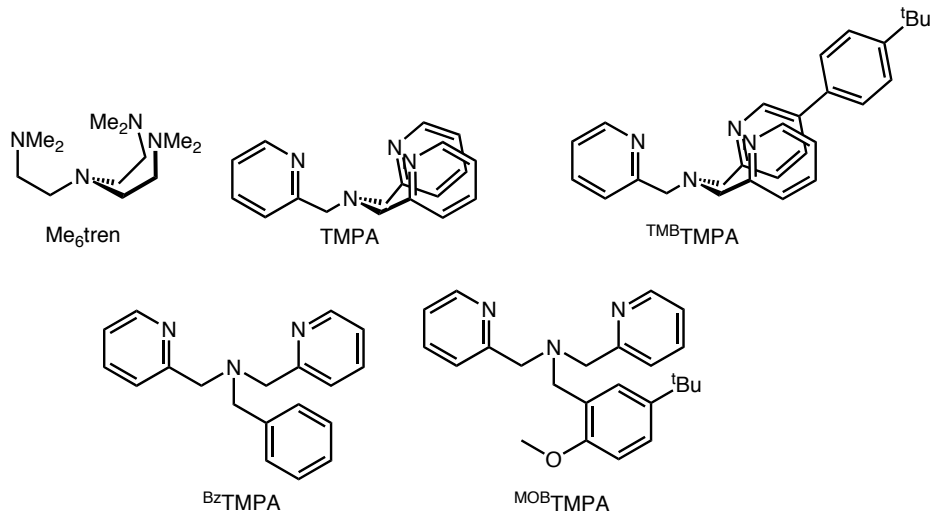

Figure 1-3. Ligands used for the synthesis of toluene oxidation catalysts of the type $[(CuL)_2(\mu\text{-}1,2\text{-}O_2)]^{2-}$.

The results of this study are summarized in Table 1-1.

Table 1-1. CO stretching frequencies, available Cu^{II}/Cu^{I} reduction potentials, and yield of benzaldehyde from toluene oxidation reactions mediated by $[(CuL)_2(\mu\text{-}1,2\text{-}O_2)]^{2-}$.

Ligand	υ_{CO}* (Nujol, cm^{-1})	υ_{CO}* (THF, cm^{-1})	$E_{1/2}$ (mV)	Benzaldehyde yield	Structurally characterized
Me_6tren	2098	2078	N/A	10%	✓
TMPA	2077	2090	-410	20%	✓
^{TMB}TMPA	2091	2092	-325	33%	-
^{Bz}TMPA	2093	2095	-225	40%	-
^{MOB}TMPA	2093	2093	N/A	40%	-

*υ_{CO} for $[Cu^{I}(CO)(L)]^{+}$ prepared separately.

The υ_{CO} of $[Cu(CO)Me_6tren]^+$ in solution indicates Me_6tren is the most electron-donating ligand of the series shown in Table 1-1. Notably, the value of the υ_{CO} is considerably lower in solution than in the solid state. This is rationalized by the hypothesis that the $[Cu(CO)Me_6tren]^+$ exists as a 4-coordinate species, with one of the ethylene arms unbound in the solid-state.[41] This explains the much higher υ_{CO}, as a lower coordination number would decrease the electron density donated to the metal center and, as a result, to the π^* orbitals of the carbonyl ligand. The general trend in this data is an increase in the benzaldehyde yield with decrease of electron donation from the ligand. Given that the reactivity of a transition metal complex is often inversely proportional to the stability of the complex, it is not surprising that the least reactive complex for toluene oxidation to benzaldehyde is that containing the most electron-donating ligand and the most reactive complex is that containing the least electron-donating ligand. This trend is further evidenced by the fact that the only of these Cu-peroxo complexes that have been structurally characterized are the most electron-donating complexes, $[((Me_6tren)Cu)_2(\mu\text{-}1,2\text{-}O_2)]^{2-}$ and $[((TMPA)Cu)_2(\mu\text{-}1,2\text{-}O_2)]^{2-}$, as they are the least reactive peroxo complexes.[36,40,42,43]

Lastly, MacBeth et al. provide an example of utilizing the second coordination sphere of a transition metal to facilitate unique reactivity and stabilize highly reactive molecules. With the goal of stabilizing a metal-oxo fragment derived from O_2, the Borovik group took their inspiration for the design of their ligand from nature.[44] Both non-heme and heme, iron-dependent enzymes are capable of stabilizing high-valent iron-oxo fragments. This is accomplished through stabilization by noncovalent interactions between the otherwise unstable iron-oxo and nearby residues in the enzyme.[45] For

example, the ferryl-oxo unit in cytochrome *C* peroxidase is stabilized by four hydrogen bonds from nearby residues and a water molecule, as shown in Figure 1-4.[46]

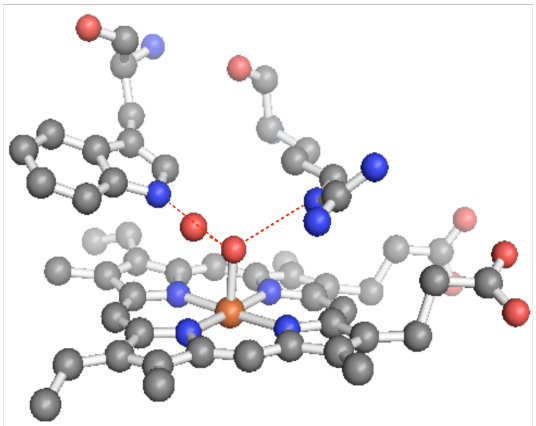

Figure 1-4. Active site of Compound I of cytochrome *C* peroxidase. Dashed lines represent hydrogen bonds between Fe=O, nearby residues, and a trapped water molecule.[46] Atoms (color): carbon (gray), iron (yellow), nitrogen (blue), oxygen (red).

With this in mind, MacBeth et al. prepared the ligand tris[(*N'*-*tert*-butylureaylato)-*N*-ethyl]aminato (Figure 1-5), which incorporates 6 basic N-H functionalities. This incorporates 3 hydrogen bonds into the second coordination sphere of the metal ion to form a positively charged cavity, thereby stabilizing an iron-oxo. Indeed, addition of 4 eq. KH and an Fe(II) salt followed by 0.5 eq. O_2 results in the formation of an isolable, structurally characterized Fe(III)-O (Scheme 1-1).

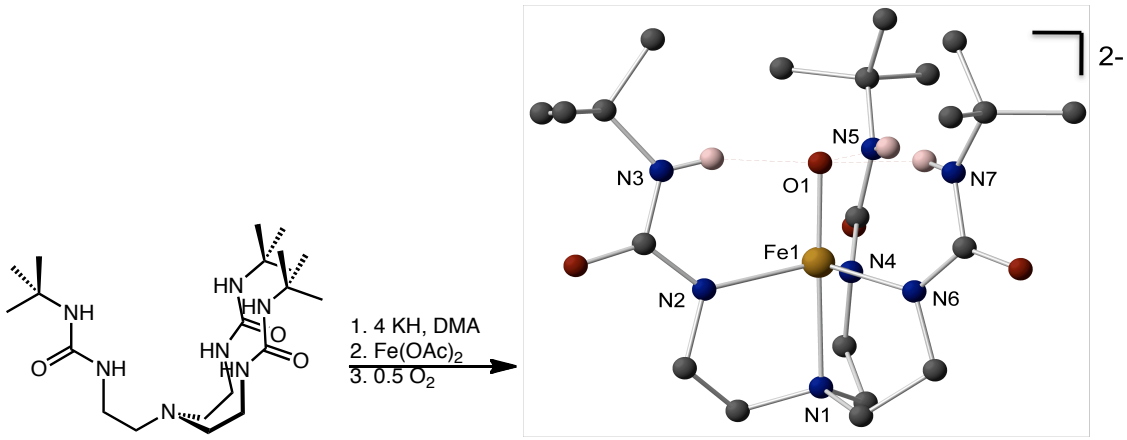

Scheme 1-1. Preparation of Fe(III)-oxo complex stabilized by nearby hydrogen bonding interactions within the transition metal's second coordination sphere.[47] Except those bound to N3, N5, and N7, hydrogen atoms have been omitted for clarity.

These examples illustrate the ability to design ligands for transition metal complexes that will be capable of unique reactivity and binding. The modularity of these tetradentate, tripodal ligands along with their robustness and propensity to direct binding and reactivity to one open coordination site make them attractive ligands for use in coordination chemistry.

Section 1-3. Ligand Design in Tetradentate Tris(carboxamide)amine Ligands

The ultimate goal of the research described in this dissertation has been to design catalysts for small molecule activation that are made from abundant, inexpensive, mid to late first-row transition metals and use environmentally benign materials (e.g. O_2 as an oxidant). We were attracted to the tetradentate triamidoamine family of ligands because of their modularity, robustness, and few examples of unwanted side reactions. With this

in mind, the tris(carboxamide)amine ligands, N(*o*-PhNCH(O)R)$_3$ (Figure 1-5), were prepared.[48]

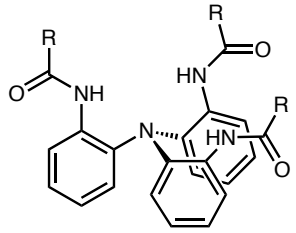

Figure 1-5. Tris(carboxamide)amine ligand, N(*o*-PhNCH(O)R).

We hypothesized that incorporation of the phenylene linkers rather than alkyl linkers would make the ligand more rigid, preventing unwanted ligand labilization, as that seen in the aforementioned Me$_6$tren and TMPA complexes. Incorporation of the carboxamide functionalities would allow for the preparation of robust, trianionic, and highly modular ligands. Lastly, these ligands have the potential to be coordinatively versatile.

Carboxamides in mononuclear transition metal complexes typically coordinate in one of three different modes, as shown in Figure 1-6.[49]

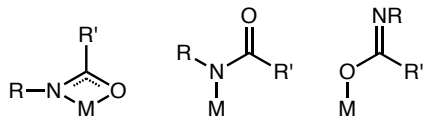

Figure 1-6. Possible coordination modes for amidate ligands in mononuclear complexes.

This versatility in the coordination mode of ligands with the general motif N(*o*-PhNCH(O)R)$_3$ was recently demonstrated by Jones et al. with a series of Ni(II) complexes that vary only in the R-substituent. Jones et al. showed that in varying the

steric bulk of the carboxamide R-substituent, different coordination modes of the carboxamides could be achieved and the geometry about the metal center could be modified. As shown in Figure 1-7, when R = Ph (L^{Ph}), the resulting Ni(II) complex has trigonal bipyramidal geometry, with the phenyl substituents wrapping around the bound solvent molecule. However, when R = ^{i}Pr (L^{iPr}), the steric bulk as well as the electron-richness of the metal center is increased, yielding a complex wherein the metal is in the somewhat rare trigonal monopyramidal geometry. Increasing the steric bulk and electron-richness even more, with R = ^{t}Bu (L^{tBu}), results in one of the ligand arms orienting itself in such a way that it minimizes the repulsive interactions between the ^{t}Bu substituents and coordinates the metal center in the monodentate *O*-amidate coordination mode.

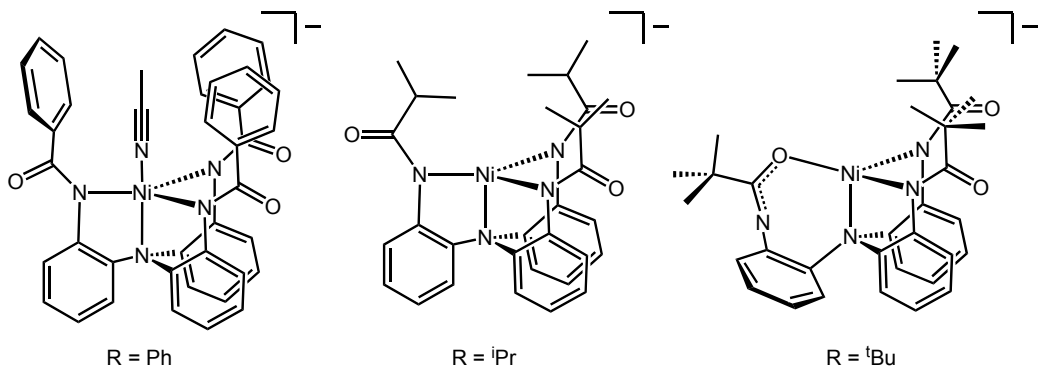

Figure 1-7. Coordination modes of a series of Ni(II) complexes that vary in their R-substituent.

Jones et al. have also described complexes (R = ^{i}Pr and ^{t}Bu) of Al(III) that coordinate to the Al(III) with the last of the possible coordination modes, the chelating κ^2-amidate.[50]

More recently the reactivity of the Fe(II) complex, $(Ph_4P)[KFe_2(L^{iPr})_2]$, in the presence of oxidants (i.e. PhIO, O_2) was described.[51] One carbonyl oxygen from each

complex interacts with the metal ion of the other complex, while another carbonyl from each ligand bridges through the potassium countercation, resulting in a dimeric species. Addition of stoichiometric oxidant results in the formation of a mononuclear Fe(III)-alkoxide—the result of intramolecular C-H activation of one of the methine protons on the ligand. Though our goal is to catalyze intermolecular C-H activation, this result was very promising. This indicated to us that (1) iron complexes of the type [Fe(N(*o*-PhNCH(O)R)$_3$)]$^-$ are capable of activating strong bonds in the presence of an oxidant, and (2) this activation can be done using dioxygen as the oxidant. These findings reaffirmed our interest in these complexes and encouraged us to tune the steric and electronic properties of the (N(*o*-PhNCH(O)R)$_3$ in order to achieve our goal of synthesizing base metal catalysts that activate small molecules using environmentally benign reagents.

Section 1-4. Dissertation Overview

In Chapter 2 of this dissertation, the preparation and properties of a series of cobalt(II) complexes of the tris(carboxamide)amine framework will be described. These complexes vary in the electronic character of the R-substituent. The cyanide binding properties of these complexes will be discussed, along with the possibility that the aromatic substituents interact noncovalently with the bound cyanide ion.

In Chapter 3 the preparation and solution- and solid-state characteristics of a series of iron(II) complexes of the tris(carboxamide)amine framework will be described. These complexes are the first of their kind to catalyze intermolecular C-H bond activation. Furthermore, they are the first examples of non-heme, iron(II) complexes that catalyze the *N*-methyl hydroxylation of *N*,*N*-dimethylformamide.

The dissertation will conclude with Chapter 4, wherein the effect of removal of one of the arms of the ligand platform will be described. The preparation and characterization of the novel, tridentate ligand will be discussed as well as the preparation, characterization, and reactivity of the corresponding cobalt(II), copper(I), and zinc(II) complexes.

References

(1) Tollenaere, J. P. *Pharmacy World and Science* **1996**, *18*, 56.

(2) Elsevier, C. J.; Reedijk, J.; Walton, P. H.; Ward, M. D. *Dalton Trans*. **2003**, 1869.

(3) Ciampolini, M.; Nardi, N. *Inorg. Chem.* **1966**, *5*, 41.

(4) Gade, L. H. *Acc. Chem. Res.* **2002**, *35*, 575.

(5) Blackman, A. G. *Polyhedron* **2005**, *24*, 1.

(6) MacBeth, C. E.; Harkins, S. B.; Peters, J. C. *Can. J. Chem.* **2005**, *83*, 332.

(7) Michalczyk, L.; de Gala, S.; Bruno, J. W. *Organometallics* **2001**, *20*, 5547.

(8) Niemoth-Anderson, J. D.; Clark, K. A.; George, T. A.; Ross, C. R., II **2000**, *122*, 3977.

(9) Redshaw, C.; Rowan, M. A.; Homden, D. M.; Dale, S. H.; Elsegood, M. R. J.; Matsui, S.; Matsuura, S. *Chem. Commun.* **2006**, 3329.

(10) Frye, C. L.; Vincent, G. A.; Hauschildt, G. L. *J. Am. Chem. Soc.* **1966**, *88*, 2727.

(11) Hu, X.; Meyer, K. *J. Organomet. Chem.* **2005**, *690*, 5474.

(12) Davies, S. C.; Durrant, M. C.; Hughes, D. L.; Richards, R. L.; Sanders, J. R. *Dalton* **2000**, 4694.

(13) Davies, S. C.; Evans, D. J.; Hughes, D. L.; Konkol, M.; Richards, R. L.; Sanders, J. R.; Sobota, P. *J. Chem. Soc., Dalton Trans.* **2002**, 2473.

(14) Phukan, A. K.; Guha, A. K. *Inorg. Chem.* **2010**, *49*, 9884.

(15) Mankad, N. P.; Whited, M. T.; Peters, J. C. *Angew. Chem., Int. Ed.* **2007**, *46*, 5768.

(16) Lee, Y.; Mankad, N. P.; Peters, J. C. *Nat. Chem.*, *2*, 558.

(17) Tsay, C.; Mankad, N. P.; Peters, J. C. *J. Am. Chem. Soc.* **2010**, *132*, 13975.

(18) Whited, M. T.; Mankad, N. P.; Lee, Y.; Oblad, P. F.; Peters, J. C. *Inorg. Chem.* **2009**, *48*, 2507.

(19) Di, V. M.; Ghilardi, C. A.; Sacconi, L. *Inorg. Chem.* **1976**, *15*, 1555.

(20) Di, V. M.; Midollini, S.; Sacconi, L. *Inorg. Chem.* **1977**, *16*, 1518.

(21) George, T. A.; Rose, D. J.; Chang, Y.; Chen, Q.; Zubieta, J. *Inorg. Chem.* **1995**, *34*, 1295.

(22) Morassi, R.; Sacconi, L. *Inorg. Synth.* **1976**, *16*, 174.

(23) Sacconi, L.; Di, V. M. *Inorg. Chem.* **1978**, *17*, 810.

(24) Stoppioni, P.; Mani, F.; Sacconi, L. *Inorg. Chim. Acta* **1974**, *11*, 227.

(25) Ambundo, E. A.; Deydier, M.-V.; Grall, A. J.; Aguera-Vega, N.; Dressel, L. T.; Cooper, T. H.; Heeg, M. J.; Ochrymowycz, L. A.; Rorabacher, D. B. *Inorg. Chem.* **1999**, *38*, 4233.

(26) Baumeister, J. M.; Alberto, R.; Ortner, K.; Spingler, B.; August, S. P.; Kaden, T. A. *J. Chem. Soc., Dalton Trans.* **2002**, 4143.

(27) Fallani, G.; Morassi, R.; Zanobini, F. *Inorg. Chim. Acta* **1975**, *12*, 147.

(28) Stavropoulos, P.; Carrie, M.; Muetterties, M. C.; Holm, R. H. *J. Am. Chem. Soc.* **1990**, *112*, 5385.

(29) Stavropoulos, P.; Muetterties, M. C.; Carrie, M.; Holm, R. H. *J. Am. Chem. Soc.* **1991**, *113*, 8485.

(30) Schrock, R. R. *Pure Appl. Chem.* **1997**, *69*, 2197.

(31) Schrock, R. R. *Acc. Chem. Res.* **1997**, *30*, 9.

(32) Yandulov, D. V.; Schrock, R. R. *Science* **2003**, *301*, 76.

(33) Schrock, R. R. *Acc. Chem. Res.* **2005**, *38*, 955.

(34) Yandulov, D. V.; Schrock, R. R.; Rheingold, A. L.; Ceccarelli, C.; Davis, W. M. *Inorg. Chem.* **2003**, *42*, 796.

(35) Suzuki, M. *Acc. Chem. Res.* **2007**, *40*, 609.

(36) Zhang, C. X.; Kaderli, S.; Costas, M.; Kim, E.-i.; Neuhold, Y.-M.; Karlin, K. D.; Zuberbühler, A. D. *Inorg. Chem.* **2003**, *42*, 1807.

(37) Lucas, H. R.; Li, L.; Sarjeant, A. A. N.; Vance, M. A.; Solomon, E. I.; Karlin, K. D. *J. Am. Chem. Soc.* **2009**, *131*, 3230.

(38) Maiti, D.; Woertink, J. S.; Narducci Sarjeant, A. A.; Solomon, E. I.; Karlin, K. D. *Inorg. Chem.* **2008**, *47*, 3787.

(39) Lucas, H. R.; Meyer, G. J.; Karlin, K. D. *J. Am. Chem. Soc.* **2010**, *132*, 12927.

(40) Würtele, C.; Sander, O.; Lutz, V.; Waitz, T.; Tuczek, F.; Schindler, S. *J. Am. Chem. Soc.* **2009**, *131*, 7544.

(41) Chu, L.; Hardcastle, K. I.; MacBeth, C. E. *Inorg. Chem.* **2010**, *49*, 7521.

(42) Komiyama, K.; Furutachi, H.; Nagatomo, S.; Hashimoto, A.; Hayashi, H.; Fujinami, S.; Suzuki, M.; Kitagawa, T. *Bull. Chem. Soc. Jpn.* **2004**, *77*, 59.

(43) Jacobson, R. R.; Tyeklar, Z.; Farooq, A.; Karlin, K. D.; Liu, S.; Zubieta, J. *J. Am. Chem. Soc.* **1988**, *110*, 3690.

(44) Hammes, B. S.; Young, V. G., Jr.; Borovik, A. S. *Angew. Chem., Int. Ed.* **1999**, *38*, 666.

(45) Springer, B. A.; Sligar, S. G.; Olson, J. S.; Jr., G. N. P. *Chem. Rev.* **1994**, *94*, 699.

(46) Bonagura, C. A.; Bhaskar, B.; Shimizu, H.; Li, H.; Sundaramoorthy, M.; McRee, D. E.; Goodin, D. B.; Poulos, T. L. *Biochemistry* **2003**, *42*, 5600.

(47) MacBeth, C. E.; Golombek, A. P.; Jr., V. G. Y.; Yang, C.; Kuczera, K.; Hendrich, M. P.; Borovik, A. S. *Science* **2000**, *289*, 938.

(48) Jones, M. B.; MacBeth, C. E. *Inorg. Chem.* **2007**, *46*, 8117.

(49) Lee, A. V.; Schafer, L. L. *European Journal of Inorganic Chemistry* **2007**, 2243.

(50) Jones, M. B.; Hardcastle, K. I.; MacBeth, C. E. *Polyhedron* **2010**, *29*, 116.

(51) Jones, M. B.; Hardcastle, K. I.; Hagen, K. S.; MacBeth, C. E. *Inorg. Chem.* **2011**, *50*, 6402.

Chapter 2: Utilizing Aromatic Substituents for Regulation of Cyanide Binding by Cobalt(II) Metal Complexes

Section 2-1. Introduction

Noncovalent interactions such as hydrogen bonding, π-stacking, electrostatic interactions, van der Waals forces, and hydrophobic interactions, charge-transfer interactions, metal coordination, and cation-π interactions have proven to be important in the field of supramolecular chemistry.[1] Hydrogen bonds are, perhaps, the most well known of these noncovalent interactions. Hydrogen bonding is responsible for many of water's unique properties—its heat capacity, cohesion and adhesion, its ability to dissolve polar compounds, and act as a ligand. In biology, they are part of the environment surrounding heme proteins that assist in controlling protein function.[2-9] They are also known to be integral players in the catalytic activity of other non-heme enzymes, such as superoxide disumutase and methane monooxygenase.[10-12] In synthetic systems, these interactions are now known to stabilize unique O_2 binding and activation[2,13-17] and aid in the selective encapsulation of environmental pollutants.[18-20]

Hydrophobic and π-π stacking interactions are largely responsible for the stability of the DNA helix.[21] Hydrophobic interactions are responsible, also, for aggregation of amphipathic biomolecules, such as phospholipids. These aggregates are essential for formation of biological membranes and play a large role in the stabilization of proteins.[22] π-π stacking also plays a role in the molecular self-assembly, folding, and stability of proteins.[23-25]

Pi-systems, like that found in benzene, can also interact with ions. The cation-π interaction was initially described as an electrostatic interaction that occurs between a cation and the negative quadrupole moment lying perpendicular to an aromatic ring that has electron-donating substituents.[26-28] Later it was demonstrated that the magnitude of this interaction is also dependent upon cation-induced polarization.[29] For instance, Li^+ has an affinity for benzene that is quantified at 159 kJ/mol, whereas NH_4^+, which has lower charge per unit area, has an affinity for benzene of 79 kJ/mol.[30] Experimental and computational evidence indicates that this is a relatively strong noncovalent interaction—similar to or stronger than the strength of hydrogen bonding and stronger than that of salt bridges.[28,31] Cation-π interactions have been proven to be virtually ubiquitous in biological systems.[26,30,32,33] They have a role in ion channels, g-protein coupled receptors, transportation across membranes, recognition proteins, and enzymes.[28] The cation-π interaction has also been shown to be prevalent in amino acid interactions. For instance, 26% of the amino acid tryptophan is involved in this type of interaction.[27]

Anions play a large role in environmental and biological systems.[34] For example, DNA, RNA, and ATP are anionic. Furthermore, anions are present in about 70% of all enzymatic sites.[34,35] Anion transport channels are used within biological systems to carry chloride, sulfate, and phosphate, and maintain osmotic balance. Malfunction of these channels has been implicated as the cause for cystic fibrosis and drug resistance.[36] Improper processing of anions in biological systems can lead to a host of problems—from renal failure due to phosphate and sulfate to acute toxicity from oxalate, arsenate, cyanide, and nitrite.[34] In the environment, many pollutants, such nitrates and phosphates, which cause river eutrophication, and pertechnetate, a byproduct of nuclear fuel

reprocessing, are anionic.[37,38] Therefore, anion sensing and selective anion binding is a large area of research.

Anion receptor chemistry has been reviewed.[39-57] The design of receptors for anions is more challenging than that for cations for several reasons.[34] First of all, anions are generally larger with lower charge density than the isolectronic cations, making electrostatic interactions less effective. Also, the charge of the anion is dependent upon the pH of the medium, as anions can be protonated and, therefore, neutral at low pH and charged in the absence of protons, at high pH. Lastly, receptors must be tailored to accomodate the size and geometric variations in anions (e.g. from small, monoatomic halides to large, double stranded DNA). Previous approaches toward the selective recognition of anions have focused on several different noncovalent interactions—electrostatic interactions, hydrogen bonding, hydrophobic interactions, and metal coordination. Often, these interactions are used in tandem to achieve selective anion binding that can be detected by NMR or X-ray diffraction.

Other efforts have focused on anion sensing.[58-63] One method of detecting the binding of anions in low concentrations is by studying the resulting electrochemical properties of the system, whether that be of the host membrane, or of an anion bound to a redox active metal complex, or by production of a chemically modified electrode that contains a redox active binding site for anions. These anion-binding systems have also be studied optically, through the formation of luminescent anion-responsive systems, and colorimetrically, using molecules that will bind anions and, as a result, absorb visible light.[37] One noncovalent interaction that has been minimally utilized in selective anion binding and recognition has been the anion-π interaction.[64-67]

In recent years, much research has focused on the anion-π interaction, and the topic has recently been reviewed.[24,68-76] An anion-π interaction is generally defined as a favorable noncovalent interaction between an electron-deficient aromatic ring and an anion.[76] The energy of these interactions varies from ~20-50 kJ mol^{-1} and act over distance that is largely dependent upon the ion, but ranges from ~3.0-3.5 Å from the centroid of the aromatic ring.[75] Figure 2-1 illustrates both the cation-π and the anion-π interactions, using benzene and hexafluorobenzene for examples. Though neither of these molecules has a permanent dipole, each of them have a region of high or low electron density through the axis that runs perpendicular to the plane of the ring, known as the quadrupole moment. Thus, the quadrupole moment of benzene is -8.48 B, whereas that of hexafluorobenzene is +9.50 B (B = 1 Buckingham = 3.336 x 10^{-40} C m^2).[77-79] Just as electron-donating substituents effect a negative quadrupole moment perpendicular to the plane of the ring, as in benzene, that can interact with cations (Figure 2-1A), electron-withdrawing substituents effect a positive quadrupole moment perpendicular to the plane of the ring, as in hexafluorobenzene, that can interact with anions (Figure 2-1B).

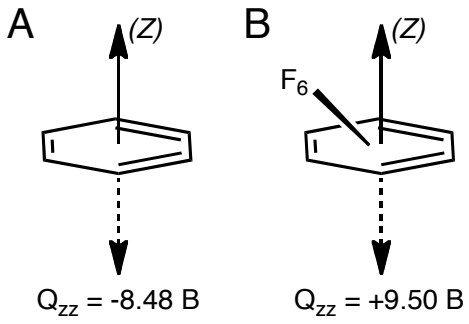

Figure 2-1. Representation of the quadruople moment induced by the area of electron-rich or electron-lacking above and below the plane of the ring of (A) benzene and (B) hexafluorobenzene.[77,79-81]

It has previously been established that benzene interacts electrostatically with cations such as sodium with an interaction energy of -27.1 kcal/mol.[26,82] Similarly, hexafluorobenzene interacts electrostatically with anions such as chloride with an interaction energy of -14.05 kcal/mol.[83] It should be noted that interaction energies for the cation-π interaction are generally more negative than those for the anion-π interaction because the cation-π interaction distances are shorter.[70]

Like cation-π interactions, anion-π interactions are dependent upon the quadrupole moment induced by the electronegativity of the bound substituents and the anion-induced polarizability.[84] For example, the series of cyanuric acids shown in Figure 2-2 exhibit decreasing quadrupole moments (Q_{zz}) and increasing polarizabilities ($a_{||}$, atomic units, a.u.). However, across the series, the chloride binding energies for the cyanuric acids remain almost constant (~15 kcal/mol).[84] This demonstrates the compensating effect that ion-induced polarization has on the interaction energies.

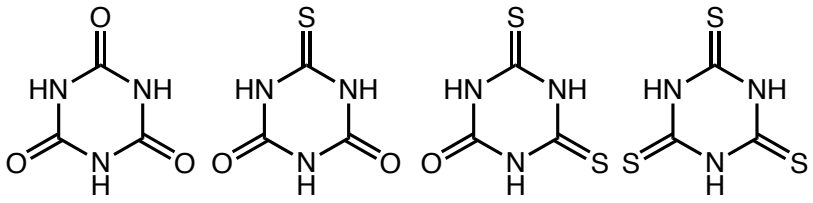

Figure 2-2. Variation in the quadrupole moment (Q_{zz}) and polarizability ($a_{||}$) of cyanuric acid, thiocyanuric acid, dithiocyanuric acid, and trithiocyanuric acid[84]

Numerous computational studies have been performed on these systems.[85-91] A thorough discussion thereof would be beyond the scope of this dissertation. However, note that these interactions have been confirmed on many different levels of theory.

Most of this computational work has been performed on small, neutral aromatic systems and either halides or small anions. The most informative of these are those that couple calculations with experiment.

In recent articles by Hay *et. al*, it was indicated that anion-π interactions may be implicated as the reason for this enhanced anion binding too frequently.[75,92] These authors stated that to truly be an anion-π interaction, the anion must be positioned directly above the centroid of the aromatic ring or DFT calculations must indicate this orientation as a minimum. Furthermore, there must be evidence for the lack of covalency exhibited by the complex. Three suggestions were made to describe the interactions that do not apply to these classifications. One of these three interactions was hydrogen bonding; the other two are strong and weak σ interactions.

Strongly covalent σ interactions are those similar to Meisenheimer complexes—intermediates in nucleophilic aromatic substitution. These are characterized by good overlap between the binding molecular orbitals of the aromatic system and the anion. Furthermore, the area in which this binding occurs is usually outside of the perimeter of the aromatic ring. The average distance from the anion to the nearest carbon atom on the aromatic ring is about 1.5 Å, which is very close to the average length of a C (sp^3) – F bond. Weakly covalent σ complexes can be identified as those where there is some overlap of bonding molecular orbitals of the anion and the aromatic system. The distance between these two moieties averages about 2.8 Å, and the anion is located away from the center, over an electron deficient part of the ring perimeter.

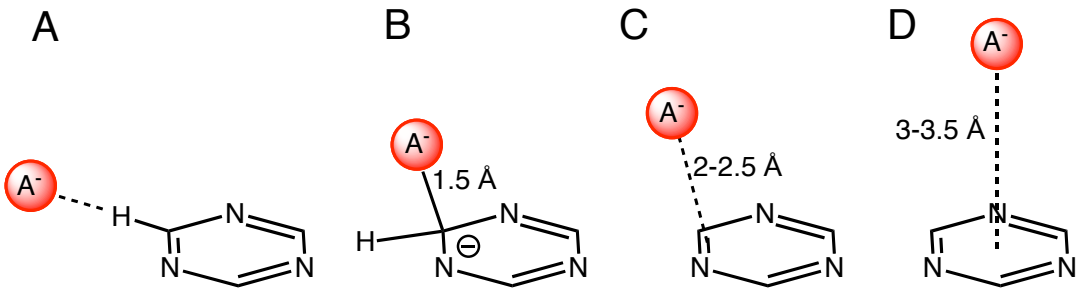

Figure 2-3. Representation of (A) aromatic hydrogen bonding with an anion, (B) a strong σ interaction, (C) a weak σ interaction, and (D) the anion-π interactions. A^- is an anion. Also shown are interaction distances.[92,93]

Favorable interactions between electron-deficient aromatic systems and anions have also been studied experimentally. Frontera *et. al* synthesized thiocyanuric acid and dithiocyanuric acid with attached flexible 2-ethyleneamine arms. These were treated with HCl, HBr, or HI to form the corresponding acid. Upon crystallization and structural determination, the investigators noted that, in the case of the dithiocyanuric acid, along with exhibiting a hydrogen bond with the amine, the halide anion was positioned almost directly above the centroid of the ring.[94]

A similar interaction was noted when an acetonitrile solution of pentafluorophenylacetimidamide was exposed to HBr, yielding the corresponding aminium salt.[95] In the solid-state, as shown in Figure 2-4, the bromide anion is positioned 3.48 Å from the centroid of the perfluorophenyl ring.

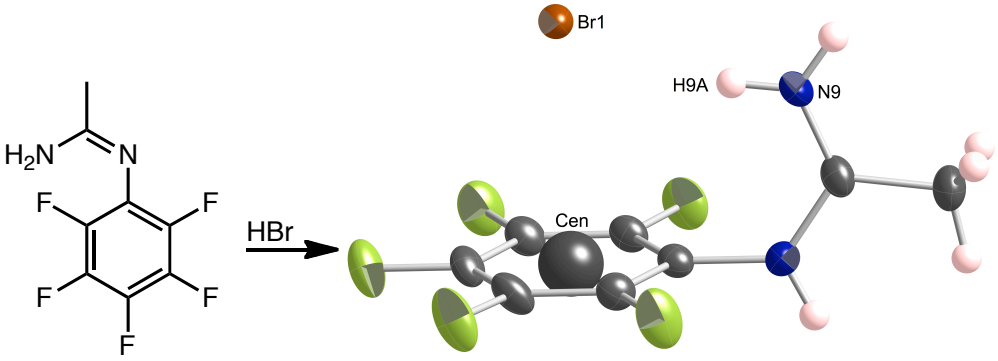

Figure 2-4. Bromide anion interaction with *N*-(1-aminoethylidene)-2,3,4,5,6-pentafluorobenzenaminium.[95]

The angle formed by this anion, the aromatic centroid, and the edge of the ring is 85.7°. Since the quadrupole moment is considered to be along the axis perpendicular to the aromatic ring, this anion appears to be aligned with the quadrupole moment. This salt also exhibits a hydrogen bonding interaction between the bromide ion and H9A, and the bromide participates in a weak σ interaction with another molecule of the aminium in the unit cell.

Solution state studies have also been used to probe interactions between electron deficient rings and anions. Titration of solutions of tetracyanopyrazine, trinitrobenzene, tetracyanopyridine, tetrachloro-*o*/*p*-benzoquinone, and tetracyanoethene with tetraalkylammonium salts of chloride, bromide, and iodide all resulted in a color change and increased absorbance in the resulting UV-visible absorption spectra.[96]

A combination solution state and computational study was also used to compare the affinities of various halide salts for a perfluorophenyl substituted aromatic system vs. that of a control, phenyl substituted aromatic compound, as seen in Figure 2-5.

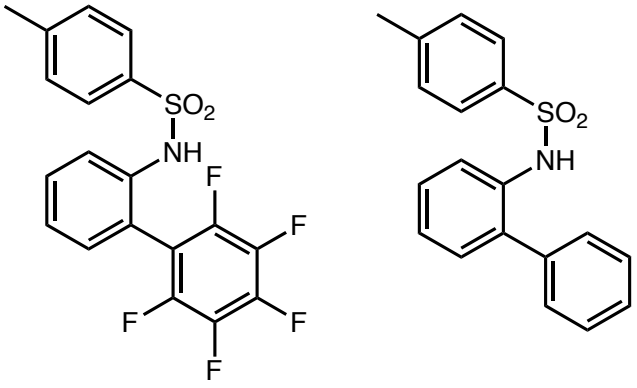

Figure 2-5. Diagrams of 2-*p*-toluenesulfonamide-2',3',4',5',6'-pentafluorobiphenyl (left) and *N*-biphenyl-2-yl-4-methyl-benzenesulfonamide (right).

These studies indicated, as expected, that the magnitude of the interaction between the electron poor, 2-*p*-toluenesulfonamide-2',3',4',5',6'-pentafluorobiphenyl, and the halides was roughly 30 M^{-1} versus the control (*N*-biphenyl-2-yl-4-methyl-benzenesulfon-amide), in which any interaction was undetectable.[97]

The first demonstration of the anion-π interaction in the gas phase was published in 1987 and relied on mass spectrometry and theory to describe halide (Cl^-, Br^-, and I^-) interactions with hexafluorobenzenethe along its C_6 axis.[98] More recent examples of anion-π interactions in the gas phase come from Chifotides et al. and Dawson et al.[67,99] Chifotides et al. found that addition of $^nBu_4N(X)$ (X = Cl^-, Br^-, I^-) solutions to solutions of the receptor 1,4,5,8,9,12-hexaazatriphenylene-hexacarbonitrile [$HAT(CN)_6$, Figure 2-6] resulted in color changes consistent with charge transfer.

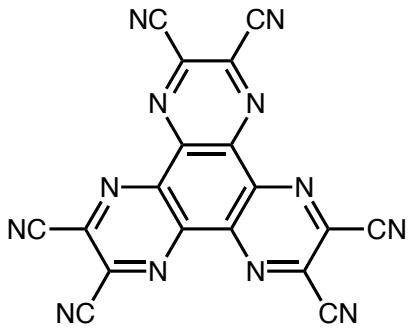

Figure 2-6. Diagram of $HAT(CN)_6$, which exhibits interactions with halides in the solid state, in solution, and in the gas phase.[67]

Crystallization of the complexes demonstrated that these species exhibited both weak σ and anion-π interactions in the solid state. Lastly, ES-MS confirmed that these interations were maintained in the gas phase, as the observed peaks were consistent with $HAT(CN)_6{:}X^-$. Similarly, Dawson et al. noted UV-vis absorption spectral changes consistent with charge transfer upon addition of Cl^-, Br^-, and NO_3^- salts to solutions of the napthalenediimides (NDIs) shown in Figure 2-7.[99]

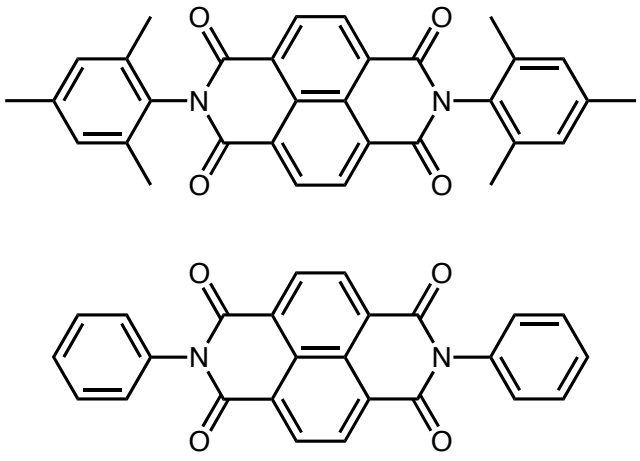

Figure 2-7. Diagram of the NDIs which exhibit interactions with Cl^-, Br^-, and NO_3^- in solution and in the gas phase.[99]

When equimolar acetonitrile solutions of the NDIs and anion salts were studied by electrospray ionization Fourier-transform ion cyclotron resonance tandem mass spectrometry, 1:1 and 2:1 adducts were observed.

Section 2-2. Results and Discussion

Despite the growth in this research area, molecular systems that incorporate both pi-acidic aromatic rings and metal ion coordination for solution-phase anion recognition have yet to be explored.[100]

The tripodal ligands containing aromatic substituents varying in quadrupole from electron-rich to electron-poor, N(*o*-PhNHC(O)(*p*-PhNMe$_2$))$_3$ (H_3L^{NMe2}), N(*o*-PhNHC(O)(*p*-PhOMe))$_3$ (H_3L^{OMe}), N(*o*-PhNHC(O)Ph)$_3$ (H_3L^{Ph}), N(*o*-PhNHC(O)(3,5-$C_6H_3F_2$))$_3$ (H_3L^{F2}), N(*o*-PhNHC(O)(2,4,6-$C_6H_2F_3$))$_3$ (H_3L^{F3}), and N(*o*-PhNHC(O)(C_6F_5))$_3$ (H_3L^{F5}), along with their Co(II) complexes, were synthesized using modifications of the previously reported procedure.[101]

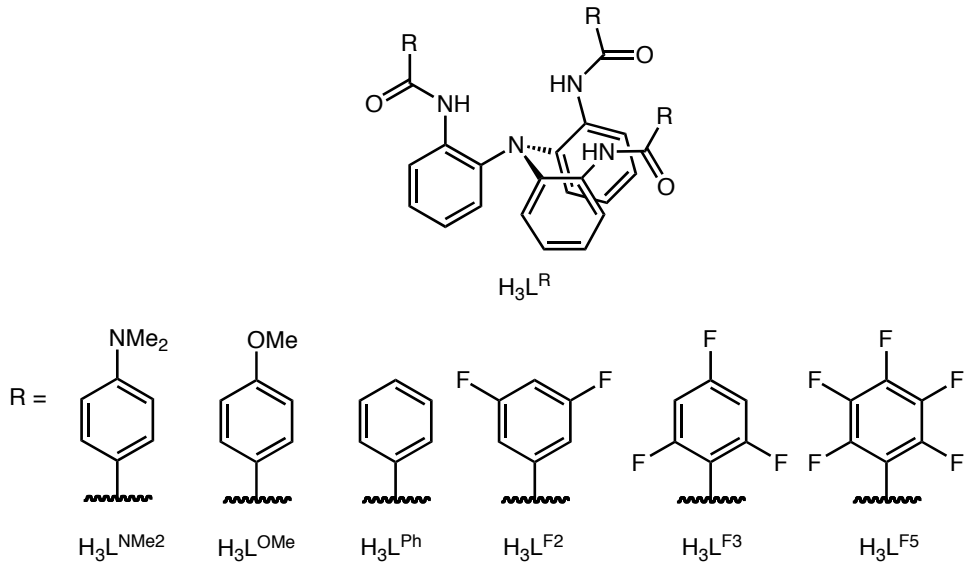

Figure 2-8. Ligands used in this study.

The aryl substituents were chosen due to the variation in the quadrupole moments that their unsubstituted moieties exhibit (see Figure 2-9). It is assumed that since the ligand remains the same throughout, the changes in the properties of the complexes described herein are primarily due to the changes in the properties of the substituent.

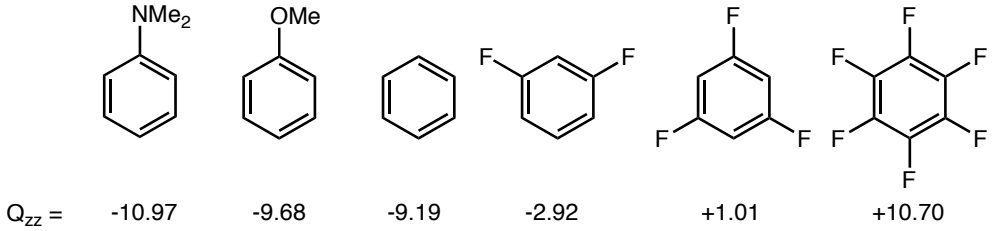

Figure 2-9. Quadrupole moments (Q_{zz} in DÅ) of ligand fragments from References 81 and 103 calculated at the RHF/6-311++G** level of theory.[80,102]

Section 2-2-1. Synthesis of Trigonal Monopyramidal and Solvento Cobalt(II) Complexes

The preparation and characterization of H_3L^{Ph} and its Co(II) complexes has previously been reported.[103] Acylation of N(*o*-$PhNH_2$)$_3$ with the corresponding aryl acid chloride yields H_3L^R, as shown in Scheme 2-1.

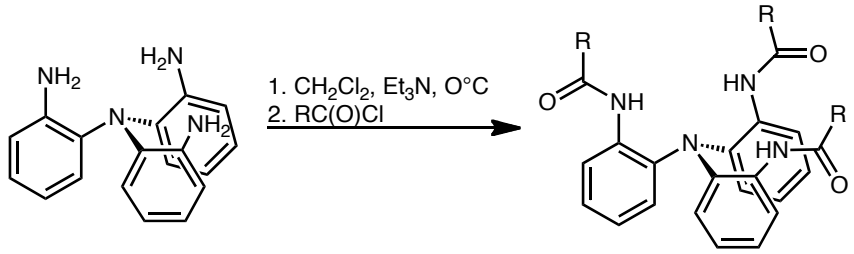

Scheme 2-1. Ligand synthesis.[101]

Deprotonation with KH followed by transmetallation with $CoBr_2$ and *in situ* salt metathesis with either tetraethylammonium bromide (Et_4NBr) or tetraphenylphosphonium bromide (Ph_4PBr) affords the corresponding anionic Co(II) complexes (Scheme 2-2).

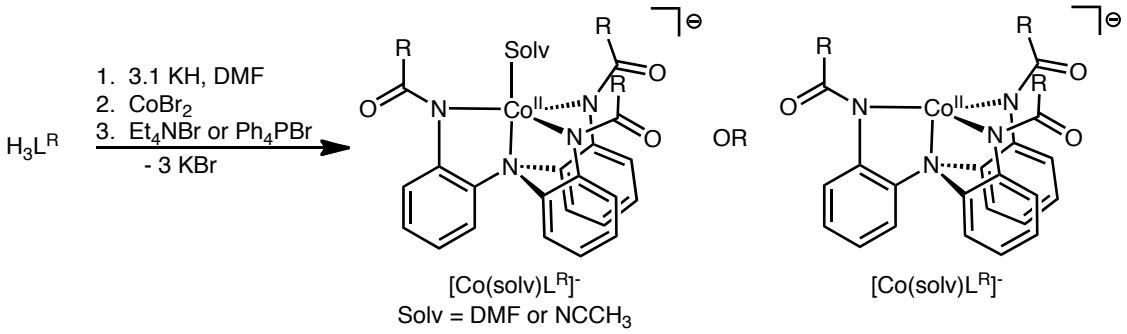

Scheme 2-2. Synthesis of solvento and trigonal monopyramidal, cobalt(II) complexes.

The complexes $Ph_4P[CoL^{NMe2}]$, $Ph_4P[CoL^{OMe}]$, and $Ph_4P[CoL^{Ph}]$,[103] can be isolated as four-coordinate, trigonal monopyramidal species by avoiding coordinating solvents in the synthesis and crystallization. $Ph_4P[CoL^{NMe2}]$ can be synthesized in good yield and remains four-coordinate in non-coordinating solvents. Conversely, the complex $Ph_4P[CoL^{OMe}]$ can only be synthesized in low yield and is very reactive and, therefore, difficult to characterize.

$Ph_4P[Co(NCCH_3)L^{NMe2}]$ can be isolated as magenta blocks by recrystallization from diffusion of diethyl ether into a 2:1 $NCCH_3$:DMF solution of the product in 60% yield. Decreasing the ratio of $NCCH_3$ to DMF results in formation of green needles ($Ph_4P[CoL^{NMe2}]$) in 92% yield. $Ph_4P[Co(NCCH_3)L^{NMe2}]$ forms a pink solution when dissolved in acetonitrile ($NCCH_3$) and a green solution when dissolved in dichloromethane (DCM), indicating that it loses the bound $NCCH_3$ solvent upon

dissolution in non-coordinating solvents and that the species exists in an equilibrium that does not strongly favor either the solvento or trigonal monopyramidal species. The ^{1}H NMR spectrum of the complex in CD_2Cl_2 (300 MHz) exhibits 7 paramagnetically shifted peaks, indicating that it is C_3-symmetric in solution. This species has a μ_{eff} of 4.33 μ_B (the method of Evans, CD_2Cl_2, 400 MHz), indicating that the metal ion is high-spin Co(II). The parent peak in the mass spectrum (ESI-MS, negative mode) has an m/z = 787.6, which is consistent with $[CoL^{NMe2}]^-$. The FT-IR spectrum of solid, pink $Ph_4P[Co(NCCH_3)L^{NMe2}]$ contains a peak at 2249 cm^{-1}, consistent with bound $NCCH_3$.

Unlike $Ph_4P[CoL^{NMe2}]$, the isolation of $Ph_4P[CoL^{OMe}]$ is not trivial. However, by avoiding the use of $NCCH_3$ in the purification of the crude material followed by crystallization from DMF, single crystals of the green product were obtained in very low yield. The difficulty in the isolation thereof as opposed to the solvento complex is a testament to the equilibrium shift towards the solvento complex, due to the more electron-deficient Co(II) center. The solvento complex, $Ph_4P[Co(NCCH_3)L^{OMe}]$, is crystallized from diffusion of diethyl ether into a 1:1 $NCCH_3$: DMF solution of the product to afford magenta blocks in 66% yield. The low intensity peak at 2253 cm^{-1} in the FT-IR spectrum of the product confirms the assignment of bound $NCCH_3$. The ^{1}H NMR spectrum of $Ph_4P[Co(NCCH_3)L^{OMe}]$ (CD_2Cl_2, 300 MHz) indicates that this species maintains C_3-symmetry in solution. Magnetic susceptibility measurements using the method of Evans (CD_2Cl_2, 300 MHz) confirm that the cobalt ion is high-spin, S = 3/2, with μ_{eff} = 4.40 μ_B.

$Ph_4P[Co(NCCH_3)L^{F2}]$ can be isolated as a pink, crystalline solid in 87% yield by diffusion of diethyl ether into a 1:1 DMF:$NCCH_3$ solution of the complex. A solution of

this complex yields an *m/z* of 766.1 (ESI-MS, negative mode), which is consistent with the formulation $[CoL^{F2}]^-$. The peak in the FT-IR (KBr pellet) at a stretching frequency of 2252 cm^{-1} is indicative of the bound $NCCH_3$ molecule. The ^1H NMR spectrum of the complex (CD_2Cl_2, 300 MHz) contains 6 signals that are paramagnetically broadened. This indicates that the molecule is likely C_3-symmetric in solution. The ^{19}F NMR confirms the assignment of C_3 symmetry in solution, as there is only one signal at -105.4 ppm. The μ_{eff} exhibited by this complex of 4.40 μ_B (the method of Evans, CD_3CN, 400 MHz) is consistent with a high-spin, S = 3/2, cobalt(II) center.

Recrystallization of $Ph_4P[Co(NCCH_3)L^{F3}]$ by the same method as $Ph_4P[Co(NCCH_3)L^{F2}]$ yields crystalline product as magenta blocks in 81% yield. The peak at 2255 cm^{-1} in the FT-IR is characteristic of the bound $NCCH_3$ molecule. The ^1H NMR spectrum of this material in CD_2Cl_2 (300 MHz) displays more peaks than would be expected for the C_3-symmetric molecule, indicating that the molecule is not C_3-symmetric in non-coordinating solvents. Magnetic susceptibility measurements yield a $\mu_{eff} = 4.28\ \mu_B$ (the method of Evans, CD_2Cl_2, 300 MHz).

Observed magnetic susceptibility measurements are the sum of the positive paramagnetic susceptibilities contributed by the unpaired electrons in a molecule and the diamagnetic susceptibilities contributed by all paired electrons in a molecule. Large molecules that contain substituents with many paired electrons tend to display lower magnetic susceptibilities, which can be deceiving when using the measurement to assign the spin state of the transition metal ion. Corrections can be made to the experimental magnetic susceptibility measurement that aid in the assignment of the paramagnetic

susceptibility of the transition metal complex.[104] The corrected value of the μ_{eff} for $Ph_4P[Co(NCCH_3)L^{F3}]$ is 4.45 μ_B.

The diamagnetic correction was also used for $Et_4N[Co(DMF)L^{F5}]$, which had an initial μ_{eff} = 4.41 μ_B and μ_{eff} = 4.53 μ_B after correction. $Et_4N[Co(DMF)L^{F5}]$ was crystallized from diffusion of diethyl ether into a DMF solution of the product at -35°C in 32% yield. This complex exhibits four peaks in its ^1H NMR spectrum (CD_2Cl_2, 300 MHz), indicating that the backbone phenylene linkers maintain C_3-symmetry in solution. However, the ^{19}F NMR spectrum (CD_2Cl_2, 400 MHz) displays many peaks (>20), indicating that the perfluorophenyl substituents are not C_3-symmetric in solution.

Section 2-2-2. Structural Characterization of Trigonal Monopyramidal and Solvento Cobalt(II) Complexes

The solid-state structures of $Ph_4P[CoL^{NMe2}]$ and $Ph_4P[CoL^{OMe}]$ are shown in Figure 2-10.

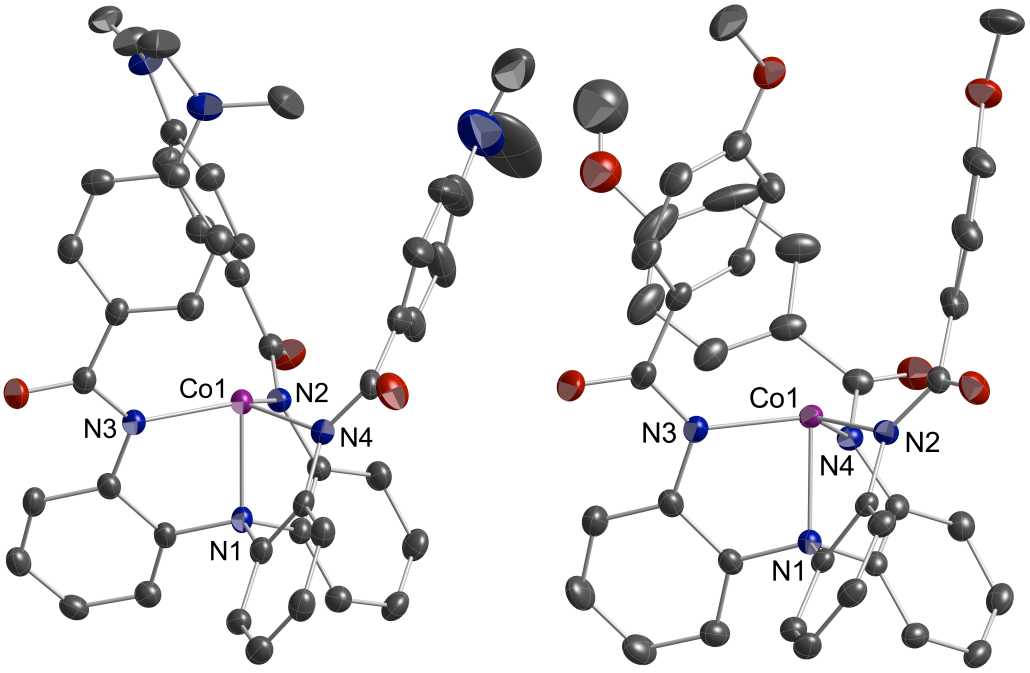

Figure 2-10: Solid-state structure of (left) $Ph_4P[CoL^{NMe2}]$ and (right) $Ph_4P[CoL^{OMe}]$. Thermal ellipsoids drawn at 40% probability. Hydrogen atoms and countercations omitted for clarity.

Table 2-1. Selected bond lengths and angles for $[CoL^{NMe2})]^-$ and $[CoL^{OMe}]^-$.

Bond Lengths (Å) and Angles (°)		
R =	*p*-NMe_2Ph	*p*-OMePh
Co1 – N1	2.115(3)	2.113(2)
Ave. Co1 – N_{eq}	1.999(2)	1.987(1)
Co1 – Eq. Plane	0.288	0.279
Ave. N1 – Co1 – N_{eq}	81.68(7)	81.90(5)
Ave. N_{eq} – Co1 – N_{eq}	117.94(8)	118.05(5)

$Ph_4P[CoL^{NMe2}]$ and $Ph_4P[CoL^{OMe}]$ crystallize with nearly ideal trigonal pyramidal geometry about the cobalt ion. The geometries of these complexes can be quantified by their τ_4 values of 0.84 and 0.85.[105] The derivation of this value is shown Equation 2-1, where α and β are equal to the two largest angles about the metal ion.

$$\tau_4 = \frac{360° - (\alpha + \beta)}{141°} \qquad \text{(Equation 2-1)}$$

This value describes the geometry about four-coordinate transition metal complexes, where τ_4 = 0.85 indicates trigonal pyramidal geometry, τ_4 = 1 indicates tetrahedral geometry because 360 – 2(109.5) = 141, and τ_4 = 0 indicates square planar geometry because 360 – 2(180) = 0.

The cobalt ion is nearer the the equatorial nitrogens in $Ph_4P[CoL^{OMe}]$, indicating greater σ donation from the equatorial nitrogens, due to the more electron-deficient Co(II) ion. The Co1-N1 distances of these two complexes are equivalent within the range of error in the measurement.

The five-coordinate, solvento complexes, $Ph_4P[Co(NCCH_3)L^{NMe2}]$, $Ph_4P[Co(NCCH_3)L^{OMe}]$, $Ph_4P[Co(NCCH_3)L^{F2}]$, $Ph_4P[Co(NCCH_3)L^{F3}]$, and $Et_4N[Co(DMF)L^{F5}]$ (Figure 2-11 and Table 2-2), display distorted trigonal bipyramidal coordination environments (τ_5 = 0.99, 1.02, 1.00, 0.96, 1.00 respectively). Five-coordinate complex geometry can be described by the τ_5 value, which is analogous to the aforementioned τ_4 value and defined in Equation 2-2.[106]

$$\tau_5 = \frac{\beta - \alpha}{60°} \qquad \text{(Equation 2-2)}$$

A τ_5 value of 1 corresponds to trigonal bipyramidal geometry because the two largest angles are 180° and 120°, and 180 – 120 = 60. A τ_5 value of 0 corresponds to square pyramidal geometry because the angles are equivalent.

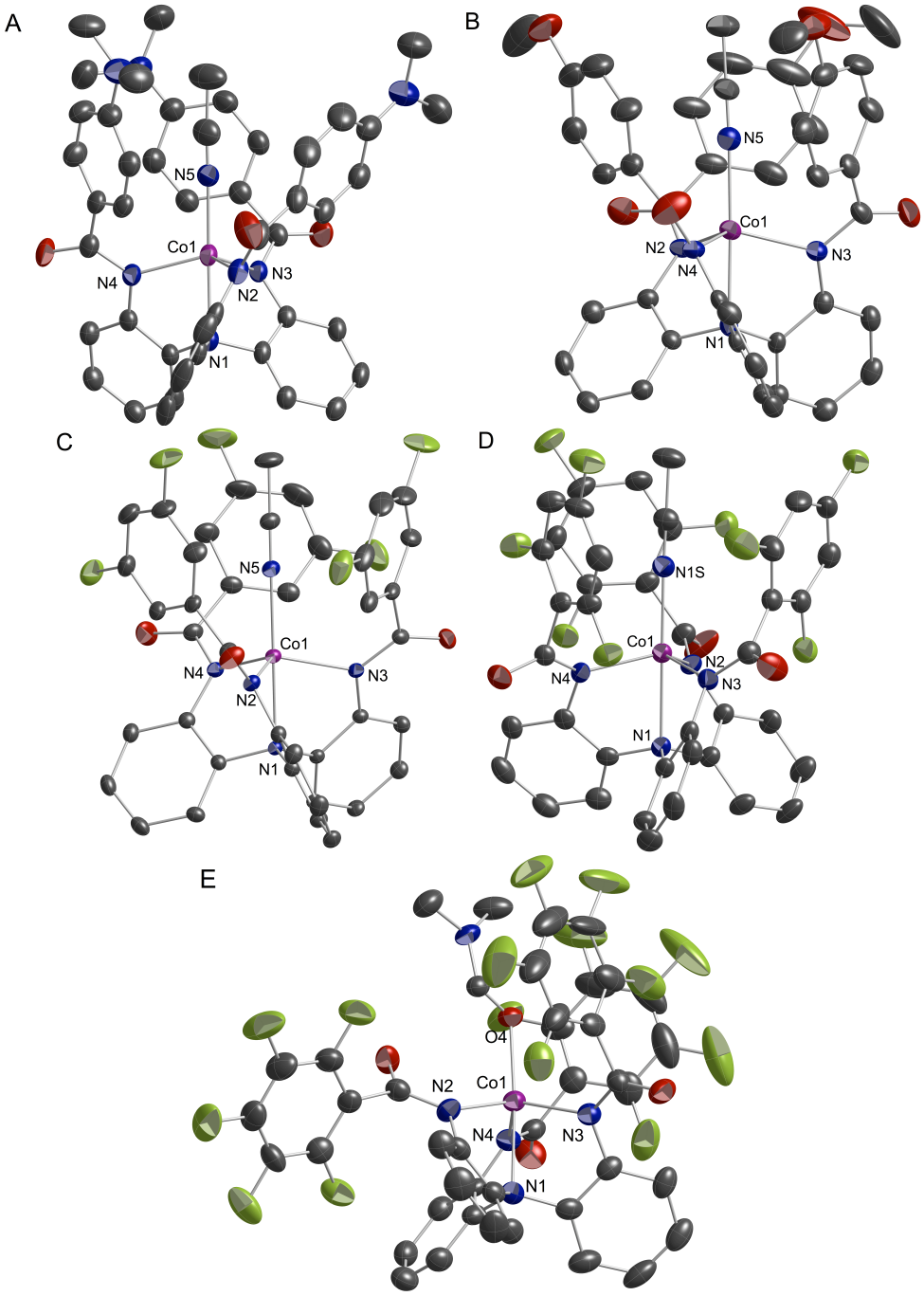

Figure 2-11: Solid-state structure of (A) $Ph_4P[Co(NCCH_3)L^{NMe2}]$, (B) $Ph_4P[Co(NCCH_3)L^{OMe}]$, (C) $Ph_4P[Co(NCCH_3)L^{F2}]$, (D) $Ph_4P[Co(NCCH_3)L^{F3}]$, and (E) $Et_4N[Co(DMF)L^{F5}]$. Thermal ellipsoids drawn at 40% probability. Hydrogen atoms and countercations omitted for clarity.

Table 2-2. Selected bond lengths and angles for $Ph_4P[Co(NCCH_3)L^{NMe2}]$, $Ph_4P[Co(NCCH_3)L^{Ph}]$, $Ph_4P[Co(NCCH_3)L^{Ph}]$ (taken from Ref. 104), $Ph_4P[Co(NCCH_3)L^{F2}]$, $Ph_4P[Co(NCCH_3)L^{F3}]$, and $Et_4N[Co(DMF)L^{F5}]$.

Bond Lengths (Å) and Angles (°)						
R =	*p*-NMe_2Ph	*p*-OMePh	Ph[103]	3,5-$C_6H_3F_2$	2,4,6-$C_6H_2F_3$	C_6F_5
Co1 – N1	2.1971(18)	2.207(3)	2.184(4)	2.2071(13)	2.254(3)	2.288(4)
Ave. Co1 – N_{eq}	2.0587(11)	2.062(2)	2.045(3)	2.0551(18)	2.044(2)	2.035(2)
Co1 – solv	2.061(2)	2.098(3)	2.064(6)	2.0875(15)	2.072(3)	2.076(4)
Co1 – Eq. Plane	0.451	0.448	0.447	0.439	0.456	0.507
Ave. N1 – Co1 – N_{eq}	77.34(4)	77.45(5)	77.39(11)	77.68(3)	77.13(6)	75.58(9)
Ave. N_{eq} – Co1 – N_{eq}	115.33(4)	115.41(5)	115.37(11)	115.57(3)	115.15(6)	114.00(10)
N1 – Co1 – solv	176.50(7)	178.40(9)	175.29(19)	177.36(5)	178.38(11)	175.90(15)

The ligand's tertiary amine nitrogen and a solvent molecule occupy the axial positions. The synthesis and solid-state structure of $Ph_4P[Co(NCCH_3)L^{Ph}]$ has previously been described.[103] One of the perfluorophenyl groups in $[Co(DMF)L^{F5}]^-$ is inverted and prevents the formation of a pseudo C_3-symmetric cavity structure in the solid-state. This inversion sterically accommodates the coordinating DMF molecule and affords a hydrogen bonding interaction between the DMF formyl C-H group and the carbonyl oxygen of the inverted ligand arm (Figure 2-11E). With the exception of $Ph_4P[Co(NCCH_3)L^{Ph}]$, the average Co – N1 length increases across this series with a corresponding decrease in the Co – N_{eq} bond length, reflecting the increase in σ-donation from the equatorial nitrogen. This also results in an increase of the distance between the

cobalt ion and the plane formed by the equatorial nitrogen atoms for the fluorinated complexes.

Section 2-2-3. Cyanide Binding

To probe the electronic effects of the aryl substitutents, we attempted to synthesize the cyano derivatives, $[Co(CN)L^{R}]^{2-}$, as previous studies had shown that treating the carboxamide substituent = ^{i}Pr derivative, $[CoL^{iPr}]^{-}$, with Et_4NCN readily formed $[Co(CN)L^{iPr}]^{2-}$ in solution.[101] It was anticipated that the cyanide-binding properties and the Co^{II}/Co^{III} redox potentials of the resulting cyano-complexes would correlate with the electron-withdrawing nature of the ligands' amide substituents (i.e. $[CoL^{iPr}]^{-}$ < $[CoL^{NMe2}]^{-}$ < $[CoL^{OMe}]^{-}$ < $[CoL^{Ph}]^{-}$ < $[CoL^{F2}]^{-}$ < $[CoL^{F3}]^{-}$ < $[CoL^{F5}]^{-}$).

However, treatment of $[CoL^{NMe2}]^{-}$, $[CoL^{OMe}]^{-}$, or $[CoL^{Ph}]^{-}$ with one equivalent of Et_4NCN does not result in formation of an isolable cyanide complex. Conversely, $[CoL^{F2}]^{-}$, $[CoL^{F3}]^{-}$, and $[CoL^{F5}]^{-}$ readily bind cyanide to form $(Et_4N)_2[Co(L^{R})(CN)]$.

Preparation of $Et_4N[CoL^{F2}]$ by a similar procedure to that described for $Ph_4P[Co(NCCH_3)L^{F2}]$, yields flocculent magenta solid. Addition of one equivalent of Et_4NCN to a solution of the complex results in a solution color change from pink to purple. Removal of solvent yields a solid with a stretch at 2121 cm^{-1} in the FT-IR spectrum (KBr pellet), which is consistent with the formation of a cyanide-bound product. The mass spectrum of this product exhibits a parent peak with m/z = 1182.6 in the positive mode (ESI-MS). This is consistent with the formulation $((Et_4N)_3[Co(CN)L^{F2}])^{+}$. The ^{1}H NMR spectrum displays six paramagnetically shifted and broadened peaks, which is indicative of a C_3-symmetric complex in solution. This is

confirmed by the presence of only one signal in the ^{19}F NMR spectrum of this complex. $(Et_4N)_2[Co(CN)L^{F2}]$ exhibits a μ_{eff} = 4.53 μ_B (the method of Evans, CD_3CN, 400 MHz) and is therefore assigned as a high-spin (S = 3/2) Co(II) complex.

Addition of one equivalent of Et_4NCN to a solution of $Et_4N[CoL^{F3}]$ results in darkening of the solution color. Recrystallization by diffusion of diethyl ether into an $NCCH_3$ solution of the product, yields crystalline material in 67% yield. The product exhibits a stretching frequency of 2116 cm^{-1} in its FT-IR spectrum (KBr pellet), indicating the formation of a cyano adduct. This species displays five paramagnetically shifted signals in the ^1H NMR spectrum, which confirms that it maintains C_3 symmetry in solution. The μ_{eff} = 4.15 μ_B (the method of Evans, CD_3CN, 300 MHz) prior to diamagnetic correction and μ_{eff} = 4.53 μ_B with the diamagnetic correction, indicating that the Co(II) ion is high-spin, S=3/2.

$(Et_4N)_2[Co(CN)L^{F5}]$ is synthesized in a similar manner. Recrystallization by diffusion of diethyl ether into a DMF solution affords the product in 62% yield. Unlike $Et_4N[Co(DMF)L^{F5}]$, $(Et_4N)_2[Co(CN)L^{F5}]$ is C_3-symmetric in solution. The ^1H NMR spectrum of this complex (CD_2Cl_2, 300 MHz) displays four paramagnetically broadened signals, and the ^{19}F NMR spectrum (CD_2Cl_2, 400 MHz) displays five distinct signals, corresponding to each fluorine on the aromatic ring, as shown in Figure 2-12B. This indicates that, unlike the aromatic substituents in $Et_4N[Co(DMF)L^{F5}]$, the aromatic substituents in $(Et_4N)_2[Co(CN)L^{F5}]$ are locked in place and do not rotate on the NMR time scale.

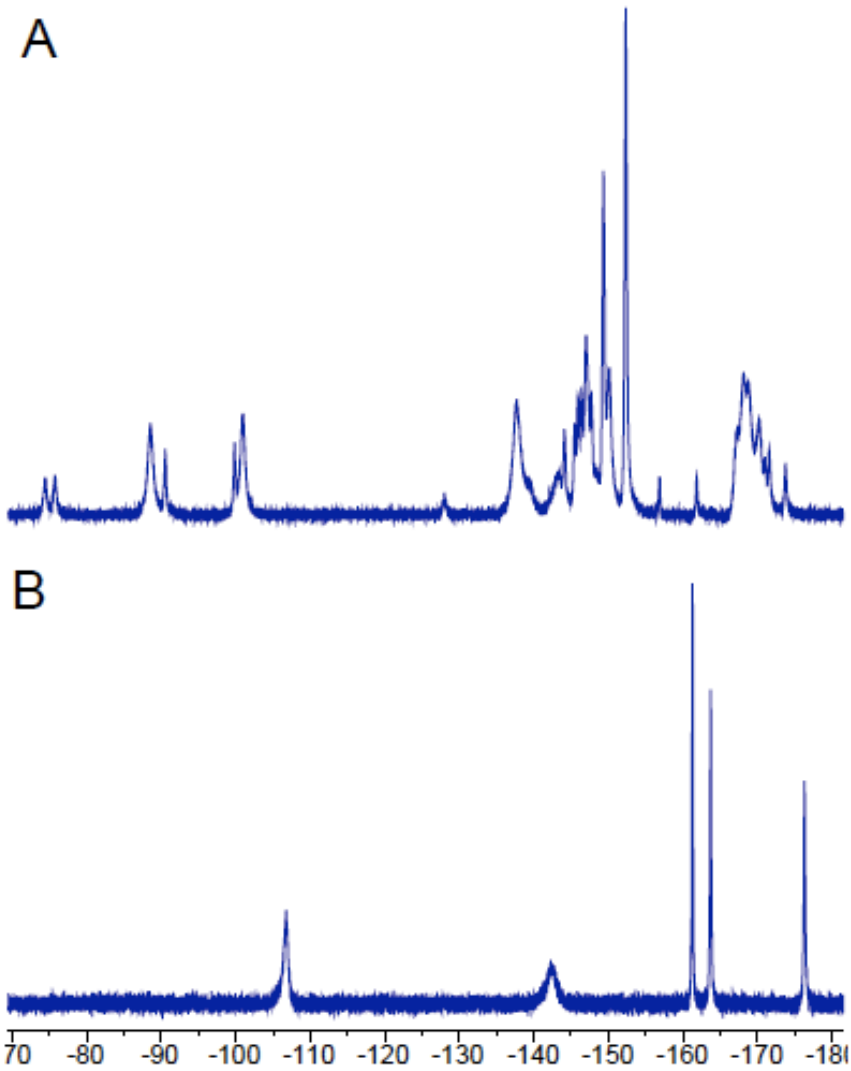

Figure 2-12. ^{19}F NMR spectra (ppm) of (A) $Et_4N[Co(DMF)L^{F5}]$ and (B) $(Et_4N)_2[Co(CN)L^{F5}]$. NMR spectra recorded in CD_2Cl_2 on a 400 MHz instrument.

The C-N stretching frequency for this complex of 2109 cm^{-1} is the lowest energy of the isolable $–CN^-$ complexes described herein, which is related to the fact that the cobalt ion is the most electron-deficient, demanding the most sigma donation from the $–CN^-$ ligand. The μ_{eff} = 4.29 μ_B (the method of Evans, CD_2Cl_2, 300 MHz) without diamagnetic

correction and μ_{eff} = 4.42 μ_B with the diamagnetic correction, indicating that the Co(II) ion is high-spin, S=3/2.

X-ray diffraction studies of $[Co(CN)L^{F3}]^{2-}$ and $[Co(CN)L^{F5}]^{2-}$ (Figure 2-13 and Table 2-3) show that the fluorinated aryl substituents form a compact cavity encapsulating the cyano ligand in the solid state, as shown in the space-filling diagram (Figure 2-14). Inspection of the structure shows close contact distances between the coordinated cyanide and aryl rings that may be indicative of noncovalent interactions. The average distances between the bound, non-fluorinated carbon of the aryl moiety and the carbon of the bound cyanide are 3.197 Å for $[Co(CN)L^{F3}]^{2-}$ and 3.160 Å for $[Co(CN)L^{F5}]^{2-}$. This is shorter than the sum of the van der Waals radii of two carbon atoms. Furthermore, the average aryl-centroid – C(CN) distances are 3.416 Å and 3.380 Å, respectively.[75,76]

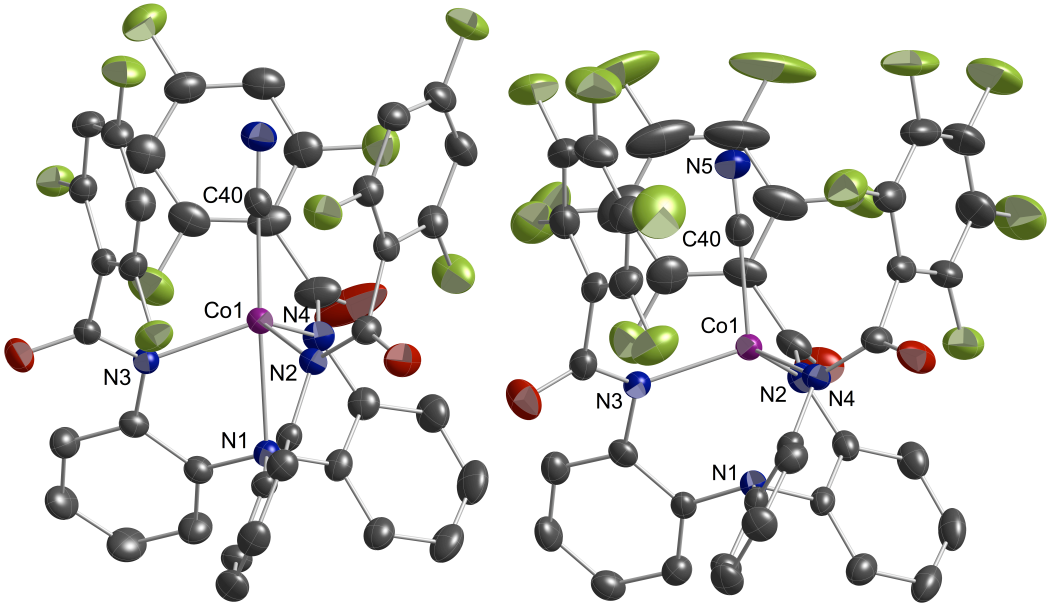

Figure 2-13. Solid-state structure of (left) $(Et_4N)_2[Co(CN)L^{F3}]$ and (right) $(Et_4N)_2[Co(CN)L^{F5}]$. Thermal ellipsoids drawn at 40% probability. Hydrogen atoms and countercations omitted for clarity.

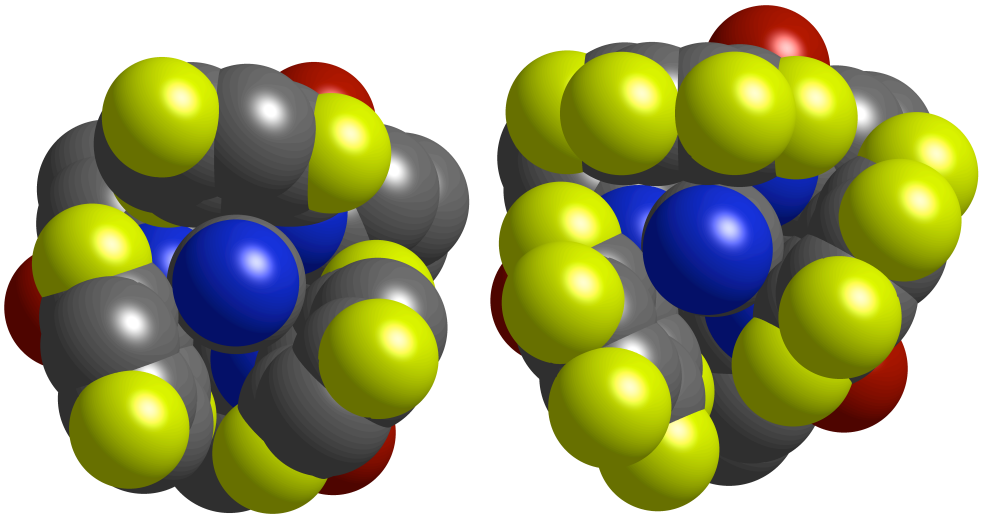

Figure 2-14. Space-filling diagrams of the structures of (left) $(Et_4N)_2[Co(CN)L^{F3}]$ and (right) $(Et_4N)_2[Co(CN)L^{F5}]$. Hydrogen atoms and countercations omitted for clarity.

Table 2-3. Selected bond lengths and angles for $[Co(CN)(L^{F3})]^{2-}$ and $[Co(CN)(L^{F5})]^{2-}$.

Bond Lengths (Å) and Angles (°)		
R =	2,4,6-$C_6H_2F_3$	C_6F_5
Co1 – N1	2.333(3)	2.393(3)
Ave. Co1 – N_{eq}	2.088(2)	2.057(2)
Co1 – C40	2.061(3)	2.049(4)
Co1 – Eq. Plane	0.556	0.572
Ave. N1 – Co1 – N_{eq}	74.59(6)	73.85(7)
Ave. N_{eq} – Co1 – N_{eq}	113.15(6)	112.56(8)
N1 – Co1 – C40	175.97(11)	176.33(14)

$[Co(CN)L^{F3}]^{2-}$ crystallizes in trigonal bipyramidal geometry, with a τ_5 value of 0.99.[106] On the other hand, in $[Co(CN)L^{F5}]^{2-}$ the bound cyanide exhibits a strong *trans* effect, causing the cobalt ion to move further out of the plane formed by the equatorial nitrogen atoms and away from the apical nitrogen. The resulting geometry about Co1 is best described as distorted tetrahedral, with $\tau_4 = 0.94$.[107] The average Co – N_{eq} distance again decreases with increase in the electron-withdrawing nature of the ligand.

The association constants for cyanide coordination to the cobalt complexes have been determined by UV-visible absorption spectroscopy titration experiments with dichloromethane as the solvent (Figure 2-15). The resulting changes in absorption were plotted vs. the added cyanide concentration and fit using non-linear methods.

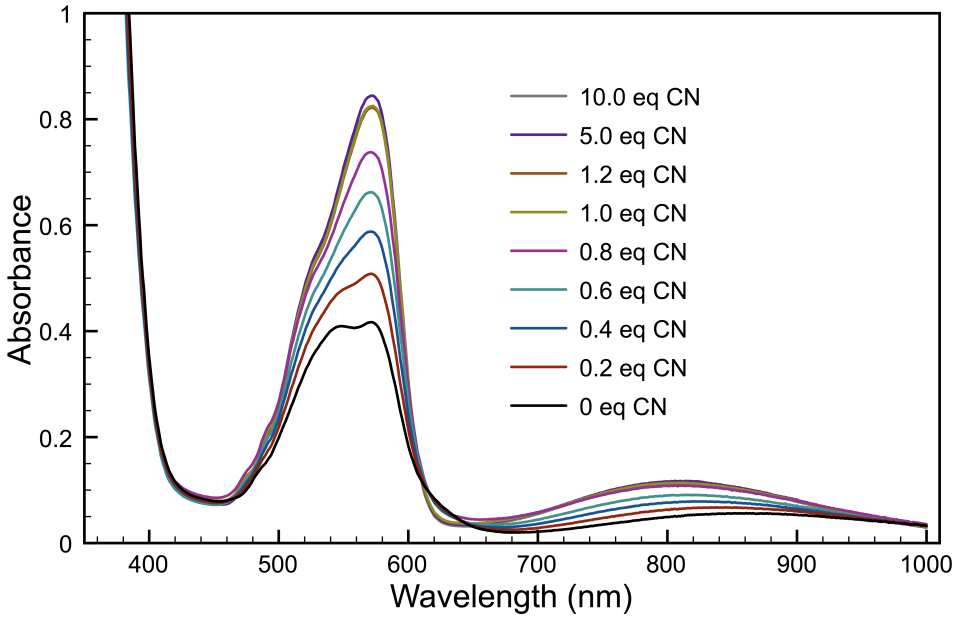

Figure 2-15. Sample UV-visible absorption spectra from cyanide binding experiments showing increasing absorbance upon addition of cyanide. Addition of cyanide to $[Co(DMF)L^{F5}]^{-}$ is shown.

When these titrations were carried out using $Ph_4P[Co(NCCH_3)L^{NMe2}]$ and $Ph_4P[Co(NCCH_3)L^{OMe}]$, the resulting changes in the UV-visible absorption spectra were not consistent with formation of the cyano adducts. Solution-state FT-IR spectra of solutions prepared in the same manner as those used for the titration studies indicated that the transition metal complex was unchanged upon addition of cyanide. The only change in the FT-IR spectra was a shift of the peak at $\nu = 528$ cm^{-1} - the peak that corresponds to the tetraphenylphosphonium cation. Furthermore, the ^1H NMR spectra display two sets of PPh_4 peaks upon addition of one equivalent of Et_4NCN to solutions of the complexes. This suggests that the cyanide ion preferentially interacts with the countercation rather than the cobalt complex. Therefore, the complexes $Et_4N[Co(NCCH_3)L^{NMe2}]$ and $Et_4N[Co(NCCH_3)L^{OMe}]$ were prepared by a similar method as their tetraphenylphosphonium analogs, using tetraethylammonium bromide for salt metathesis. Titration of the tetraethylammonium salt of $[CoL^{OMe}]$ with Et_4NCN resulted in changes in the UV-visible absorption spectra that were consistent with cyanide binding. Titration of $Et_4N[Co(NCCH_3)L^{NMe2}]$ with CN^-, however, yielded very little change in the UV-visible absorption spectrum from 0-1.2 eq. At higher $[CN^-]$, the complex appeared to demetallate, which is indicated by the lack of a charge transfer band in the UV-visible absorption spectrum and formation of a yellow solution. This is consistent with formation of low-spin $[Co^{II}(CN)_5]^{3-}$, which is yellow in non-coordinating solvents.[108-110] However this complex absorbs UV-visible light at wavelengths less than 400 nm in organic solvents. Due to the π-π^* transitions of the $(L^R)^{3-}$, these could not be identified in the spectra. $[CoL^{OMe}]^-$ also appeared to demetallate with the addition of a large excess of CN^- (5 and 10 eq.) but was well behaved from 0-2 eq.

Titration of $[CoL^{F2}]^-$ with $(CN)^-$ yielded similar results. Addition of more than 1 eq. CN^- to the solution containing $[CoL^{F2}]^-$ resulted in a marked decrease in absorbance that was proportional to the excess CN^- added with no shift in the absorption maximum. Demetallation is confirmed by the appearance of diamagnetic signals in the ^1H NMR spectrum (CD_2Cl_2) of the complex, new C-N stretches at 2109 and 2064 cm^{-1} in the FT-IR spectrum (KBr pellet), and free ligand as the parent peak in the mass spectrum (ESI-MS, negative mode) after addition of excess CN^- to a solution of $[CoL^{F2}]^-$. Demetallation of nickel complexes of macrocyclic and open-chain, tetraamine ligands by excess cyanide has previously been described.[111-113]

Insight into why the weak-binding complexes tend to demetallate while the strong-binding complexes stay intact is given by the ^{19}F NMR spectra. $(Et_4N)_2[Co(CN)L^{F2}]$ exhibits one fluorine signal in its ^{19}F NMR spectrum, as shown in Figure 2-16.

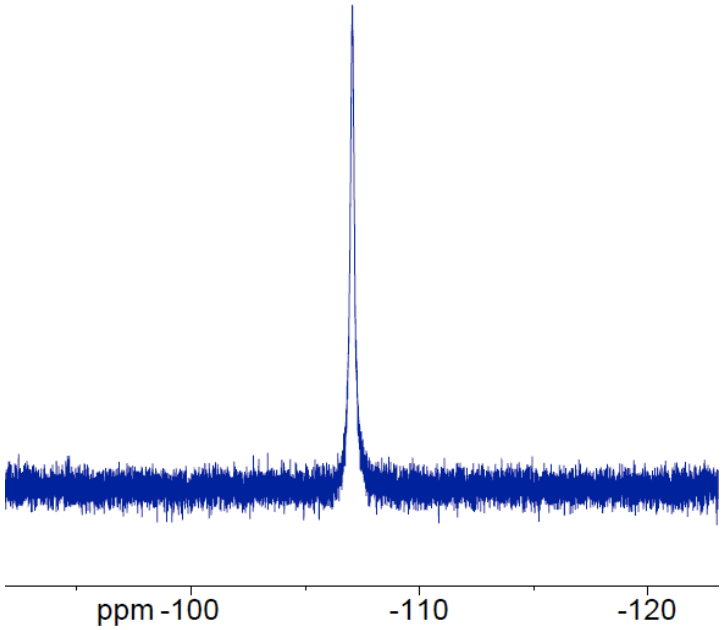

Figure 2-16. ^{19}F NMR spectrum of $(Et_4N)_2[Co(CN)L^{F2}]$ recorded in CD_2Cl_2 on a 400 MHz instrument.

This indicates that the difluorophenyl substituents rotate on the NMR time scale. Conversely, $(Et_4N)_2[Co(CN)L^{F5}]$ has five fluorine signals in its ^{19}F NMR spectrum, which indicates that the perfluorophenyl substituents are "locked" in place and do not rotate on the NMR time scale (refer to Figure 2-12B). Given that the complex' demetallation by cyanide is the result of cyanide association followed by ligand dissociation, this indicates that the interaction between the perfluorophenyl substituent and the bound cyanide prevents this ligand labilization. In the weak-bonding complexes, where this interaction does not appear to occur to as great of an extent, the ligand arms remain labile, allowing for dissociation followed by demetallation at high $[(CN)^-]$.

The weak-binding $[CoL^{OMe}]^-$, $[CoL^{Ph}]^-$, and $[CoL^{F2}]^-$ were fit using a one-site binding hyperbola. However, this did not provide a satisfactory fit for the strong-binding

$[CoL^{F3}]^-$ and $[CoL^{F5}]^-$. The assumption made when fitting most binding curves with a one-site binding hyperbola is that most of the metal complex in solution is not bound to the ligand.[114] This assumption does not hold in strong binding scenarios, as the equilibrium is shifted much more toward product. Therefore, these data were fit using a modification of the parabolic function recently described by Chiang *et al*.[115] Equation 2-3 was used to fit the strong-binding scenarios and is shown below, where CF is a correction factor on the same order of magnitude as the extinction coefficent for the complexes. Examples of the resulting data fitting curves are shown in Figure 2-17.

$$[ML] = \frac{\left([M]_0 + [L]_0 + \frac{1}{K_{eq}}\right) - \left\{\left([M]_0 + [L]_0 + \frac{1}{K_{eq}}\right)^2 - 4[L]_0[M]_0\right\}^{\frac{1}{2}}(CF)}{2}$$

Equation 2-3

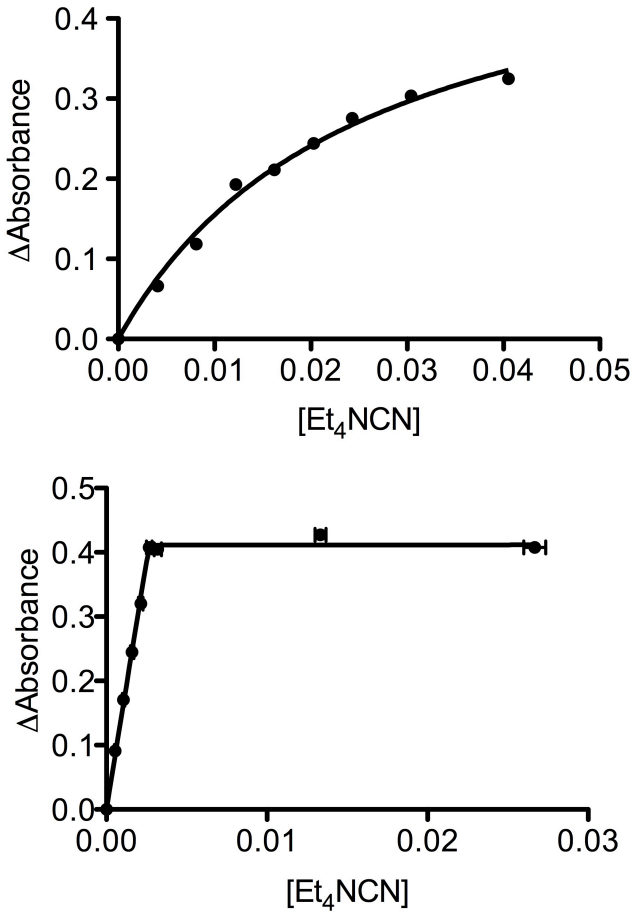

Figure 2-17. Sample data fitting resulting from cyanide binding experiments using (top) a one-site binding hyperbola for weakly binding complexes ($[Co(NCCH_3)L^{OMe}]^-$ shown) and (bottom) a modification of that described by Chiang et al. for strongly binding complexes ($[Co(DMF)L^{F5}]^-$ shown).[115]

The cyanide association constants for $[CoL^{F3}]^-$ and $[CoL^{F5}]^-$ ($1.29 \pm 0.072 \times 10^5\ M^{-1}$ and $1.38 \pm 0.69 \times 10^6\ M^{-1}$, respectively) are considerably higher than those measured for the more electron-releasing species, $[CoL^{OMe}]^-$, $[CoL^{Ph}]^-$, and $[CoL^{F2}]^-$ ($K_a = 40 \pm 6\ M^{-1}$, $197 \pm 10\ M^{-1}$, $1732 \pm 131\ M^{-1}$ and respectively). The 1:1 binding stoichiometry in solution was confirmed using the method of continuous variations, resulting in Job plots like that seen in Figure 2-18.

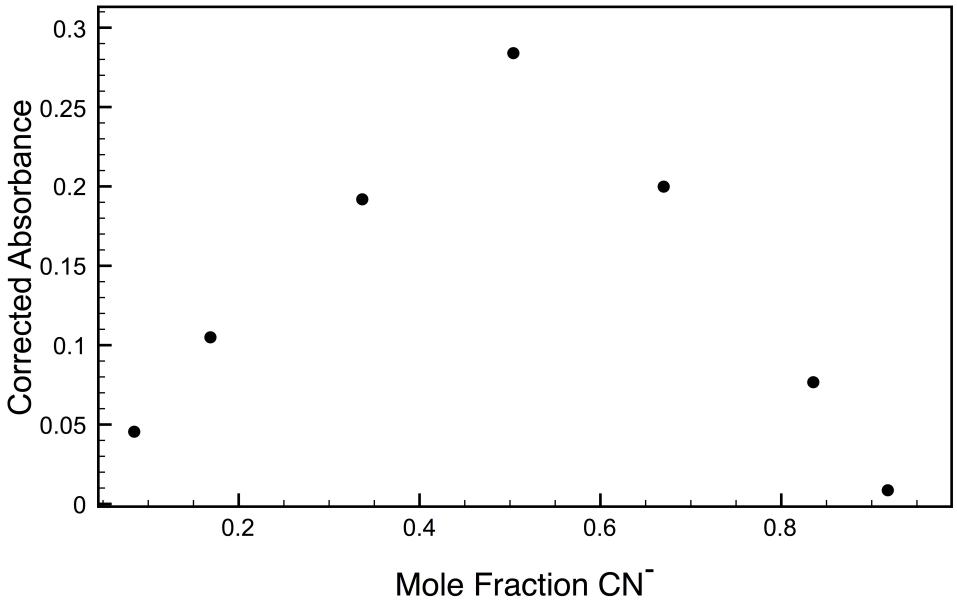

Figure 2-18. Sample Job Plot confirming 1:1 binding of cyanide by $[Co(DMF)L^{F5}]^-$.

These results show that the complexes that incorporate electron-withdrawing aromatic substituents into the ligand framework exhibit cyanide association constants that are up to five orders of magnitude greater than those that incorporate electron-donating substituents into the ligand framework. However, it could be hypothesized that this only occurs due to the change in electronic character at the metal center, with the most electron-poor cobalt ion exhibiting the highest cyanide association constant. The electrochemistry of these species along with the cyanide association properties of the complexes with alkyl substituents, $Ph_4P[Co(NCCH_3)L^{CF3}]$ and $Ph_4P[CoL^{iPr}]$, were therefore investigated.

Section 2-2-4. Electrochemistry and Alkyl-Substituted Complexes

Typically, solvento complexes of this type do not show reversible electrochemical features in their cyclic voltammograms. However, addition of cyanide to form the respective cyano complexes often results in reversible electrochemical events within the solvent window. The cyclic voltammograms (0.2 M $TBAPF_6$ in DMF, corrected vs. Fc/Fc^+, referenced vs. Ag/Ag^+, glassy carbon working electrode) of $[Co(CN)L^{F3}]^{2-}$ and $[Co(CN)L^{F5}]^{2-}$ in DMF display reversible $Co^{II/III}$ couples at -208 mV and +28 mV, respectively. A $Co^{II/III}$ couple could not be detected when $[Co(L^{NMe2})]^-$ or $[Co(L^{OMe})]^-$ was treated with Et_4NCN, which is consistent with their low cyanide association constants.

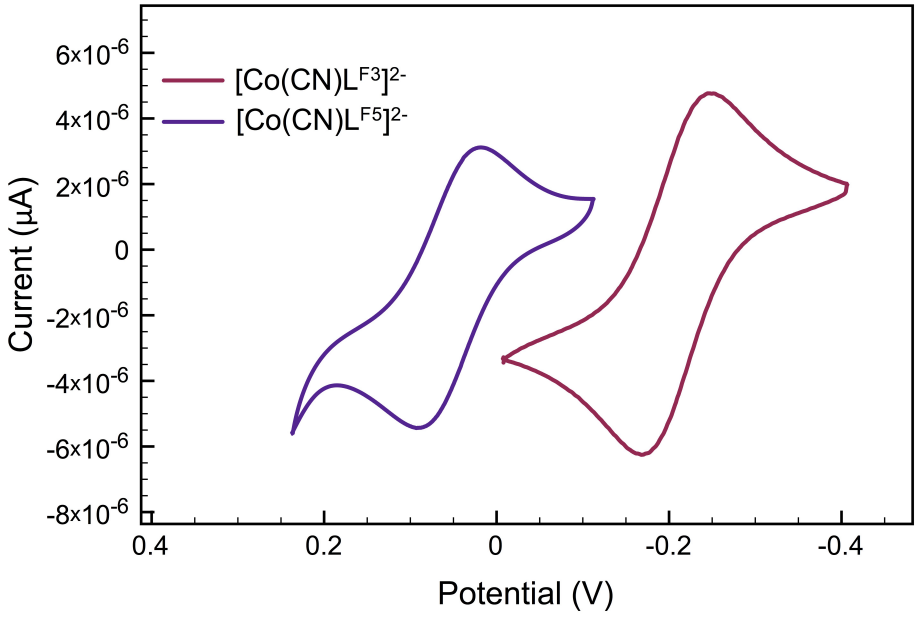

Figure 2-19. Cyclic voltammograms of (left) $(Et_4N)_2[Co(CN)L^{F5}]$ (10 mV/s, $E_{1/2}$ = +28 mV) and (right) $(Et_4N)_2[Co(CN)L^{F3}]$ (50 mV/s, $E_{1/2}$ = -208 mV) with 0.2 M $TBAPF_6$ in DMF as the supporting electrolyte, referenced vs. Fc/Fc^+, Ag/Ag^+ as the reference electrode, using a glassy carbon working electrode, and scans are initially negative.

$Ph_4P[CoL^{iPr}]$ has previously been synthesized, and its cyanide association constant ($600 \pm 36\ M^{-1}$) as well as its isolable and structurally characterized cyano complex have been reported.[101,103] The cyano adduct exhibits an $E_{1/2}$ of -327 mV (0.2 M $TBAPF_6$ in DMF, corrected vs. Fc/Fc^+, referenced vs. Ag/Ag^+, glassy carbon working electrode).

$Ph_4P[Co(NCCH_3)L^{CF3}]$ is synthesized using a modification of the procedure described *vide supra*—via acylation of $N(o\text{-}(PhNH_2)_3)$ with trifluoroacetic anhydride, deprotonation with KH, metallation with $CoBr_2$, and salt metathesis with Ph_4PBr. Lavender needles were obtained in 90% yield by recrystallization from diffusion of diethyl ether into an $NCCH_3$ solution of the product. The solid-state structure of this complex, as determined by X-ray diffraction, is shown in Figure 2-20.

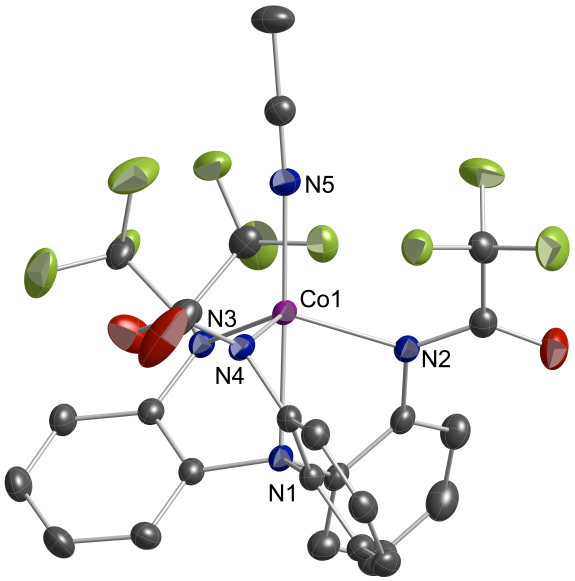

Figure 2-20. Solid-state structure of $Ph_4P[Co(NCCH_3)L^{CF3}]$. Thermal ellipsoids drawn at 40% probability. Hydrogen atoms and countercations omitted for clarity.

Table 2-4. Selected bond lengths and angles for $Ph_4P[Co(NCCH_3)(L^{CF3})]$.

Bond Lengths (Å) and Angles (°)			
Co1 – N1	2.297(2)	N1 – Co1 – Neq (Ave.)	74.79(5)
Co1 – Neq (Ave.)	2.0459(1)	Neq – Co1 – Neq (Ave.)	113.36(5)
Co1 – N5	2.056(2)	N1 – Co1 – N1S	177.85(8)
Co1 – Eq. Plane	0.541		

$Ph_4P[Co(NCCH_3)(L^{CF3})]$ exhibits trigonal bipyramidal geometry in the solid state, with τ_5 = 1.0. The equatorial nitrogen atoms bind the cobalt with an average distance of 2.0459(1) Å. The Co ion binds the apical nitrogen atom at a distance of 2.297(2) Å, which is longer than any of the previously discussed, aryl-substituted complexes. Thus, the cobalt ion also is furthest from the plane formed by the equatorial nitrogen atoms (0.541 Å).

The cyclic voltammogram of the cyano adduct of this complex in DMF displays a reversible oxidation event at +299 mV (0.2 M $TBAPF_6$ in DMF, corrected vs. Fc/Fc^+, referenced vs. Ag/Ag^+, glassy carbon working electrode). This is significantly more positive than any of the previously described oxidation potentials.

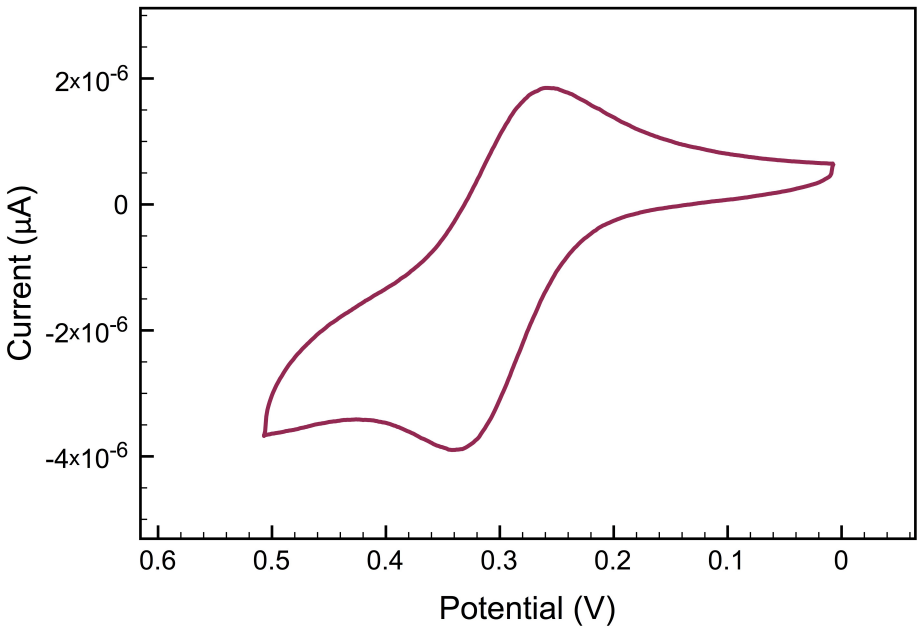

Figure 2-21. Cyclic voltammogram of $(Et_4N)_2[Co(CN)L^{CF3}]$ (50 mV/s, $E_{1/2}$ = +299 mV) with 0.2 M $TBAPF_6$ in DMF as the supporting electrolyte, referenced vs. Fc/Fc^+, using Ag/Ag^+ as the reference electrode and a glassy carbon working electrode. The scan direction is negative.

Addition of one equivalent of Et_4NCN to the Et_4N^+ salt of the complex results in a magenta product that exhibits a C-N stretching frequency of 2110 cm^{-1} in its FT-IR spectrum (KBr pellet) in 85% yield. The solid-state structure of the product, $(Et_4N)_2[Co(CN)L^{CF3}]$, as determined by X-ray diffraction, is shown in Figure 2-22.

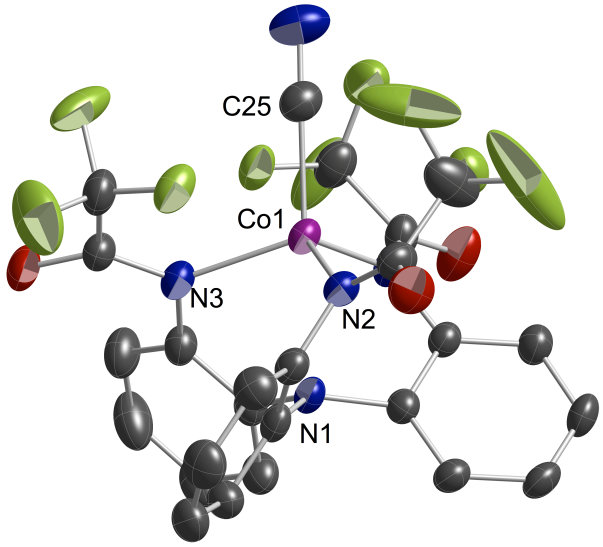

Figure 2-22. Solid-state structure of $(Et_4N)_2[Co(CN)L^{CF3}]$. Thermal ellipsoids drawn at 40% probability. Hydrogen atoms and countercations omitted for clarity.

Table 2-5. Selected bond lengths and angles for $[Co(L^{CF3})(CN)]^{2-}$.

Bond Lengths (Å) and Angles (°)			
Co1 ••• N1	2.409(4)	N1 ••• Co1 – N_{eq} (Ave.)	71.99(8)
Co1 – N_{eq} (Ave.)	2.082(2)	N_{eq} – Co1 – N_{eq} (Ave.)	110.86(9)
Co1 – C25	2.040(6)	N1 ••• Co1 – C25	174.58(17)
Co1 – Eq. Plane	0.644		

$[Co(CN)L^{CF3}]^{2-}$ exhibits distorted tetrahedral geometry in the solid state (τ_4 = 0.94), and the average angle made by the equatorial nitrogen atoms and the cobalt ion is close to 109.5°. The equatorial nitrogen atoms bind the cobalt with an average distance of 2.082(2) Å, which is similar to the corresponding distances in $[Co(CN)L^{F3}]^{2-}$ and $[Co(CN)L^{F5}]^{2-}$. The Co1 – C_{CN} bond is slightly shorter than that in $[Co(CN)L^{F3}]^{2-}$ and $[Co(CN)L^{F5}]^{2-}$, which is likely a result of the lack of sigma donation from the apical nitrogen atom of the ligand. The cobalt ion interacts with the apical nitrogen atom at a

distance of 2.409(4) Å and sits 0.644 Å above the plane formed by the equatorial nitrogen atoms.

Due to its significantly more positive oxidation potential, a reasonable hypothesis would be that $Ph_4P[Co(NCCH_3)L^{CF3}]$ would exhibit a significantly higher cyanide association constant. Titration of this complex with a solution of Et_4NCN, as indicated by UV-visible absorption spectroscopy, results in a cyanide association constant of 3.09 x 10^5 (5.60 x 10^3) M^{-1}, which is one order of magnitude less than that displayed by the perfluorophenyl-substituted complex.

These results indicate that the relatively high K_a values measured for cyanide binding to $[Co(L^{F3})]^-$ and $[Co(L^{F5})]^-$ are due to the fluorinated aryl substituents giving rise to an electron-poor cobalt center and interacting electrostatically with the electron-rich pi-bond of the coordinated cyanide ligand. Additionally, the low cyanide association constants found for $Ph_4P[Co(NCCH_3)L^{NMe2}]$, $Ph_4P[Co(NCCH_3)L^{OMe}]$, and $Ph_4P[Co(NCCH_3)L^{Ph}]$ as compared to the higher cyanide association constant exhibited by the more electron-rich $Ph_4P[CoL^{iPr}]$ suggest that the electron-rich aryl groups are suppressing cyanide binding. Specifically, repulsive interactions between the electron-rich aromatic rings positioned near the vacant coordination site and the incoming anionic cyanide ligand may deter cyanide binding.

Section 2-3. Conclusion

In conclusion, we have used a series of coordinatively unsaturated cobalt complexes to demonstrate that, when incorporated into tripodal ligands as substituents, aromatic rings may give rise to secondary electrostatic interactions. Specifically, it

appears the electron deficient aromatic system in $[Co(L^{F3})]^-$ and $[Co(L^{F5})]^-$ stabilizes cyanide binding to these complexes by forming an electropositive cavity around the coordinated cyanide ligand. In contrast, the electron-rich substituents in $Ph_4P[Co(NCCH_3)L^{NMe2}]$, $Ph_4P[Co(NCCH_3)L^{OMe}]$, $Ph_4P[Co(NCCH_3)L^{Ph}]$ and $Ph_4P[Co(NCCH_3)L^{F2}]$ appear to discourage cyanide binding at the cobalt center. The results of these studies are summarized in Table 2-6.

Table 2-6: Summary of quadrupole moments of the unsubstituted fragments (taken from Refs. 81 and 103), oxidation potentials, and cyanide association constants for the cobalt complexes described herein. Data for $Ph_4P[CoL^{iPr}]$ and $Ph_4P[Co(NCCH_3)L^{Ph}]$ taken from Refs. 102 and 104.

R	**iPr**	***p*-NMe$_2$Ph**	***p*-OMePh**	**Ph**	**3,5-C$_6$H$_3$F$_2$**	**2,4,6-C$_6$H$_2$F$_3$**	**C$_6$F$_5$**	**CF$_3$**
Q_{zz} (DÅ)	-	-10.97	-9.68	-9.19	-2.92	+1.01	+10.70	-
$E_{1/2}$ (mV)	-327	-	-	-	-	-208	+28	+299
K_a (M^{-1})	600	-	40 ± 6	197 ± 10	1732 ± 131	1.29 ± 0.072 x 10^5	1.38 ± 0.69 x 10^6	3.09 ± 0.056 x 10^5

Aromatic rings are often incorporated into ligand platforms as a means of sterically protecting metal ions and stabilizing reactive species.[116-118] The studies presented here suggest steric, electronic, and possible secondary electrostatic interactions should be considered when incorporating aromatic rings into ligand frameworks.[119]

Section 2-4. Experimental Section

General Considerations and Materials

All manipulations were carried out using standard Schlenk techniques or conducted in an MBraun Labmaster 130 drybox under a nitrogen atmosphere. All reagents used were purchased from commercial vendors and used as received unless otherwise noted. Anhydrous solvents were purchased from Sigma-Aldrich and further purified by sparging with Ar gas followed by passage through activated alumina columns. Deuterated NMR solvents were purchased from Cambridge Isotopes and degassed and dried according to standard procedures[120] prior to use. Elemental analyses were performed either by Columbia Analytical Services, Tucson, AZ, Midwest Microlab, Indianapolis, IN, or Atlantic Microlab, Inc, Norcross, GA. ^{1}H and ^{13}C NMR spectra were recorded on Varian Mercury 300 MHz or Inova 400 MHz spectrometers at ambient temperature. Chemical shifts were referenced to residual solvent peaks. ^{19}F NMR recorded on an Inova 400 MHz spectrometer at ambient temperature and referenced versus trifluorotoluene (-63.73 ppm). Infrared spectra were recorded as KBr pellets on a Varian Scimitar 800 Series FT-IR spectrometer. UV-Visible absorption spectra were recorded on a Varian Cary 50 spectrophotometer using 1.0 cm quartz cuvettes. Solution state magnetic moments were measured using the the method of Evans.[121,122] Diamagnetic corrections were made as described by Berry et al.[104] Mass spectra were recorded in the Mass Spectrometry Center at Emory University on a JEOL JMS-SX102/SX102A/E mass spectrometer. X-ray diffraction studies were carried out in the X-ray Crystallography Laboratory at Emory University on a Bruker Smart 1000 CCD diffractometer. Cyclic voltammetric experiments were carried out using a CH Instruments (Austin, TX) Model 660C

potentiostat. All experiments were conducted in anhydrous solvents with 0.10 M tetrabutylammonium hexafluorophosphate ($TBAPF_6$) as the supporting electrolyte. Electrochemical experiments were conducted under a nitrogen atmosphere in a three-component cell consisting of a Pt wire auxiliary electrode, a non-aqueous reference electrode ($Ag/AgNO_3$), and a platinum working electrode (3 mm). All electrochemical measurements are referenced and reported versus the ferrocene/ferrocenium couple.[123] Tris(2-aminophenyl)amine, $N(o\text{-}PhNH_2)_3$, was prepared according to a literature method.[5]

Ligand Syntheses

H_3L^{NMe2}. A suspension of $N(o\text{-}PhNH_2)_3$ (1.14 g, 3.93 mmol) in dichloromethane (110 mL) was cooled to 0 °C under an atmosphere of N_2. Triethylamine (2.0 mL, 14.0 mmol) was added and stirred for 15 min. To this mixture, 4-(dimethylamino)benzoyl chloride (2.37 g, 12.9 mmol) was added and stirred for 20 minutes at 0 °C. The reaction mixture was warmed to room temperature and stirred overnight. The resulting tan solution was washed three times with saturated sodium bicarbonate solution (50 mL) then two times with water (75 mL). The organic layer was dried over magnesium sulfate, filtered, and then concentrated in vacuo, yielding a tan oil. The oil was triturated once with 200 mL boiling hexanes. The resulting white solid was collected by filtration and recrystallized from hot methanol to yield 1.66 g (58%) off-white solid. ^{1}H NMR (δ, $CDCl_3$, 300 MHz): 8.61 (bs, 3H, NH), 7.70 (dd, 3H, J = 5.2 Hz, J = 2.4 Hz, ArH), 7.44 (d, 6H, J = 9.0 Hz, ArH), 6.97 (m, 9H ArH), 6.47 (d, 6H, J = 8.7 Hz, ArH), 2.96 (s, 18H, MeH). $^{13}C[^1H]$ NMR (δ, $CDCl_3$, 400 MHz): 165.51, 152.01, 138.05, 131.92, 129.02, 125.77, 124.93, 124.53, 120.98, 110.87, 40.28, 40.26. HRMS(ESI-MS): $C_{42}H_{31}N_7O_3$ m/z $[M+1]^+$ Calcd.

732.36174. Found 732.36567. FTIR (KBr, cm^{-1}): ν(CO) 1661, ν(NH) 3386, 3280; 3061, 2894, 2804, 1608, 1511, 1441, 1366, 1302, 1266, 1200, 1170, 1135, 1063, 946, 830, 761, 693, 578, 474.

H_3L^{OMe}. A suspension of N(*o*-$PhNH_2$)$_3$ (3.0 g, 10.3 mmol) in dichloromethane (100 mL) was cooled to 0 °C under an atmosphere of N_2. Triethylamine (5.2 mL, 36.9 mmol) was added to the mixture and stirred for 30 min. 4-methoxybenzoyl chloride (5.0 mL, 36.9 mmol) was added dropwise and stirred for 15 minutes at 0 °C. The reaction mixture was warmed to room temperature and stirred for an additional 3 hrs. The resulting orange solution was washed three times with 0.1 M HCl solution (50 mL) then three times with water (50 mL). The organic layer was dried over magnesium sulfate then concentrated in vacuo, yielding a sage-colored oil. The oil was triturated once with 350 mL boiling hexanes. The resulting white solid was collected by filtration (5.59 g, 78.7%). ^{1}H NMR (δ, $CDCl_3$, 300 MHz): 8.75 (bs, 3H, NH), 7.58 (T, 3H, *J* = 5.4 Hz, ArH), 7.41 (d, 6H, *J* = 8.7 Hz, ArH), 6.93 (m, 9H ArH), 6.71 (d, 6H, *J* = 9.0 Hz, ArH), 3.78 (s, 9H, MeH). ^{13}C[^{1}H] NMR (δ, $CDCl_3$, 400 MHz): 165.24, 162.34, 138.18, 131.53, 129.32, 126.37, 126.19, 125.94, 124.85, 124.46, 113.36, 55.46. HRMS(ESI-MS): $C_{42}H_{37}N_4O_6$ *m/z* $[M+1]^+$ Calcd. 693.26684. Found 693.27177. FTIR (KBr, cm^{-1}): ν(CO) 1664, ν(NH) 3249; 3111, 3069, 3006, 2957, 2934, 2838, 1638, 1607, 1531, 1508, 1439, 1302, 1252, 1177, 1114, 1028, 844, 759, 678, 625, 583.

H_3L^{F2}. A suspension of N(*o*-$PhNH_2$)$_3$ (1.00 g, 3.45 mmol) in dichloromethane (50 mL) was cooled to 0 °C under an atmosphere of N_2. Triethylamine (1.7 mL, 12.4 mmol) was

added and stirred for 10 min. To the suspension was added 3,5-difluorobenzoyl chloride (1.3 mL, 11.4 mmol), dropwise. The reaction mixture was warmed to room temperature and stirred for 2 hrs. The resulting yellow solution was washed three times with 0.1 M HCl solution (50 mL) then three times with water (50 mL). The organic layer was dried over magnesium sulfate, filtered, and then concentrated in vacuo, yielding a yellow oil. The oil was triturated once with 400 mL boiling hexanes. The resulting pale yellow solid was collected by filtration (1.80 g, 73%). ^{1}H NMR (δ, $CDCl_3$, 400 MHz): 8.57 (bs, 3H, NH), 7.64 (bs, 3H, ArH), 7.12 (bs, 6H), 6.95 (dd, 3H, *J* = 5.2 Hz, *J* = 2.4 Hz, ArH), 6.87 (m, 9H ArH). ^{13}C[^{1}H] NMR (δ, $CDCl_3$, 400 MHz): 164.03 (d, *J* = 47.2 Hz), 163.52 (s), 161.54 (d, *J* = 48.4 Hz), 137.89, 137.21 (t, *J* = 38.0 Hz), 130.76 (s), 127.25 (s), 125.83 (d, *J* = 57.6 Hz), 125.67 (s), 110.54 (dd, *J* = 75.6 Hz, *J* = 30.4 Hz), 107.40 (t, *J* = 100.0 Hz). ^{13}C[^{19}F] NMR (δ, $CDCl_3$, 400 MHz): 163.54 (s), 162.78 (t, *J* = 20.8 Hz), 137.88 (s), 137.21 (s), 130.71 (m), 128.03 (m), 126.61 (m), 125.01 (m), 123.91 (m), 111.33 (d, *J* = 18.4 Hz), 109.72 (m), 108.23 (m), 106.57 (m). ^{19}F NMR (δ, $CDCl_3$, 400 MHz): -108.72 (s). HRMS(ESI-MS): $C_{39}H_{25}F_6N_4O_3$ *m/z* $[M+1]^+$ Calcd. 711.17861. Found 711.18254. FTIR (KBr, cm^{-1}): ν(CO) 1684, ν(NH) 3338, 3254; 1648, 1597, 1535, 1492, 1447, 1329, 1265, 1125, 990, 887, 855, 761, 667, 627, 554, 510, 474.

H_3L^{F3}. A suspension of N(*o*-$PhNH_2$)$_3$ (1.6 g, 5.39 mmol) in dichloromethane (50 mL) was cooled to 0 °C under an atmosphere of N_2. Triethylamine (2.5 mL, 17.8 mmol) was added and stirred for 20 min. 2,4,6-trifluorobenzoyl chloride (2.3 mL, 17.8 mmol) was added dropwise and stirred for 45 minutes at 0 °C. The reaction mixture was slowly warmed to room temperature and stirred for an additional 23 hrs. The resulting orange

solution was washed three times with saturated sodium bicarbonate solution (30 mL) then three times with water (30 mL). The organic layer was dried over magnesium sulfate then concentrated in vacuo, yielding a dark brown oil. The oil was triturated once with 200 mL boiling hexanes. The resulting off-white solid was collected by filtration (3.28 g, 79.6%). ^{1}H NMR (δ, $CDCl_3$, 400 MHz): 8.62 (bs, 3H, NH), 7.80 (d, 3H, J = 7.6 Hz, ArH), 7.15 (dt, 6H, J = 19.6 Hz, J = 7.2 Hz, ArH), 6.85 (dd, 3H, J = 8.0 Hz, J = 1.6 Hz, ArH), 6.55 (t, 3H, J = 8.0 Hz, ArH). ^{13}C[^{1}H] NMR (δ, $CDCl_3$, 400 MHz): 163.65 (m), 160.59 (m), 157.78 (s), 138.40 (s), 131.31 (s), 126.80 (s), 125.74 (s), 125.05 (s), 124.41 (s), 110.34 (m), 100.65 (m). ^{13}C[^{19}F] NMR (δ, $CDCl_3$, 400 MHz): 163.47 (t, $^{2}J_{CH}$ = 6.03 Hz), 160.36 (t, $^{2}J_{CH}$ = 3.02 Hz), 157.74 (s), 138.29 (s), 131.35 (t, $^{2}J_{CH}$ = 6.), 126.85 (dd, $^{1}J_{CH}$ = 109.6 Hz, $^{2}J_{CH}$ = 9.1 Hz), 125.75 (br), 124.20 (br d, $^{1}J_{CH}$ = 161.9 Hz), 124.43 (dd, $^{1}J_{CH}$ = 53.3 Hz, $^{2}J_{CH}$ = 7.0 Hz), 110.34 (t, $^{2}J_{CH}$ = 4.0 Hz), 100.42 (dd, $^{1}J_{CH}$ = 168.9 Hz, $^{2}J_{CH}$ = 3.0 Hz). ^{19}F NMR (δ, $CDCl_3$, 400 MHz): -104.08 (t, 3F, J = 8.4 Hz, $C_6H_2F_3$), -108.86 (s, 6F, $C_6H_2F_3$). HRMS(ASAP-MS): $C_{39}H_{22}F_9N_4O_3$ m/z $[M+1]^+$ Calcd. 765.15427. Found 765.15352. FTIR (KBr, cm^{-1}): ν(CO) 1691, ν(NH) 3237, 3120, 1655, 1641, 1605, 1527, 1494, 1449, 1317, 1262, 1129, 1043, 1000, 843, 758.

H_3L^{F5}. A suspension of N(*o*-$PhNH_2$)$_3$ (1.5 g, 5.17 mmol) in dichloromethane (50 mL) was cooled to 0 °C under an atmosphere of N_2. Triethylamine (2.2 mL, 16.0 mmol) was added and stirred for 20 min. Perfluorobenzoyl chloride (2.2 mL, 16.0 mmol) was added dropwise and stirred for 45 minutes at 0 °C. The reaction mixture was slowly warmed to room temperature and stirred for an additional 16 hrs. The resulting brown solution was washed two times with HCl solution (1M, 25 mL) then two times with water (25 mL).

The organic layer was dried over magnesium sulfate then concentrated in vacuo, yielding a dark brown oil. The oil was triturated once with 100 mL boiling hexanes. The resulting off-white solid was collected by filtration (3.407 g, 75.5%). ^{1}H NMR (δ, $CDCl_3$, 400 MHz): 8.46 (bs, 3H, NH), 7.81 (dd, 3H, *J* = 7.6 Hz, *J* = 1.6 Hz, ArH), 7.25 (td, 3H, *J* = 7.6 Hz, *J* = 1.2 Hz, ArH), 7.20 (td, 3H, *J* = 15.2 Hz, *J* = 7.6 Hz, *J* = 1.6 Hz, ArH), 6.89 (dd, 3H, *J* = 8.0 Hz, *J* = 1.6 Hz, ArH). ^{13}C NMR (δ, $CDCl_3$, 400 MHz): 155.68 (s), 145.58 (m), 144.18 (m), 143.05 (m), 141.65 (m), 138.94 (m), 138.22 (s), 136.42 (m), 130.46 (s), 127.70 (s), 126.40 (s), 125.16 (s), 124.68 (s), 110.52 (m). ^{13}C[^{19}F] NMR (δ, CDCl3, 400 MHz): 155.79 (s), 144.11 (s), 142.67 (s), 138.24 (br), 137.56 (s), 130.51 (br), 128.41 (d, *J* = 9.0 Hz), 126.85 (t, *J* = 8.0 Hz), 125.98 (br), 125.28 (d, *J* = 7.0 Hz), 124.41 (br), 123.64 (br), 110.62 (s). ^{19}F NMR (δ, $CDCl_3$, 400 MHz): -141.68 (d, 6F, *J* = 16.17 Hz, C_6F_5), -150.07 (t, 6F, *J* = 20.68 Hz, C_6F_5), -160.91 (t, 3F, *J* = 17.48 Hz, C_6F_5). HRMS(ESI): $C_{39}H_{16}F_{15}N_4O_3$ *m/z* $[M+1]^+$ Calcd. 873.09774 Found 873.09772. FTIR (KBr, cm^{-1}): ν(CO) 1702, ν(NH) 3237, 3060, 1655, 1599, 1519, 1501, 1451, 1420, 1330, 1300, 1264, 1205, 1119, 1092, 995, 961, 784, 758.

H_3L^{CF3}. This ligand was prepared using a modified published method.[124] A suspension of N(*o*-$PhNH_2$)$_3$ (3.2 g, 10.9 mmol) in dichloromethane (50 mL) was cooled to 0 °C under an atmosphere of N_2. To the mixture, triethylamine (5.5 mL, 39.3 mmol) was added. Trifluoroacetic anhydride (5.0 mL, 36.0 mmol) was then added dropwise to the mixture and stirred for 15 minutes at 0 °C. The reaction mixture was slowly warmed to room temperature and stirred for an additional 1.5 hrs. The product was washed three times with saturated $NaHCO_3$ solution (60 mL) and then three times with water (60 mL).

The organic layer was dried over magnesium sulfate, filtered, then concentrated in vacuo, yielding a tan oil. The oil was triturated once with 200 mL boiling hexanes. The resulting off-white solid was collected by filtration (4.84 g, 76.8%). ^{1}H NMR (δ, $CDCl_3$, 300 MHz): 8.59 (bs, 3H, NH), 7.69 (d, 3H, *J* = 6.6, ArH), 7.23 (m, 6H, ArH), 6.88 (d, 3H, *J* = 7.2, ArH). ^{13}C[^{1}H] NMR (δ, CDCl3, 400 MHz): 155.18 (d, *J* = 38.4 Hz), 138.29 (s), 128.78 (s), 127.97 (s), 126.50 (s), 126.23 (s), 124.56 (s), 115.61 (q, *J* = 289.9 Hz). ^{19}F NMR (δ, $CDCl_3$, 400 MHz): -76.34 (s). ESI-MS: $C_{24}H_{16}F_9N_4O_3$ *m/z* $[M+1]^+$ Calcd. 579.1 Found 579.1 . FTIR (KBr, cm^{-1}): ν(CO) 1733, 1706; ν(NH) 3249, 3134; 1661, 1599, 1542, 1487, 1287, 1159, 907, 758, 625.

Syntheses of Cobalt Complexes

$Ph_4P[Co^{II}(NCCH_3)L^{NMe2}]$. To a solution of H_3L^{NMe2} (309.7 mg, 0.423 mmol) in dimethylformamide (DMF, 10 mL) was added potassium hydride (52.7 mg, 1.314 mmol) as a solid. After stirring 2 hours, hydrogen evolution had ceased, yielding a yellow solution that contained colorless solid. $CoBr_2$ (92.4 mg, 0.422 mmol) was added to this mixture as a solid. After stirring for 1 hour, Ph_4PBr (177.8 mg, 0.424 mmol) was added as a solid to the purple solution. After stirring overnight, DMF was removed in vacuo. The resulting solid was extracted with acetonitrile (10 mL), yielding a red solution and colorless solid (KBr). The mixture was filtered to remove solid KBr. The solvent was removed from the filtrate, and the resulting crude product was recrystallized by slow diffusion of diethyl ether into a 2:1 DMF:acetonitrile solution to yield magenta blocks (294.4 mg, 59.6%). ^{1}H NMR (δ, CD_3CN, 400 MHz): 17.23, 15.89, 7.95 (s, Ph_4P), 7.77(s, Ph_4P), 3.31, 2.58, -1.5. FTIR (KBr, cm^{-1}): ν(CO) 1608; 3056, 2928, 1656, 1518,

1480, 1439, 1389, 1351, 1259, 1193, 1107, 997, 828, 756, 724, 691, 660, 528, 492. UV-vis ($NCCH_3$) λ_{max}, nm (ε, $M^{-1}\,cm^{-1}$): 532 (156), 745 (25). μ_{eff} = 4.24 μ_B (the method of Evans, CD_3CN, 400 MHz).

$Ph_4P[Co^{II}L^{NMe2}]$. To a solution of H_3L^{NMe2} (253.8 mg, 0.347 mmol) in dimethylformamide (DMF, 10 mL) was added potassium hydride (43.2 mg, 1.077 mmol) as a solid. After stirring 1.5 hours, hydrogen evolution had ceased, yielding a yellow solution. $CoBr_2$ (76.8 mg, 0.351 mmol) was added to this mixture as a solid. After stirring for 1.25 hours, Ph_4PBr (146.0 mg, 0.348 mmol) was added as a solid to the purple solution. After stirring overnight, DMF was removed in vacuo. The resulting solid was extracted with acetonitrile (10 mL), yielding a red solution and colorless solid (KBr). The mixture was filtered to remove KBr. The solvent was removed from the filtrate, and the resulting crude product was recrystallized by slow diffusion of diethyl ether into a 2:1 DMF:acetonitrile solution to yield green needles (358.8 mg, 91.8%). ^1H NMR (δ, CD_2Cl_2, 300 MHz): 24.48, 11.30, 8.69 (m, Ph_4P), 7.92, 2.27, 0.04, -1.63, -20.21. FTIR (KBr, cm^{-1}): ν(CO) 1608; 3055, 2924, 2856, 1669, 1577, 1542, 1522, 1474, 1439, 1344, 1186, 1108, 1063, 1043, 996, 941, 827, 773, 754, 723, 689, 623, 526, 473. UV-vis (DCM) λ_{max}, nm (ε, $M^{-1}\,cm^{-1}$): 589 (75). μ_{eff} = 4.33 μ_B (the method of Evans, CD_2Cl_2, 400 MHz).

$Et_4N[Co^{II}(NCCH_3)L^{NMe2}]$. To a solution of H_3L^{NMe2} (205.3 mg, 0.281 mmol) in dimethylformamide (DMF, 10 mL) was added potassium hydride (34.9 mg, 0.870 mmol) as a solid. After stirring 30 mins, hydrogen evolution had ceased, yielding a yellow solution. $CoBr_2$ (62.0 mg, 0.283 mmol) was added to this mixture as a solid. After

stirring for 10 minutes, Et_4NBr (59.5 mg, 0.283 mmol) was added as a solid to the purple solution. DMF was removed in vacuo. The resulting pink solid was extracted with acetonitrile (10 mL). The mixture was filtered to remove KBr. The solvent was removed from the filtrate, and the resulting crude product was recrystallized by slow diffusion of diethyl ether into a 1:1 DMF:acetonitrile solution to yield magenta blocks (128.1 mg, 47.6%). ^{1}H NMR (δ, CD_3CN, 400 MHz): 40.86, 17.26, 15.89, 3.25, 2.55, 1.27, -1.08. FTIR (KBr, cm^{-1}): ν(CO) 1607; 3051, 2984, 2797, 2254, 1656, 1576, 1519, 1474, 1342, 1244, 1187, 1128, 1040, 1003, 945, 822, 776, 623, 584, 499. UV-vis (DCM) λ_{max}, nm (ε, M^{-1} cm^{-1}): 584 (72). μ_{eff} = 4.79 μ_B (the method of Evans, CD_3CN, 400 MHz). Anal. Calcd (found) for $Et_4N[Co^{II}(NCCH_3)L^{NMe2}]$: C, 68.88 (68.68); H, 6.84 (6.83); N, 13.14 (12.96).

$Ph_4P[Co^{II}(NCCH_3)L^{OMe}]$. To a solution of H_3L^{OMe} (295.9 mg, 0.427 mmol) in dimethylformamide (DMF, 5 mL) was added potassium hydride (53.4 mg, 1.324 mmol) as a solid. After stirring 4 hrs, hydrogen evolution had ceased, yielding a yellow solution. $CoBr_2$ (93.4 mg, 0.427 mmol) was added to this mixture as a solid. After stirring for 1.5 hours, Ph_4PBr (179.1 mg, 0.427 mmol) was added as a solid to the purple solution. After stirring for an additional hour, DMF was removed in vacuo. The resulting purple solid was extracted with a mixture of acetonitrile (5 mL) and dichloromethane (5 mL), yielding a purple solution and a colorless precipitate (KBr). The mixture was filtered to remove KBr. Solvent was removed from the filtrate, and the resulting crude product was recrystallized by slow diffusion of diethyl ether into a 3:1 DMF:acetonitrile solution to yield pink blocks (239.4 mg, 49.6%). ^{1}H NMR (δ, CD_2Cl_2,

300 MHz): 19.00, 12.86, 12.67, 8.07 (m), 2.45, 1.99. FTIR (KBr, cm^{-1}): ν(CO) 1605; 3057, 2932, 1655, 1596, 1474, 1440, 1348, 1246, 1169, 1108, 1028, 997, 845, 775, 753, 724, 690, 528. UV-vis (DCM) λ_{max}, nm (ε, M^{-1} cm^{-1}): 575 (54), 813 (11). μ_{eff} = 4.40 μ_B (the method of Evans, CD_2Cl_2, 300 MHz). Anal. Calcd (found) for $Ph_4P[Co^{II}(NCCH_3)L^{OMe}]$: C, 72.33 (72.09); H, 5.00 (5.26); N, 6.20 (6.35).

$Et_4N[Co^{II}(NCCH_3)L^{OMe}]$. To a solution of H_3L^{OMe} (335.5 mg, 0.484 mmol) in dimethylformamide (DMF, 8 mL) was added potassium hydride (60.3 mg, 1.503 mmol) as a solid. After stirring 1 hour, $CoBr_2$ (105.7 mg, 0.483 mmol) was added to the yellow solution as a solid. After stirring for 1 hour, Et_4NBr (105.2 mg, 0.501 mmol) was added as a solid to the purple solution. DMF was removed in vacuo. The resulting magenta powder was extracted with a mixture of acetonitrile (5 mL) and dichloromethane (5 mL), yielding a purple solution and a colorless precipitate (KBr). The mixture was filtered to remove KBr. Solvent was removed from the filtrate in vacuo. The crude product was recrystallized by slow diffusion of diethyl ether into a 1:1 DMF:acetonitrile solution to yield purple blocks (293.9 mg, 66.0%). ^1H NMR (δ, CD_3CN, 400 MHz): 36.25, 17.17, 15.95, 4.29, 3.53, 3.34, 3.28 (-CH_2-, Et_4N), 1.30 (-CH_3, Et_4N), -1.57. FTIR (KBr, cm^{-1}): ν(CO) 1605; 3057, 2993, 2951, 2836, 1656, 1556, 1508, 1475, 1446, 1350, 1247, 1170, 1031, 923, 846, 826, 774, 756, 627, 587, 496, 460, 425. UV-vis (DCM) λ_{max}, nm (ε, M^{-1} cm^{-1}): 584 (69). μ_{eff} = 4.97 μ_B (the method of Evans, CD_3CN, 400 MHz).

$Ph_4P[Co^{II}(NCCH_3)L^{F2}]$. To a solution of H_3L^{F2} (150.7 mg, 0.212 mmol) in DMF (5 mL) was added potassium hydride (26.3 mg, 0.656 mmol) as a solid. After stirring for 1 hour,

hydrogen evolution had ceased, yielding a yellow solution. $CoBr_2$ (47.4 mg, 0.217 mmol) was added to this mixture as a solid. After stirring for 1 hour, Ph_4PBr (90.1 mg, 0.215 mmol) was added as a solid to the purple solution. After stirring for an additional 1.5 hours, DMF was removed in vacuo. The resulting magenta solid was extracted with acetonitrile (10 mL), and the mixture was filtered to remove KBr. Solvent was removed from the filtrate in vacuo, and the resultant crude, magenta solid was recrystallized by slow diffusion of diethyl ether into a 1:1 DMF:acetonitrile solution to yield pink blocks (211.3 mg, 86.9%). ^{1}H NMR (δ, CD_3CN, 400 MHz): 30.60, 17.23, 15.59, 7.92 (s, Ph_4P), 7.74 (s, Ph_4P), 3.83, 1.76, -2.64. FTIR (KBr, cm^{-1}): ν(CO) 1579; 3060, 2971, 2931, 2864, 1476, 1422, 1355, 1273, 1227, 1111, 1042, 985, 887, 869, 772, 754, 724, 690, 620, 527, 487. UV-vis (DCM) λ_{max}, nm (ε, M^{-1} cm^{-1}): 588 (38). μ_{eff} = 4.42 μ_B (the method of Evans, CD_3CN, 400 MHz). ESI-MS (*m/z*) for $[CoL^{F2}]^-$, $(C_{30}H_{21}CoF_6N_4O_3)^-$ calcd 766.09; found 766.09.

$(Et_4N)_2[Co^{II}(CN)L^{F2}]$. To a solution of H_3L^{F2} (199.2 mg, 0.280 mmol) in dimethylformamide (DMF, 5 mL) was added potassium hydride (35.4 mg, 0.826 mmol) as a solid. After stirring 1.25 hours, hydrogen evolution had ceased, yielding a yellow solution. $CoBr_2$ (60.9 mg, 0.278 mmol) was added to this mixture as a solid. After stirring for 3 hours, Et_4NBr (59.7 mg, 0.284 mmol) was added as a solid to the purple solution. After stirring for an additional hour, DMF was removed in vacuo. The resulting purple solid was extracted with a mixture of acetonitrile (5 mL) and dichloromethane (5 mL), yielding a purple solution and a colorless precipitate (KBr). Solvent was removed from the product in vacuo. The product was recrystallized by slow

diffusion of diethyl ether into a 1:1 DMF:acetonitrile solution to yield flocculent pink needles. To a DCM solution (5 mL) of the product (40.4 mg, 0.043 mmol) was added Et_4NCN (8.2 mg, 0.052 mmol) as a solid, forming a magenta solution. DCM was removed in vacuo. The product was crystallized from diffusion of diethyl ether into a 1:1 DMF: $NCCH_3$ solution of the product to yield flocculent pink solid (26.6 mg, 58.6%). ^{1}H NMR (δ, CD_3CN, 400 MHz): 28.19, 16.87, 10.12, 8.93, 5.30, 3.13, 1.18. ^{1}H NMR (δ, CD_3CN, 376 MHz): -98.94. FT-IR (KBr, cm^{-1}): ν(CO) 1625, ν(CN) 2121; 3062, 2988, 1592, 1557, 1477, 1446, 1370, 1354, 1276, 1241, 1173, 1110, 1040, 1002, 982, 883, 862, 773, 753, 677, 621, 568, 513. UV-vis (DCM) λ_{max}, nm (ε, M^{-1} cm^{-1}): 580 (295), 847 (56). μ_{eff} = 4.53 μ_B (the method of Evans, CD_3CN, 400 MHz, 298). ESI-MS (*m/z*) for $(Et_4N)_3[Co(CN)L^{F2}]^+$, $(C_{64}H_{81}CoF_6N_8O_3)^+$ calcd 1182.6; found 1182.6.

$Ph_4P[Co^{II}(NCCH_3)L^{F3}]$. To a solution of H_3L^{F3} (110.4 mg, 0.144 mmol) in dimethylformamide (DMF, 10 mL) was added potassium hydride (19.4 mg, 0.484 mmol) as a solid. After stirring overnight, hydrogen evolution had ceased, yielding an orange solution. $CoBr_2$ (31.4 mg, 0.144 mmol) was added to this mixture as a solid. After stirring for two hours, Ph_4PBr (60.9 mg, 0.145 mmol) was added as a solid to the purple solution. After stirring for an additional hour, DMF was removed in vacuo. The resulting purple solid was extracted with a mixture of acetonitrile (5 mL) and dichloromethane (5 mL), yielding a purple solution and a colorless precipitate (KBr). The mixture was filtered to remove KBr (48.0 mg). Solvent was removed from the filtrate in vacuo, yielding a crude, magenta solid. The product was recrystallized by slow diffusion of diethyl ether into a 1:1 DMF:acetonitrile solution to yield purple blocks

(139.9 mg, 80.7%). ^{1}H NMR (δ, CD_2Cl_2, 300 MHz): 15.36, 14.42, 12.67, 12.02, 11.61, 11.38, 10.57, 7.84 (m). FTIR (KBr, cm^{-1}): ν(CO) 1637; 3059, 2927, 2869, 1673, 1606, 1580, 1485, 1369, 1246, 1115, 1034, 997, 837, 753, 724, 690, 620, 528. UV-vis (DMF) λ_{max}, nm (ε, $M^{-1}\,cm^{-1}$): 569 (179), 869 (22). μ_{eff} = 4.45 μ_B (the method of Evans, CD_2Cl_2, 300 MHz). Anal. Calcd (found) for $Ph_4P[Co^{II}(NCCH_3)L^{F3}]\cdot DMF\cdot Et_2O$: C, 64.14 (64.00); H, 4.34 (4.07); N, 6.23 (5.91).

$(Et_4N)_2[Co^{II}(CN)L^{F3}]$. To a solution of H_3L^{F3} (158.9 mg, 0.208 mmol) in dimethylformamide (DMF, 10 mL) was added potassium hydride (25.6 mg, 0.638 mmol) as a solid. After stirring for five hours, hydrogen evolution had ceased, yielding an orange solution. $CoBr_2$ (45.8 mg, 0.209 mmol) was added to this mixture as a solid. After stirring for two hours, Et_4NBr (44.3 mg, 0.211 mmol) was added as a solid to the purple solution. After stirring for an additional hour, DMF was removed in vacuo. The resulting purple solid was extracted with dichloromethane (5 mL), yielding a purple solution and a colorless precipitate (KBr). The mixture was filtered to remove KBr (62.2 mg). Solvent was removed from the filtrate in vacuo, and the resultant crude, magenta product was recrystallized by slow diffusion of diethyl ether into acetonitrile solution to yield purple blocks 108.7 mg, 55.0%). The product was dissolved in 5 mL DMF. Et_4NCN was added as a solid (18.2 mg, 0.116 mmol). After stirring for one hour, DMF was removed from the violet solution in vacuo. The product was recrystallized by slow diffusion of diethyl ether into an acetonitrile solution to yield magenta needles (92.0 mg, 67.0%). Crystals that were suitable for x-ray diffraction were grown by layering THF onto a DMF solution of the product, resulting in purple blocks. ^{1}H NMR (δ, CD_2Cl_2, 300

MHz): 16.96, 10.75, 8.09, 7.95, 7.60. FTIR (KBr, cm^{-1}): ν(CO) 1638; ν(CN) 2116; 3059, 2990, 1610, 1549, 1483, 1440, 1335, 1172, 1112, 1033, 996, 834, 755, 631, 547, 513. UV-vis (DMF) λ_{max}, nm (ε, M^{-1} cm^{-1}): 574 (239), 811 (33). μ_{eff} = 4.53 μ_B (the method of Evans, CD_2Cl_2, 300 MHz). Anal. Calcd (found) for $(Et_4N)_2[Co^{II}(CN)L^{F3}]$: C, 60.76 (60.70); H, 5.28 (5.33); N, 8.86 (9.25).

$Et_4N[Co^{II}(DMF)L^{F5}]$. To a solution of H_3L^{F5} (114.5 mg, 0.131 mmol) in dimethylformamide (DMF, 3 mL) was added potassium hydride (17.2 mg, 0.429 mmol) as a solid. After 1 hour, hydrogen evolution had ceased, yielding an amber solution and a colorless precipitate. $CoBr_2$ (29.0 mg, 0.133 mmol) was added to this mixture as a solid. After stirring for 30 mins, Et_4NBr (27.8 mg, 0.132 mmol) was added as a solid to the dark purple solution. After stirring for an additional hour, DMF was removed in vacuo. The resulting purple solid was extracted with acetonitrile (5 mL), yielding a purple solution and a colorless precipitate (KBr). The mixture was filtered to remove KBr (40.5 mg). Acetonitrile was removed from the filtrate in vacuo. The resultant purple solid was washed with diethyl ether and collected by filtration (132.8 mg, 89.3%). The product was recrystallized by slow diffusion of diethyl ether into DMF solution followed by storage in a freezer (-35 °C) to yield magenta blocks (52.4 mg, 31.6%). ^1H NMR (δ, CD_2Cl_2, 300 MHz): 15.37, 14.12, 11.69, 7.35 (s), 3.44, 1.45. FTIR (KBr, cm^{-1}): ν(CO) 1607; 3061, 2931, 2879, 1655, 1584, 1572, 1518, 1490, 1449, 1394, 1365, 1301, 1240, 1172, 1093, 988, 916, 868, 816, 789, 752, 669, 622, 567. UV-vis (DMF) λ_{max}, nm (ε, M^{-1} cm^{-1}): 570 (173), 874 (25). μ_{eff} = 4.53 μ_B (the method of Evans, CD_2Cl_2, 298K). Anal. Calcd (found) for $Et_4N[Co^{II}(DMF)L^{F5}]$: C, 53.06 (52.86); H, 3.47 (3.62); N, 7.43 (7.26).

$(Et_4N)_2[Co^{II}(L^{F5})(CN)]$. To a solution of H_3L^{F5} (131.6 mg, 0.151 mmol) in dry dimethylformamide (DMF, 4 mL) was added potassium hydride (19.7 mg, 0.491 mmol) as a solid. After 1 hour, hydrogen evolution had ceased, yielding an amber solution with colorless preciptate. $CoBr_2$ (33.5 mg, 0.153 mmol) was added as a solid. After stirring for 30 mins, Et_4NBr (31.5 mg, 0.150 mmol) was added as a solid to the dark purple solution. After stirring for an additional hour, DMF was removed in vacuo. The resulting purple solid was extracted with acetonitrile (5 mL), yielding a purple solution and a colorless precipitate (KBr). The mixture was filtered to remove KBr (46.6 mg). To the purple solution in 5 mL acetonitrile Et_4NCN (24.0 mg, 0.154 mmol) was added as a solid. The solution was stirred overnight. Acetonitrile was then removed in vacuo. The resulting purple solid was washed with tetrahydrofuran and diethyl ether. The crude purple powder was collected (139.7 mg, 76.3%). The product was recrystallized by slow diffusion of diethyl ether into DMF solution to yield purple blocks (112.6 mg, 61.5%). ^{1}H NMR (δ, CD_2Cl_2, 300 MHz): 16.96, 11.18, 6.77, 3.17, 1.22. FTIR (KBr, cm^{-1}): ν(CO) 1600; ν(CN) 2109; 2990, 1673, 1567, 1519, 1500, 1449, 1417, 1370, 1285, 1243, 1173, 1115, 1086, 1041, 987, 874, 818, 791, 756, 670, 623, 566, 493, 439. UV-vis (DMF) λ_{max}, nm (ε, M^{-1} cm^{-1}): 569 (224), 807 (39). μ_{eff} = 4.42 μ_B (the method of Evans, CD_2Cl_2, 298K). Anal. Calcd (found) for $(Et_4N)_2[Co^{II}(L^{F5})(CN)]$: C, 55.36 (55.43); H, 4.31 (4.72); N, 8.07 (8.03).

$Ph_4P[Co^{II}(NCCH_3)L^{CF3}]$. To a solution of H_3L^{CF3} (239.5 mg, 0.414 mmol) in dimethylformamide (DMF, 3 mL) was added potassium hydride (51.4 mg, 1.281 mmol)

as a solid. After 1.5 hours, hydrogen evolution had ceased, yielding a yellow solution. $CoBr_2$ (91.6 mg, 0.419 mmol) was added to this mixture as a solid. After stirring for 1.5 hours, Ph_4PBr (178.8 mg, 0.426 mmol) was added as a solid to the dark purple solution. After stirring overnight, DMF was removed in vacuo. The resulting purple solid was extracted with acetonitrile (10 mL), yielding a purple solution and a colorless precipitate (KBr). The mixture was filtered to remove KBr. Acetonitrile was removed from the filtrate in vacuo. The resultant crude, purple solid was recrystallized by slow diffusion of diethyl ether into an $NCCH_3$ solution to yield fine, lavender-colored needles (376.5 mg, 89.6%). ^{1}H NMR (δ, CD_3CN, 400 MHz): 16.53, 11.95, 7.92, 7.74, 4.75, -4.68. FTIR (KBr, cm^{-1}): ν(CO) 1651; 3063, 2974, 2928, 2874, 1590, 1482, 1442, 1254, 1205, 1139, 1110, 948, 774, 725, 690, 527, 494. UV-vis (DCM) λ_{max}, nm (ε, M^{-1} cm^{-1}): 580 (30). μ_{eff} = 4.93 μ_B (the method of Evans, CD_3CN, 400 MHz, 298K).

$(Et_4N)_2[Co^{II}(CN)L^{CF3}]$. To a solution of H_3L^{CF3} (279.4 mg, 0.483 mmol) in dry dimethylformamide (DMF, 5 mL) was added potassium hydride (60.2 mg, 1.498 mmol) as a solid. After 6 hours, the solution was beige with a colorless preciptate. $CoBr_2$ (105.6 mg, 0.483 mmol) was added as a solid. After stirring for 1 hour, Et_4NBr (101.5 mg, 0.483 mmol) was added as a solid to the dark purple solution. After stirring overnight, Et_4NCN (78.2 mg, 0.500 mmol) was added as a solid. DMF was removed in vacuo. The resulting purple solid was extracted with acetonitrile (10 mL), yielding a purple solution and a colorless precipitate (KBr). The mixture was filtered to remove KBr. Acetonitrile was removed from the filtrate, and the crude, magenta product was crystallized by slow diffusion of diethyl ether into an $NCCH_3$ solution to yield magenta needles (376.9 mg,

84.7%). (δ, CD_3CN, 400 MHz): 16.56, 14.82, 11.95, 11.40, 3.19, 1.21, -4.78. FTIR (KBr, cm^{-1}): ν(CO) 1626; ν(CN) 2110; 2992, 2891, 1588, 1483, 1453, 1397, 1248, 1185, 1149, 1126, 1036, 1003, 941, 776, 748, 729, 564, 467. UV-vis (DCM) λ_{max}, nm (ε, M^{-1} cm^{-1}): 580 (311), 930 (37). $\mu_{eff} = 5.05\ \mu_B$ (the method of Evans, CD_3CN, 400 MHz, 298 K).

Cyanide Binding Studies

General procedure. Under an N_2 atmosphere, a known amount of the analytically pure**,** five-coordinate cobalt complex was placed in a volumetric flask and dissolved in enough dichloromethane to produce 10.0 or 25.0 mL of stock solution (typically concentration range 4 - 6 mM). A dichloromethane stock solution of Et_4NCN was prepared in a similar fashion. One or two milliliters of the cobalt complex solution was transferred from the volumetric flask to a quartz cuvette using a transfer pipette. An aliquot of known concentration of Et_4NCN was then transferred to the cuvette containing the cobalt complex. The resulting solution was then diluted with enough dichloromethane to produce exactly 3.0 mL of solution. The cuvette was sealed. The UV-visible spectrum was then recorded at room temperature. All flasks and containers were kept sealed between transfers and measurements to minimize evaporation. This procedure was repeated for each cobalt sample (gradually increasing the concentration from 0.2 equivalents to 10 equivalents when possible) until 8 – 14 measurements were obtained. These measurements were then overlaid and used to create a titration curve. The association constants (K_a) were calculated by generating and fitting a one-site binding isotherm (plot of ΔAbs for the wavelength that exhibited greatest change upon cyanide

binding vs. cyanide ion concentration). This binding curve was then fitted using non-linear regression methods to generate the association constants. The curve fitting technique that was used depended on the strength of binding. In weak-binding scenarios, a standard one-site binding hyperbola was used and fit the data well. A reasonable fit could not be obtained using a hyperbolic fit for the strongly binding complexes.[114] For these complexes, a parabolic function was used as recently described by the Holland group.[115]

A 1:1 binding ratio can be confirmed using the method of continuous variations by generating a Job's plot (corrected absorbance vs. mole fraction CN^-).[125] This was done for each complex that demonstrated binding in dichloromethane. The data points were obtained by varying the mole fraction of complex: Et_4NCN in dichloromethane and recording the spectra. Each of the complexes studied by this method demonstrated a corrected absorbance maximum at a mole fraction of 0.5, indicating a 1:1 binding ratio.

Crystallographic Data

For each complex, crystals were coated with Paratone N oil, and suitable crystals were suspended in small fiber loops. They were mounted in a cooled nitrogen gas stream at 173 K on a Bruker D8 APEX II CCD sealed tube diffractometer with graphite monochromated Mo Kα (0.71073 Å) radiation. Data was collected using a series of phi and omega scans with 10s frame exposures and 0.5° frame widths.

The structures were solved using direct methods and difference Fourier techniques (Shelxtl, V6.12). Hydrogen atoms were added with the HFIX command. These were included in the final cycles of least squares refinement, with isotropic U_{ij}'s

that were determined by the riding model. All non-hydrogen atoms in the main residues were refined anisotropically. Residual solvent molecules in the unit cells were not refined anisotropically. Structure solution, refinement, and generation of publication materials were performed by using SHELX, V6.12 software.

The complex $PPh_4[CoL^{NMe2}]$ was solved in the space group $P2_1/c$. The asymmetric unit is comprised of 1 molecule of the complex and its countercation, and 1 molecule of DMF that exhibits partial occupancy (modeled at 67%). The main residue was refined anisotropically. The residual solvent molecule was refined isotropically. Residual electron density peaks (81 electrons) that could not be refined were omitted using the SQUEEZE function.[126] The complex $PPh_4[CoL^{OMe})]$ was solved in the space group $P2_1/c$. The asymmetric unit is comprised of 1 molecule of the complex and its countercation, and 2 molecules of DMF. All atoms were refined anisotropically. The complexes $PPh_4[Co(NCCH_3)L^{NMe2}]$ and $Ph_4P[Co(NCCH_3)L^{OMe}]$ were solved in the space group P-1. The asymmetric unit is comprised of 1 molecule of the complex and its countercation. These were refined anisotropically. The unit cell of $Ph_4P[Co(NCCH_3)L^{OMe}]$ also contained electron density peaks (106 electrons) that could not be refined. These were removed using the SQUEEZE function.[126] The complex $Ph_4P[Co(NCCH_3)L^{F2}]$ was solved in the space group P-1. The asymmetric unit is comprised of 1 molecule of the complex and its countercation, and 1 molecule of DMF. These were refined anisotropically. The complex $Ph_4P[Co(NCCH_3)L^{F3}]$ was solved in the space group $P2_1/c$. The asymmetric unit is comprised of 4 molecules of the complex and its countercation, 1 molecule of diethyl ether, 1 molecule of residual *N,N*-dimethylformamide that exhibits partial occupancy (modeled at 20%). The main residue

was refined anisotropically. Residual solvent molecules were refined isotropically. The complex $(Et_4N)_2[Co(CN)L^{F3}]$ was solved in the space group $P2_1/c$. The asymmetric unit is comprised of 1 molecule of the complex and its two countercations, and 1 molecule of diethyl ether that exhibits partial occupancy (modeled at 45%). The main residue was refined anisotropically. Residual solvent molecules were refined isotropically. The complex $Et_4N[Co(DMF)L^{F5}]$ was solved in the space group $P2_1/c$. The asymmetric unit is comprised of 4 molecules of the complex and its countercation, 1 molecule of residual *N,N*-dimethylformamide, and 3 molecules of diethyl ether that exhibit partial occupancy (modeled at 50% for each of two molecules and 75% for another). The main residue was refined anisotropically. Residual solvent molecules were refined isotropically. The complex $(Et_4N)_2[Co(CN)L^{F5}]$ was solved in the space group $P2_1/c$. The asymmetric unit is comprised of 1 molecule of the complex and its two countercations, and 1 molecule of tetrahydrofuran (THF) that exhibits partial occupancy (modeled at 50%). The main residue and residual solvent molecules were refined anisotropically. The complexes $PPh_4[Co(NCCH_3)L^{CF3}]$ and $(Et_4N)_2[Co(CN)L^{CF3}]$ were solved in the space group $P2_1/c$. The asymmetric unit of $PPh_4[Co(NCCH_3)L^{CF3}]$ is comprised of 1 molecule of the complex and its countercation, and 1 molecule of $NCCH_3$ that is fully occupied and one that exhibits partial occupancy (modeled at 50%). The asymmetric unit of $(Et_4N)_2[Co(CN)L^{CF3}]$ is comprised of 1 molecule of the complex and its countercation. All atoms in each of these two structures were refined anisotropically.

Table 2-7. Crystal data and structure refinement parameters for $PPh_4[CoL^{NMe2}]$•0.67 DMF, $PPh_4[CoL^{OMe})]$•2 DMF, and $PPh_4[Co(NCCH_3)L^{NMe2}]$.

	$PPh_4[CoL^{NMe2}]$•0.67 DMF	**$PPh_4[CoL^{OMe})]$•2 DMF**	**$PPh_4[Co(NCCH_3)L^{NMe2}]$**
Formula	$C_{71.01}H_{66.69}CoN_{7.67}O_{3.67}P$	$C_{72}H_{65}CoN_6O_8P$	$C_{69}H_{62}CoN_7O_3P$
Crystal size (mm^3)	0.43 × 0.12 × 0.02	0.28 × 0.21 × 0.08	0.20 × 0.19 × 0.14
Form. wt. (g/mol)	1176.13	1232.20	1127.16
Space group	$P2_1/c$	$P2_1/c$	P -1
a (Å)	19.7745(6)	19.1712(5)	10.9028(2)
b (Å)	29.5175(8)	29.5066(8)	13.9367(3)
c (Å)	11.3386(3)	11.1333(3)	21.7563(5)
α (deg)	90	90	93.3780(10)
β (deg)	105.963(2)	105.3050(10)	91.572(2)
γ (deg)	90	90	102.8030(10)
V ($Å^3$)	6363.1(3)	6074.5(3)	3215.27(12)
Z	4	4	2
T (K)	173(2)	173(2)	173(2)
ϱ, calcd (g/cm)	1.228	1.347	1.164
Reflns collected	42389	38322	36845
Unique reflns	11394	10022	11018
Par/restr.	530/0	780/0	811/0
μ Kα (mm^{-1})	2.775	2.981	2.715
GOF[b]	1.079	1.113	1.029
Final *R* indices [I > 2σ(*I*)][b]	R_1 = 0.0771	R_1 = 0.0500	R_1 = 0.0442
All data	wR_2 = 0.2244	wR_2 = 0.1384	wR_2 = 0.1396

Table 2-8. Crystal data and structure refinement parameters for $Ph_4P[Co(NCCH_3)L^{OMe}]$, $Ph_4P[Co(NCCH_3)L^{F2}]$•DMF, and $Ph_4P[Co(NCCH_3)L^{F3}]$•Et_2O, 0.2 DMF

	$Ph_4P[Co(NCCH_3)L^{OMe}]$	**$Ph_4P[Co(NCCH_3)L^{F2}]$ •DMF**	**$Ph_4P[Co(NCCH_3)L^{F3}]$ •Et_2O, 0.2 DMF**
Formula	$C_{68}H_{56}CoN_5O_6P$	$C_{69}H_{54}CoF_6N_5O_4P$	$C_{69.60}H_{52.40}CoF_9N_{5.20}O_{4.20}P$
Crystal size (mm^3)	0.26 × 0.11 × 0.08	0.53x 0.31 x 0.29	0.17 x 0.09 x 0.07
Form. wt. (g/mol)	1129.08	1221.07	1289.67
Space group	P-1	P-1	$P2_1/c$
a (Å)	10.776(8)	10.8114(9)	14.747(4)
b (Å)	13.751(10)	13.6329(11)	28.861(7)
c (Å)	20.652(15)	21.4103(17)	17.576(5)
α (deg)	91.325(11)	99.8580(10)	90
β (deg)	91.101(12)	102.9960(10)	113.740(4)
γ (deg)	103.805(12)	102.1160(10)	90
V ($Å^3$)	2970(4)	2926.3(4)	6858(3)
Z	2	2	4
T (K)	173(2)	173(2)	173(2)
ϱ, calcd (g/cm)	1.263	1.386	1.251
Reflns collected	48935	59755	128110
Unique reflns	14056	17758	19142
Par/restr.	731/0	775/0	803/6
μ Kα (mm^{-1})	0.372	0.395	0.348
GOF[b]	1.155	1.051	1.047
Final *R* indices [I > $2\sigma(I)$][b]	R_1 = 0.0629	R_1 = 0.0488	R_1 = 0.0754
All data	wR_2 = 0.1020	wR_2 = 0.1378	wR_2 = 0.2328

Table 2-9. Crystal data and structure refinement parameters for $Et_4N[Co(DMF)L^{F5}]]$•0.44 Et_2O, 0.25 DMF, $(Et_4N)_2[Co(CN)L^{F3}]$•Et_2O, and $(Et_4N)_2[Co(CN)L^{F5}]$•0.5 Et_2O

	$Et_4N[Co(DMF)L^{F5}]$ •0.44 Et_2O, 0.25 DMF	**$(Et_4N)_2[Co(CN)L^{F3}]$ •Et_2O**	**$(Et_4N)_2[Co(CN)L^{F5}]$ •0.5 Et_2O**
Formula	$C_{52.50}H_{45.13}CoF_{15}N_{6.25}O_{4.69}$	$C_{60}H_{66}CoF_9N_7O_4$	$C_{58}H_{56}CoF_{15}N_7O_{3.50}$
Crystal size (mm^3)	0.30 × 0.22 × 0.12	0.20 x 0.17 x 0.17	0.08 x 0.07 x 0.06
Form. wt. (g/mol)	1182.50	1179.13	1251.03
Space group	$P2_1/c$	$P2_1/c$	$P2_1/c$
a (Å)	20.4727(5)	16.2560(9)	11.889(5)
b (Å)	23.0888(6)	12.9238(7)	19.445(8)
c (Å)	46.9865(13)	26.8628(15)	25.921(11)
α (deg)	90	90	90
β (deg)	91.1730(10)	96.5520(10)	90.353(7)
γ (deg)	90	90	90
V ($Å^3$)	22205.4(10)	5606.7(5)	5992(4)
Z	16	4	4
T (K)	173(2)	173(2)	173(2)
ϱ, calcd (g/cm)	1.415	1.397	1.387
Reflns collected	209015	105033	106394
Unique reflns	45208	16439	16993
Par/restr.	2834/12	730/0	759/0
μ Kα (mm^{-1})	0.410	0.390	0.383
GOF[b]	1.229	1.005	1.022
Final *R* indices [I > 2σ(*I*)][b]	R_1 = 0.0903	R_1 = 0.0648	R_1 = 0.0791
All data	wR_2 = 0.2513	wR_2 = 0.2082	wR_2 = 0.2766

Table 2-10. Crystal data and structure refinement parameters for $PPh_4[Co(NCCH_3)L^{CF3}]\bullet 1.5\ NCCH_3$ and $(Et_4N)_2[Co(CN)L^{CF3}]$.

	$PPh_4[Co(NCCH_3)L^{CF3}]\bullet 1.5\ NCCH_3$	**$(Et_4N)_2[Co(CN)L^{CF3}]$**
Formula	$C_{35}H_{36.50}CoF_9N_{6.50}O_3P$	$C_{41}H_{52}CoF_9N_7O_3$
Crystal size (mm^3)	0.41 × 0.32 × 0.23	0.30 × 0.24 × 0.02
Form. wt. (g/mol)	826.14	920.83
Space group	$P2_1/c$	$P2_1/c$
a (Å)	14.0630(2)	19.457(17)
b (Å)	19.4987(3)	12.279(11)
c (Å)	15.1501(3)	18.993(16)
α (deg)	90	90
β (deg)	119.972(1)	90.251(4)
γ (deg)	90	90
V ($Å^3$)	3852.57(10)	4538(7)
Z	4	4
T (K)	173(2)	173(2)
ϱ, calcd (g/cm)	1.424	1.348
Reflns collected	30389	77248
Unique reflns	7389	11270
Par/restr.	511/0	550/0
μ Kα (mm^{-1})	0.532	0.459
GOF[b]	1.079	1.027
Final *R* indices [$I > 2\sigma(I)$][b]	$R_1 = 0.0467$	$R_1 = 0.0791$
All data	$wR_2 = 0.1565$	$wR_2 = 0.2538$

References:

(1) Reinhoudt, D. N.; Crego-Calama, M. *Science* **2008**, *295*, 2403.

(2) Borovik, A. S. *Acc. Chem. Res.* **2005**, *38*, 54.

(3) Fulop, V.; Phizackerley, R. P.; Soltis, S. M.; Clifton, I. J.; Wakatsuki, S.; Erman, J.; Hajdu, J.; Edwards, S. L. *Structure* **1994**, *2*, 201.

(4) Gerber, N. C.; Sligar, S. G. *J. Am. Chem. Soc.* **1992**, *114*, 8742.

(5) Mukai, M.; Nagano, S.; Tanaka, M.; Ishimori, K.; Morishima, I.; Ogura, T.; Watanabe, Y.; Kitagawa, T. *J. Am. Chem. Soc.* **1997**, *119*, 1758.

(6) Ozaki, S.-i.; Roach, M. P.; Matsui, T.; Watanabe, Y. *Acc. Chem. Res.* **2001**, *34*, 818.

(7) Perutz, M. F.; Fermi, G.; Luisi, B.; Shaanan, B.; Liddington, R. C. *Acc. Chem. Res.* **1987**, *20*, 309.

(8) Sono, M.; Roach, M. P.; Coulter, E. D.; Dawson, J. H. *Chem. Rev.* **1996**, *96*, 2841.

(9) Springer, B. A.; Sligar, S. G.; Olson, J. S.; Phillips, G. N., Jr. *Chem. Rev.* **1994**, *94*, 699.

(10) Vance, C. K.; Miller, A.-F. *Biochemistry* **2001**, *40*, 13079.

(11) Xie, J.; Yikilmaz, E.; Miller, A.-F.; Brunold, T. C. *J. Am. Chem. Soc.* **2002**, *124*, 3769.

(12) Du Bois, J.; Mizoguchi, T. J.; Lippard, S. J. *Coord. Chem. Rev.* **2000**, *200,Äì202*, 443.

(13) Ghosh, S.; Roehm, B.; Begum, R. A.; Kut, J.; Hossain, M. A.; Day, V. W.; Bowman-James, K. *Inorg. Chem.* **2007**, *46*, 9519.

(14) MacBeth, C. E.; Gupta, R.; Mitchell-Koch, K. R.; Young, V. G., Jr.; Lushington, G. H.; Thompson, W. H.; Hendrich, M. P.; Borovik, A. S. *J. Am. Chem. Soc.* **2004**, *126*, 2556.

(15) MacBeth, C. E.; Golombek, A. P.; Young, V. G., Jr.; Yang, C.; Kuczera, K.; Hendrich, M. P.; Borovik, A. S. *Science* **2000**, *289*, 938.

(16) Collman, J. P.; Zhang, X.; Wong, K.; Brauman, J. I. *J. Am. Chem. Soc.* **1994**, *116*, 6245.

(17) Momenteau, M.; Reed, C. A. *Chem. Rev.* **1994**, *94*, 659.

(18) Lakshminarayanan, P. S.; Ravikumar, I.; Suresh, E.; Ghosh, P. *Chem. Commun.* **2007**, 5214.

(19) Rudkevich, D. M.; Verboom, W.; Brzozka, Z.; Palys, M. J.; Stauthamer, W. P. R. V.; van, H. G. J.; Franken, S. M.; Harkema, S.; Engbersen, J. F. J.; Reinhoudt, D. N. *J. Am. Chem. Soc.* **1994**, *116*, 4341.

(20) Walton, P. H.; Raymond, K. N. *Inorg. Chim. Acta* **1995**, *240*, 593.

(21) Mueller-Dethlefs, K.; Hobza, P. *Chem. Rev.* **2000**, *100*, 143.

(22) Nelson, D. L.; Cox, M. M. *Principles of Biochemistry*; Fourth Edition ed.; W.H. Freeman and Company: New York City, NY, 2005.

(23) Claessens, C. G.; Stoddart, J. F. *J. Phys. Org. Chem.* **1997**, *10*, 254.

(24) Salonen, L. M.; Ellermann, M.; Diederich, F. *Angew. Chem., Int. Ed.* **2011**, *50*, 4808.

(25) Meyer, E. A.; Castellano, R. K.; Diederich, F. *Angew. Chem., Int. Ed.* **2003**, *42*, 1210.

(26) Ma, J. C.; Dougherty, D. A. *Chem. Rev.* **1997**, *97*, 1303.

(27) Gallivan, J. P.; Dougherty, D. A. *Proc. Natl. Acad. Sci. U. S. A.* **1999**, *96*, 9459.

(28) Zacharias, N.; Dougherty, D. A. *Trends Pharmacol. Sci.* **2002**, *23*, 281.

(29) Cubero, E.; Orozco, M.; Luque, F. J. *J. Phys. Chem. A* **1999**, *103*, 315.

(30) Dougherty, D. A. *Science* **1996**, *271*, 163.

(31) Gallivan, J. P.; Dougherty, D. A. *J. Am. Chem. Soc.* **2000**, *122*, 870.

(32) Gallivan, J. P.; Dougherty, D. A. *Proc. Natl. Acad. Sci. USA* **1999**, *96*, 9459.

(33) Scrutton, N. S.; Raine, A. R. C. *Biochem. J.* **1996**, *319*, 1.

(34) Sessler, J. L.; Gale, P.; Cho, W.-S. *Anion Receptor Chemistry*; The Royal Society of Chemistry: Los Angeles, CA, 2006.

(35) Lange, L. G.; Riordan, J. F.; Vallee, B. L. *Biochemistry* **1974**, *13*, 4361.

(36) Leslie, E. M.; Deeley, R. G.; Cole, S. P. C. *Toxicol. Appl. Pharmacol.* **2005**, *204*, 216.

(37) Beer, P. D.; Gale, P. A. *Angew. Chem., Int. Ed.* **2001**, *40*, 486.

(38) Beer, P. D.; Hayes, E. J. *Coord. Chem. Rev.* **2003**, *240*, 167.

(39) Best, M. D.; Tobey, S. L.; Anslyn, E. V. *Coord. Chem. Rev.* **2003**, *240*, 3.

(40) Bondy, C. R.; Loeb, S. J. *Coord. Chem. Rev.* **2003**, *240*, 77.

(41) Choi, K.; Hamilton, A. D. *Coord. Chem. Rev.* **2003**, *240*, 101.

(42) Davis, A. P.; Joos, J.-B. *Coord. Chem. Rev.* **2003**, *240*, 143.

(43) Gale, P. A. *Coord. Chem. Rev.* **2003**, *240*, 191.

(44) Hosseini, M. W. *Coord. Chem. Rev.* **2003**, *240*, 157.

(45) Lambert, T. N.; Smith, B. D. *Coord. Chem. Rev.* **2003**, *240*, 129.

(46) Llinares, J. M.; Powell, D.; Bowman-James, K. *Coord. Chem. Rev.* **2003**, *240*, 57.

(47) Wedge, T. J.; Hawthorne, M. F. *Coord. Chem. Rev.* **2003**, *240*, 111.

(48) Sessler, J. L.; Camiolo, S.; Gale, P. A. *Coord. Chem. Rev.* **2003**, *240*, 17.

(49) Sessler, J. L.; Gale, P. A.; Cho, W.-S. *Anion Receptor Chemistry*, 2006.

(50) Dydio, P.; Lichosyt, D.; Jurczak, J. *Chem. Soc. Rev.* **2011**, *40*, 2971.

(51) Gale, P. A. *Chem. Soc. Rev.* **2010**, *39*, 3746.

(52) Gale, P. A. *Acc. Chem. Res.* **2011**, *44*, 216.

(53) Gale, P. A. *Chem. Commun.* **2011**, *47*, 82.

(54) Gogoi, P. K.; Bordoloi, S. *Proc. Natl. Acad. Sci., India, Sect. A* **2008**, *78*, 179.

(55) Lima, L. M. P.; Tripier, R. *Curr. Inorg. Chem.* **2011**, *1*, 36.

(56) Steed, J. W. *Chem. Soc. Rev.* **2009**, *38*, 506.

(57) Wenzel, M.; Hiscock, J. R.; Gale, P. A. *Chem. Soc. Rev.* **2012**, *41*, 480.

(58) Beer, P. D. *Chem. Commun.* **1996**, 689.

(59) Beer, P. D. *Acc. Chem. Res.* **1998**, *31*, 71.

(60) Beer, P. D.; Cadman, J. *Coord. Chem. Rev.* **2000**, *205*, 131.

(61) Czarnik, A. W. *Acc. Chem. Res.* **1994**, *27*, 302.

(62) Duke, R. M.; Veale, E. B.; Pfeffer, F. M.; Kruger, P. E.; Gunnlaugsson, T. *Chem. Soc. Rev.* **2010**, *39*, 3936.

(63) Martinez-Manez, R.; Sancenon, F. *Chem. Rev.* **2003**, *103*, 4419.

(64) Guha, S.; Saha, S. *J. Am. Chem. Soc.* **2010**, *132*, 17674.

(65) Hung, C.-Y.; Singh, A. S.; Chen, C.-W.; Wen, Y.-S.; Sun, S.-S. *Chem. Commun.* **2009**, 1511.

(66) Mahanta, S. P.; Kumar, B. S.; Baskaran, S.; Sivasankar, C.; Panda, P. K. *Org. Lett.* **2012**, *14*, 548.

(67) Chifotides, H. T.; Schottel, B. L.; Dunbar, K. R. *Angew. Chem., Int. Ed.* **2010**, *49*, 7202.

(68) Ballester, P. *Acc. Chem. Res.*, Ahead of Print.

(69) Frontera, A.; Gamez, P.; Mascal, M.; Mooibroek, T. J.; Reedijk, J. *Angew. Chem., Int. Ed.* **2011**, *50*, 9564.

(70) Frontera, A.; Quinonero, D.; Deya, P. M. *Wiley Interdiscip. Rev.: Comput. Mol. Sci.* **2011**, *1*, 440.

(71) Garau, C.; Frontera, A.; Quinonero, D.; Ballester, P.; Costa, A.; Deya, P. M. *Recent Res. Dev. Chem. Phys.* **2004**, *5*, 227.

(72) Schneider, H.-J. *Acc. Chem. Res.*, Ahead of Print.

(73) Watt, M. M.; Collins, M. S.; Johnson, D. W. *Acc. Chem. Res.*, Ahead of Print.

(74) Ballester, P. *Structure and Bonding (Berlin, Germany)* **2008**, *129*, 127.

(75) Hay, B. P.; Bryantsev, V. S. *Chem. Commun.* **2008**, 2417.

(76) Schottel, B. L.; Chifotides, H. T.; Dunbar, K. R. *Chem. Soc. Rev.* **2008**, *37*, 68.

(77) Battaglia, M. R.; Buckingham, A. D.; Williams, J. H. *Chem. Phys. Lett.* **1981**, *78*, 421.

(78) Garau, C.; Frontera, A.; Quinonero, D.; Ballester, P.; Costa, A.; Deya, P. M. *ChemPhysChem* **2003**, *4*, 1344.

(79) Vrbancich, J.; Ritchie, G. L. D. *J. Chem. Soc., Faraday Trans.* **1980**, *76*, 648.

(80) Cormier, K. W.; Watt, M.; Lewis, M. *J. Phys. Chem. A* **2010**, *114*, 11708.

(81) Garau, C.; Frontera, A.; Quinonero, D.; Ballester, P.; Costa, A.; Deya, P. M. *Chem. Phys. Lett.* **2004**, *399*, 220.

(82) Mecozzi, S.; West, A. P.; Dougherty, D. A. *J. Am. Chem. Soc.* **1996**, *118*, 2307.

(83) Estarellas, C.; Bauza, A.; Frontera, A.; Quinonero, D.; Deya, P. M. *Phys. Chem. Chem. Phys.* **2011**, *13*, 5696.

(84) Frontera, A.; Saczewski, F.; Gdaniec, M.; Dziemidowicz-Borys, E.; Kurland, A.; Deya, P. M.; Quinonero, D.; Garau, C. *Chem.--Eur. J.* **2005**, *11*, 6560.

(85) Alkorta, I.; Rozas, I.; Elguero, J. *J. Am. Chem. Soc.* **2002**, *124*, 8593.

(86) Kim, D.; Lee, E. C.; Kim, K. S.; Tarakeshwar, P. *J. Phys. Chem. A* **2007**, *111*, 7980.

(87) Kim, D.; Tarakeshwar, P.; Kim, K. S. *J. Phys. Chem. A* **2004**, *108*, 1250.

(88) Kim, D. Y.; Singh, N. J.; Kim, K. S. *J. Chem. Theory Comput.* **2008**, *4*, 1401.

(89) Kim, D. Y.; Singh, N. J.; Lee, J. W.; Kim, K. S. *J. Chem. Theory Comput.* **2008**, *4*, 1162.

(90) Mascal, M.; Armstrong, A.; Bartberger, M. D. *J. Am. Chem. Soc.* **2002**, *124*, 6274.

(91) Quinonero, D.; Garau, C.; Rotger, C.; Frontera, A.; Ballester, P.; Costa, A.; Deya, P. M. *Angew. Chem., Int. Ed.* **2002**, *41*, 3389.

(92) Berryman, O. B.; Bryantsev, V. S.; Stay, D. P.; Johnson, D. W.; Hay, B. P. *J. Am. Chem. Soc.* **2007**, *129*, 48.

(93) Hay, B. P.; Bryantsev, V. S. *Chem. Commun.* **2008**, 2417.

(94) Frontera, A.; Saczewski, F.; Gdaniec, M.; Ewa Dziemidowicz-Borys; Kurland, A.; Deya, P. M.; Quinonero, D.; Garau, C. *Chem.--Eur. J.* **2005**, *11*, 6560.

(95) Albrecht, M.; Wessel, C.; de Groot, M.; Rissanen, K.; Luechow, A. *J. Am. Chem. Soc.* **2008**, *130*, 4600.

(96) Rosokha, Y. S.; Lindeman, S. V.; Rosokha, S. V.; Kochi, J. K. *Angew. Chem., Int. Ed.* **2004**, *43*, 4650.

(97) Berryman, O. B.; Hof, F.; Hynes, M. J.; Johnson, D. W. *Chem. Commun.* **2006**, 506.

(98) Hiraoka, K.; Mizuse, S.; Yamabe, S. *J. Phys. Chem.* **1987**, *91*, 5294.

(99) Dawson, R. E.; Hennig, A.; Weimann, D. P.; Emery, D.; Ravikumar, V.; Montenegro, J.; Takeuchi, T.; Gabutti, S.; Mayor, M.; Mareda, J.; Schalley, C. A.; Matile, S. *Nat. Chem.* **2010**, *2*, 533.

(100) Mooibroek, T. J.; Black, C. A.; Gamez, P.; Reedijk, J. *Cryst. Growth Des.* **2008**, *8*, 1082.

(101) Jones, M. B.; MacBeth, C. E. *Inorg. Chem.* **2007**, *46*, 8117.

(102) Korenaga, T.; Kawauchi, Y.; Kosaki, T.; Ema, T.; Sakai, T. *Bull. Chem. Soc. Jpn.* **2005**, *78*, 2175.

(103) Jones, M. B. Ph.D. Dissertation, Emory University, 2010.

(104) Bain, G. A.; Berry, J. F. *J. Chem. Ed.* **2008**, *85*, 532.

(105) Yang, L.; Powell, D. R.; Houser, R. P. *Dalton Trans.* **2007**, 955.

(106) Addison, A. W.; Rao, T. N.; Reedijk, J.; Van Rijn, J.; Verschoor, G. C. *J. Chem. Soc., Dalton Trans.* **1984**, 1349.

(107) Yang, L.; Powell, D. R.; Houser, R. P. *Dalton Trans.* **2007**, 955.

(108) Alexander, J. J.; Gray, H. B. *J. Am. Chem. Soc.* **1967**, *89*, 3356.

(109) Brown, L. D.; Raymond, K. N. *Inorg. Chem.* **1975**, *14*, 2590.

(110) King, N. K.; Winfield, M. E. *J. Am. Chem. Soc.* **1961**, *83*, 3366.

(111) Kolski, G. B.; Margerum, D. W. *Inorg. Chem.* **1969**, *8*, 1125.

(112) Curtis, N. F. *Coord. Chem. Rev.* **1968**, *3*, 3.

(113) Siegfried, L.; Kaden, T. A. *Helv. Chim. Acta* **2005**, *88*, 380.

(114) Connors, K. A. *Binding constants: the measurement of molecular complex stability*; John Wiley & Sons, Inc.: New York City, NY, 1987.

(115) Chiang, K. P.; Barrett, P. M.; Ding, F.; Smith, J. M.; Kingsley, S.; Brennessel, W. W.; Clark, M. M.; Lachicotte, R. J.; Holland, P. L. *Inorg. Chem.* **2009**, *48*, 5106.

(116) Schrock, R. R. *Acc. Chem. Res.* **2005**, *38*, 955.

(117) Hu, X.; Meyer, K. *J. Organomet. Chem.* **2005**, *690*, 5474.

(118) Wampler, K. M.; Schrock, R. R. *Inorg. Chem.* **2007**, *46*, 8463.

(119) Gagliardo, M.; Chase, P. A.; Lutz, M.; Spek, A. L.; Hartl, F.; Havenith, R. W. A.; Klink, G. P. M. v.; Koten, G. v. *Organometallics* **2005**, *24*, 4553.

(120) Armarego, W., L.F.; Chai, Christina, L.L. *Purification of Laboratory Chemicals*; 5th ed.; Elsevier, 2003.

(121) Evans, D. F. *J. Chem. Soc.* **1959**, 2003.

(122) Sur, S. K. *J. Magn. Reson.* **1989**, *82*, 169.

(123) Connelly, N. G.; Geiger, W. E. *Chem. Rev.* **1996**, *96*, 877.

(124) Paraskevopoulou, P.; Ai, L.; Wang, Q.; Pinnapareddy, D.; Acharyya, R.; Dinda, R.; Das, P.; Celenligil-Cetin, R.; Floros, G.; Sanakis, Y.; Choudhury, A.; Rath, N. P.; Stavropoulos, P. *Inorg. Chem.* **2010**, *49*, 108.

(125) Harris, D. C. I. Q. C. Q. *Quantitative Chemical Analysis*; 4th ed.; W. H. Freeman and Company: New York City, NY, 1995.

(126) Sluis, P. v. d.; Spek, A. L. *Acta Crystallogr., Sect. A* **1990**, *A46*, 194.

Chapter 3: Biomimetic Aerobic Oxidation of *N*-alkyl C-H Bonds by a Non-heme Iron(II) Catalyst

Section 3-1. Introduction

The ability to selectively transform C-H bonds to alternative organic functional groups remains an important and challenging problem.[1] The selective activation/functionalization of "unactivated" C-H bonds, specifically those found in aliphatic hydrocarbons, is particularly challenging because the C-H bond strengths of these moieties typically range from ~96 - 105 kcal/mol.[2] The selectivity of C-H bond activation is dictated by sterics, with the least hindered C-H bond being the most reactive, or bond strength trends, with tertiary C-H bonds being the most reactive and primary C-H bonds the least. The development of catalysts capable of "non-directed", selective, primary C-H bond oxidation, is an even more complex and challenging problem, as selectivity must be engendered by the catalyst's architecture.[3]

Research in the area of C-H activation catalysis has seen rapid growth in the past ten years.[4] This research surge has led to two generally accepted mechanistic pathways for achieving C-H activation, inner-sphere and outer-sphere. The inner-sphere C-H activation/oxidation mechanism (Scheme 3-1) is based on two separate steps. The first step involves transition metal insertion into a carbon-hydrogen bond to form an organometallic intermediate. The second step requires that the organometallic intermediate react with an external reagent (usually a chemical oxidant) to form the C-H functionalized product.

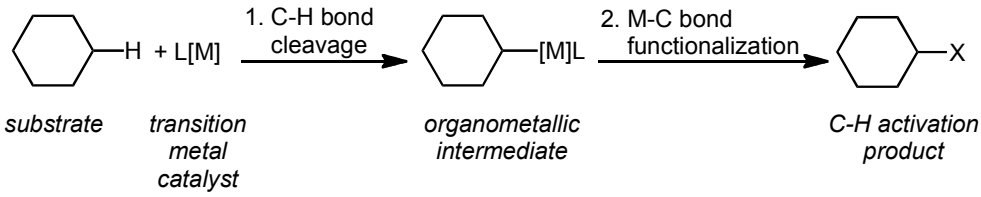

Scheme 3-1. An inner-sphere C-H activation reaction.

Transition metal catalysts capable of selective C-H activation by the inner-sphere mechanism have been realized. For example, an early report by Periana and co-workers demonstrated methane C-H activation using a simple platinum catalyst.[5] This catalyst (Scheme 3-2) remains the most efficient methane oxidation system, converting methane to methyl hydrogen sulfate in 90% yield. The selectivity in this system arises from the installation of the sulfonic acid group, rendering the product inert to subsequent oxidation. However, this catalytic system only functions under extreme reaction conditions (conc. H_2SO_4, T > 175 °C) and renders this system applicable to only very simple substrates.

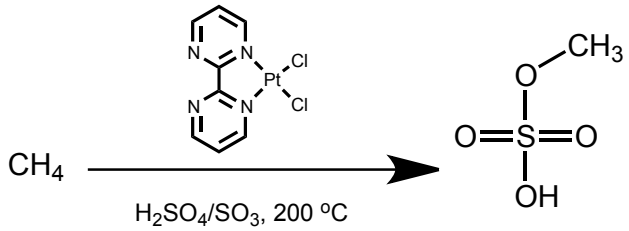

Scheme 3-2. Catalyst for methane C-H activation employed by Periana et al.

An alternative strategy for achieving selective C-H oxidation via an inner-sphere mechanism involves using substrates that contain directing groups (Scheme 3-3).[6] These directing groups interact with the transition metal catalysts via coordination, poising specific C-H bonds near the transition metal for activation. Sanford and co-workers have

recently employed this approach to achieve selective C-H acetoxylation in good yields using a simple palladium salt, $Pd(OAc)_2$, as the catalyst.[7-9]

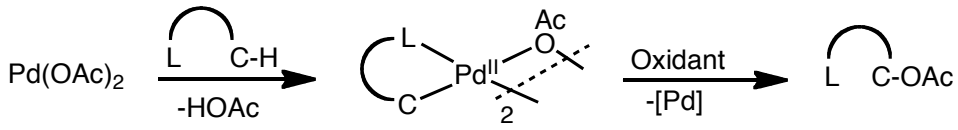

Scheme 3-3. Inner-sphere C-H oxidation that utilizes directing groups, as employed by Sanford et al.

In contrast to the inner-sphere mechanism, the first step of the outer-sphere C-H oxidation mechanism entails the formation of a reactive transition metal intermediate (Scheme 3-4). These intermediates are generated by reacting a reduced transition metal center (M^n) with a potent chemical oxidant (i.e., PhIO, $PhI(OAc)_2$, oxone, or permanganate) to form a high-valent (M^{n+2}) metal-oxidant intermediate. These high-valent intermediates are intriguing chemical species, as they are reminiscent of the proposed active intermediates in biological C-H activating enzymes, such as cytochrome P_{450} and methane monooxygenase. Once the metal-oxidant species is formed, it reacts with a C-H bond either by direct insertion or by a radical rebound mechanism (Scheme 3-4). The distinct feature of the outer sphere mechanism is that the metal center doesn't have to react directly with the substrate.

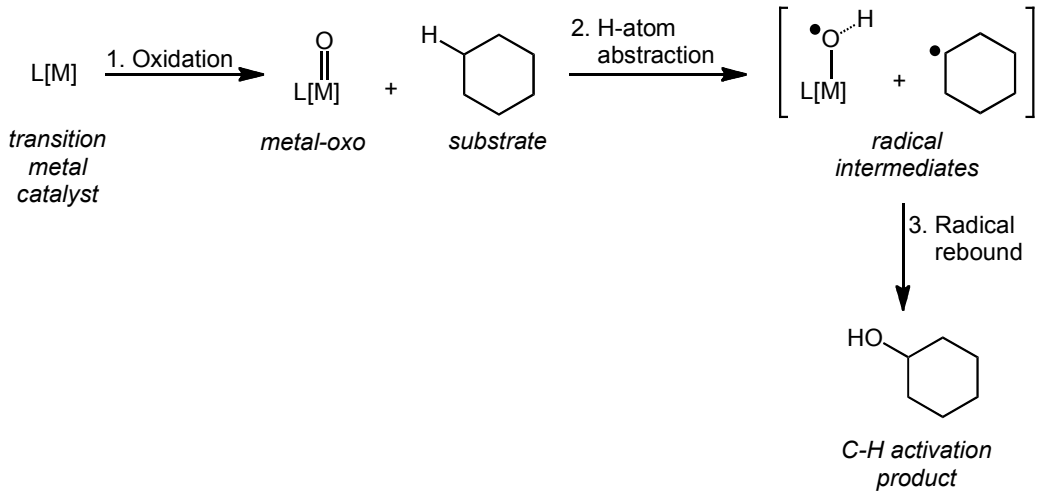

Scheme 3-4. Outer-sphere C-H bond activation reaction.

Metalloporphyrin complexes containing manganese, iron, cobalt, and ruthenium ions have been the most widely examined outer-sphere C-H oxidation catalysts.[10] These systems are appealing because porphyrin-type ligands are employed in a variety of C-H activating enzymes, such as cytochrome P_{450}. These catalytic systems, in general, show selectivity for relatively weak, or "activated", C-H bonds. Early synthetic work by Groves[11,12] has shown that it is possible to modify a porphyrin with a vaulted binapthyl capping-group to create a chiral pocket above the transition metal center that directs substrate approach through steric interactions to achieve asymmetric oxidation (Figure 3-1). This catalyst achieves slightly better selectivity than non-capped metalloporphyrin species.

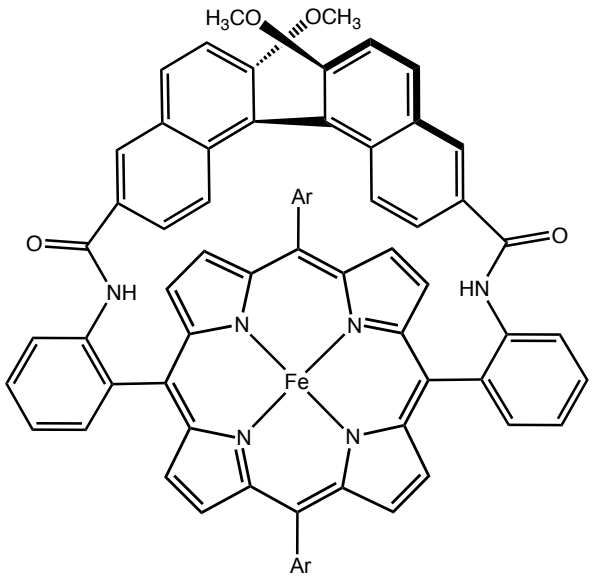

Figure 3-1: Binapthyl-capped metalloporphyrin employed by Groves et al. for C-H bond activation.

An alternative strategy for achieving selectivity in outer-sphere C-H oxidation reactions has been based on the use of noncovalent interactions (typically hydrogen bonding) to selectively position substrates prior to oxidation. Crabtree and Brudvig recently used this approach to design a dimanganese catalyst that uses a hydrogen bonding interaction between the substrate and the ligand backbone to achieve selective oxidation.[13] Though systems that utilize ligand architectures to achieve selective C-H oxidation through steric or noncovalent interactions demonstrate the power of this approach, catalysts based on these principles have not seen widespread application. One of major drawbacks of this approach is the difficulty associated with synthesizing and systematically modifying these complex ligand scaffolds.

Recent examples employing the inner-sphere and outer-sphere strategies of achieving selective C-H oxidation have led to significant advances in the field. Both

strategies, however, still have significant limitations. There remains a need to develop metal catalysts that function at mild temperatures and selectively oxidize strong, unactivated C-H bonds, such as those found in alkanes. In addition, catalysts that can use environmentally benign and readily available oxidants, like dioxygen, need to be identified.

Section 3-2. Background and Significance

Our group has been exploring new catalysts for bioinspired C-H activation reactions. We have been specifically interested in developing non-heme iron(II) catalysts that can hydroxylate C-H bonds. While iron is often used in biological systems for C-H hydroxylation, it has found very little use in synthetic oxidation chemistry until very recently.[14] Specifically, the White group reported a non-heme Fe(II) complex that exhibits mixed hydroxylation/desaturation activity with aliphatic C-H bonds, using peroxides as the oxidants. Though these results are promising, the products are highly substrate dependent and unpredictable.

In biological systems, cytochrome P_{450} activates C-H bonds through an outer-sphere mechanism that involves what is believed to be an Fe(IV)=O intermediate.[15] This intermediate is stabilized by a nitrogenous heme ligand as well as by hydrogen bonding in its secondary coordination sphere. This intermediate, specifically as it applies to the N-methyl C-H bond activation of anilines and amides, is believed to be primarily high-spin (S=2), as established through kinetic isotope effect studies and density functional theory (DFT).[16-18] Similarly, many of the non-heme iron enzymes that are capable of C-H

bond activation exist in a nitrogen-rich ligand environment and act through a high-spin, Fe(IV)=O intermediate.[19-23]

Until recently, most attempts to mimic the reactivity of these intermediates have involved synthesis of octahedral, Fe(II) complexes with S=1, which resulted in decreased activity towards substrate when compared to the enzymes.[24] DFT studies indicate that this decrease in reactivity is due to the low-spin state of the Fe(IV)=O, which should be less reactive than its S=2 counterpart.[25] Que hypothesized that a trigonal bipyramidal geometry would better stabilize an high-spin Fe(IV)=O moiety, due to the resulting degeneracy of the d_{xy} and $d_{x^2-y^2}$ orbitals, which makes spin pairing too energetically costly.[26]

Our group has been exploring the reactivity of Fe(II) complexes that utilize tripodal, tetraamine ligands for the activation of C-H bonds. To this end, our group has been exploring the coordination chemistry of C_3-symmetric triamidoamine ligand platforms, [N(*o*-PhNHC(O)R)$_3$] (where R = alkyl or aryl), derived from tris(2-aminophenyl)amine, N(*o*-PhNH$_2$)$_3$.[27-29] These highly modular platforms were designed to contain sterically encumbered and oxidatively robust cavities around potent transition metal oxidants. When formed, we envisaged using these rigid cavities to limit substrate approach through steric interactions. Reports from our laboratory have demonstrated that the R-groups of these ligand platforms can be tuned to achieve geometric control of ligand binding.[30] However, first row transition metal complexes that utilize these ligands typically exhibit high spin states and trigonal bipyramidal geometry. Recently, we have started exploring these ligands as platforms for biomimetic iron catalysis. Most relevant

to the work described herein, is the work on Fe(II) systems that can carry out bond activation processes with dioxygen.

The diiron(II) complex of the tris(isobutyrylamido)triphenylamine (H_3L^{iPr}) ligand[28] reacts with 2 eq. PhIO or 1 eq. O_2 to replace the methine proton of the ligand, forming the Fe(III)-alkoxide (Scheme 3-5).[31]

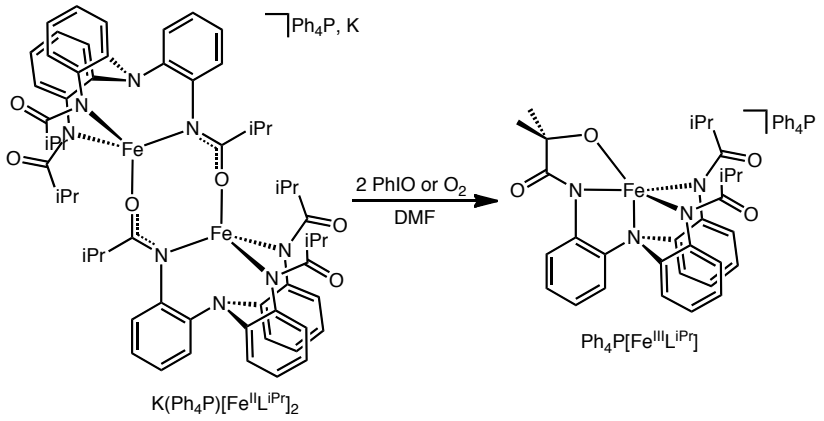

Scheme 3-5. Intramolecular C-H bond activation promoted by $K(Ph_4P)(FeL^{iPr})_2$.

This type of transformation is not unheard of, as activation of the methine C-H bond of the isopropyl group has been seen before in cobalt[32] and copper complexes.[33,34] However, it indicates that iron complexes of these trisamidate ligands are capable of effecting C-H bond activation. Though the mechanism of this process has not been determined, it is believed that it may proceed via a high-valent diiron intermediate that contains either μ-oxo or μ-hydroxo-bridging ligands, because either an oxygen transfer reagent or dioxygen can act as the oxidant.

In an attempt to effect intermolecular C-H bond oxidation by removing nearby oxidizeable C-H bonds, the iron(II) complex of the ligand $[N(o\text{-}PhNC(O)C_6F_5)_3]^{3-}$ (L^{F5}) was prepared.[35] Addition of oxidant (e.g. PhIO, O_2) to the resulting complex,

K[Fe(NCCH$_3$)L^{F5}], yields 0.5 eq. of an iron(III) aryloxide species that results from C-F bond oxidation of the ligand and 0.5 eq. K[Fe(F)L^{F5}] (Scheme 3-6).

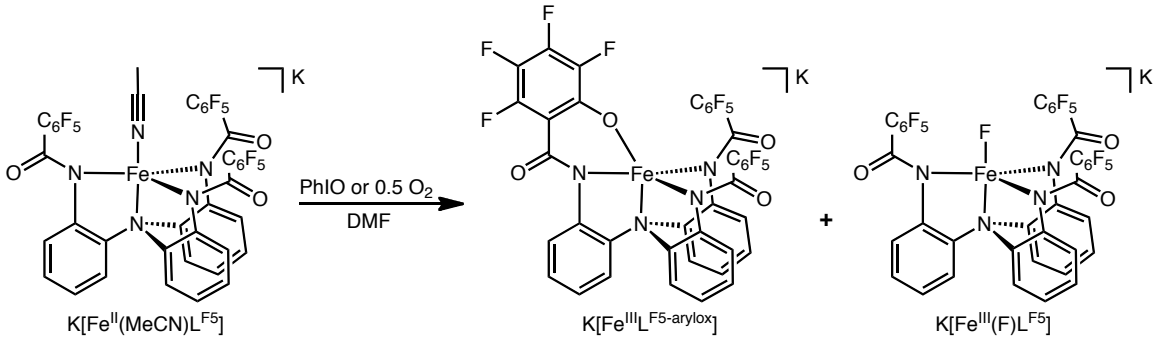

Scheme 3-6. Intramolecular C-F bond activation promoted by K[Fe(NCCH$_3$)(L^{F5})].

It was believed that this reaction could proceed through two different mechanisms. The first began with H-atom abstraction from solvent by a high-valent Fe=O followed by nucleophilic aromatic substitution by the corresponding alcohol, producing HF through radical rebound, which would react with a nearby molecule of starting material. The other option, as shown in Scheme 3-7, was that an Fe^{IV}=O is formed followed by intermolecular electron transfer with another molecule of K[Fe(NCCH$_3$)L^{F5}]. The iron(III)-oxide would then perform nucleophilic aromatic substitution on the ligand arm, releasing F$^-$, which would bind the other 0.5 eq. of Fe^{III}L^{F5}.

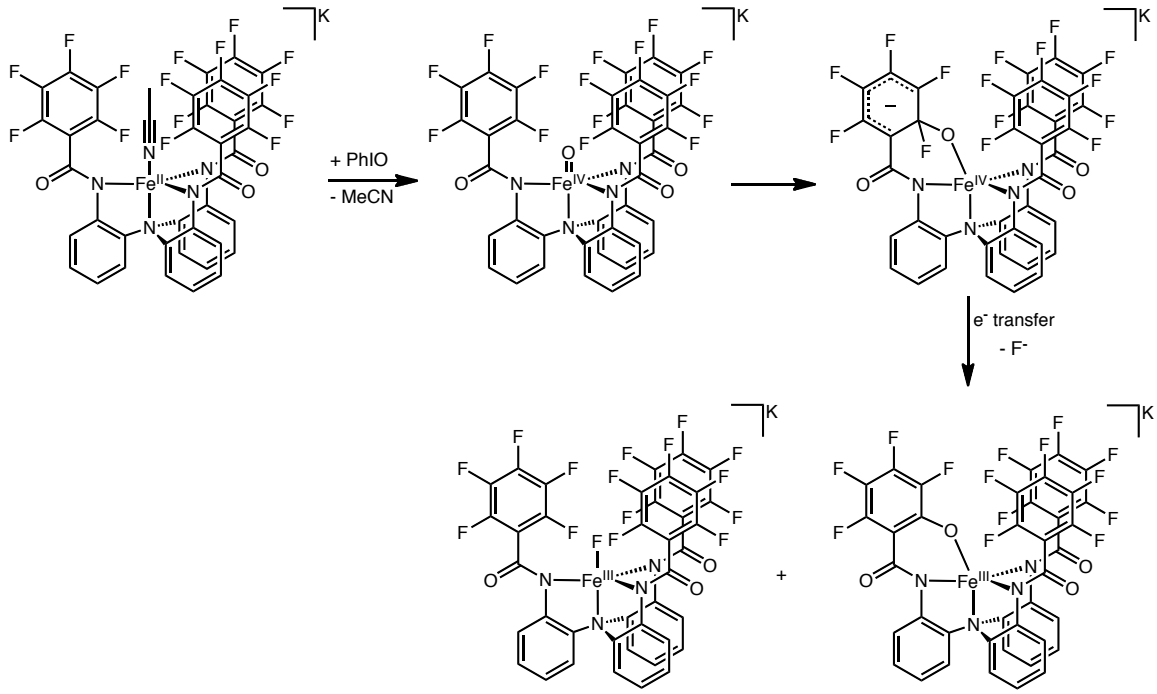

Scheme 3-7. Proposed mechanism for intramolecular C-F bond activation promoted by K[Fe(NCCH$_3$)(L^{F5})].

The product distribution of this reaction, the substantially more positive oxidation potential, and the fact that K[Fe(NCCH$_3$)L^{F5}] does not react with 9,10-dihydroanthracene, indicated that the reaction proceeded via the latter.[36] This was confirmed by titrating K[Fe(NCCH$_3$)L^{F5}] with a solution of PhIO and following the reaction by UV-visible absorption spectroscopy. The maximum absorbance for the reaction is consistently reached at 0.6 eq. PhIO, as shown in Figure 3-2, lending further support to a mechanism involving nucleophilic aromatic substitution without H-atom abstraction.

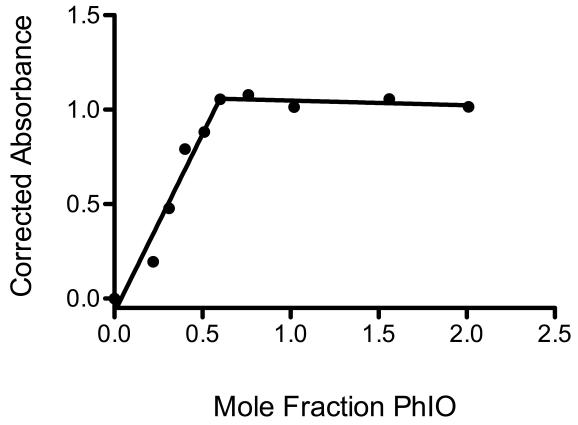

Figure 3-2. Corrected absorbance vs. mole fraction PhIO obtained from titration of an $NCCH_3$ solution of $K[Fe(NCCH_3)(L^{F5})]$ with an $NCCH_3$ solution of PhIO. The two lines intersect at a mole fraction of 0.6.

Analysis of the related complex, $K(Et_4N)[Fe(CN)(L^{F5})]$, reveals that this species exhibits an $E_{1/2}$ = -310 mV, which is 464 mV more positive than that of the complex $K(Et_4N)[Fe(CN)(L^{iPr})]$ ($E_{1/2}$ = -774 mV). Therefore, the change in the electronic character at the iron(II) center caused the proposed iron-oxo to react as a nucleophile in the presence of oxidant rather than an electrophile.

In summary, this work by Jones et al. demonstrates that a diiron(II) complex containing bridging amidate ligands can effect the intramolecular, aliphatic C-H activation of an isopropyl group using either an oxygen atom transfer reagent or O_2 as the oxidant. This study supports the hypothesis that chelating ligand scaffolds that incorporate amidate ligands are promising candidates for development of functional models of diiron(II) hydroxylase enzymes. It also indicates that the electronic character at the iron center greatly impacts the kind of reactivity that the complex displays. Therefore, to effect intermolecular C-H bond activation, it is necessary to prepare a

complex that is resistant to intramolecular oxidation reactions while maintaining an electron rich iron center.

Section 3-2. Results and Discussion

These results led to the hypothesis that a ligand with phenyl substituents would be more robust in the presence of strong oxidants than its alkyl counterpart. The stronger aryl C–H bonds should by less prone to abstraction by an intermediate, high-valent "Fe–oxygen" species, while maintaining the electrophilicity of the putative oxo.

The synthesis of the phenyl derivative of the $[(L^{R})]^{3-}$ ligand scaffold has been published.[37,38] The Fe(II) complex of the ligand, $Ph_4P[Fe(NCCH_3)(L^{Ph})]$, is synthesized using a route similar to those for the Co(II) and Ni(II) analogues of this type of ligand, and has been described.[27,35,38-40] The synthesis, as shown in Scheme 3-8, begins with deprotonation of the ligand, N(*o*-PhNCH(O)Ph)$_3$ (H_3L^{Ph}), using three equivalents of KH in DMF to afford its tripotassium salt. This species is then transmetallated with $Fe(OAc)_2$ to generate the potassium salt, $K[Fe(L^{Ph})]$, and afford two equivalents of KOAc. Salt metathesis using tetraphenylphosphonium bromide affords the more soluble salt, $Ph_4P[Fe(L^{Ph})]$. Extraction of the product into $NCCH_3$ and subsequent filtration allows for the removal of the potassium salt by-products. Recrystallization of the filtrate by diffusion of diethyl ether into an $NCCH_3$ solution containing the complex provides analytically pure $Ph_4P[Fe(NCCH_3)L^{Ph}]$ as bright yellow, X-ray quality crystals in good yield (74%). Use of dichloromethane (DCM) instead of $NCCH_3$ for the extraction, followed by recrystallization by diffusion of diethyl ether into a DMF solution of the

product yields analytically pure $Ph_4P[Fe(DMF)L^{Ph}]$ as bright yellow, X-ray quality crystals in moderate yield (57%).

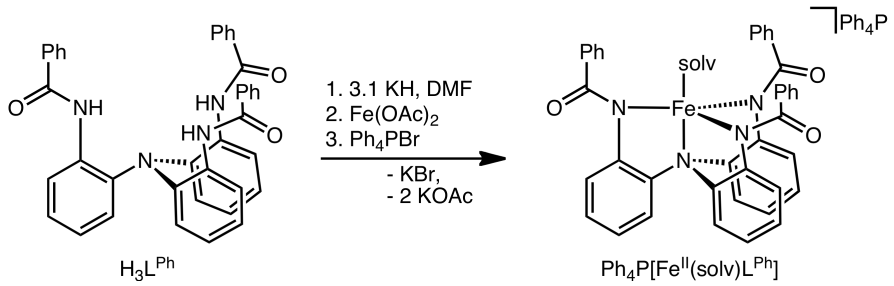

Scheme 3-8. Synthesis of $Ph_4P[Fe(solv)L^{Ph}]$.

The molecular structures of $Ph_4P[Fe(NCCH_3)L^{Ph}]$ and $Ph_4P[Fe(DMF)L^{Ph}]$, as determined by XRD, are shown in Figure 3-3 and feature five-coordinate Fe(II) centers in approximately trigonal bipyramidal geometry (τ_5 = 0.95 and 0.97, respectively).[41] In these complexes, the primary coordination sphere about the Fe(II) ion is made up of the three *N*-amidate donors of the ligand, with distances averaging 2.089(3) Å and 2.088(9) Å, respectively, from Fe1, which define the trigonal coordination plane (Table 3-1). The tertiary amine of the ligand backbone is coordinated to one of the axial positions, with a shorter Fe1-N1 distance for $Ph_4P[Fe(NCCH_3)L^{Ph}]$ than for $Ph_4P[Fe(DMF)L^{Ph}]$. This causes the iron to sit further above the plane formed by the equatorial nitrogen atoms in $Ph_4P[Fe(DMF)L^{Ph}]$. The second axial site contains the $NCCH_3$ or DMF solvent molecule.

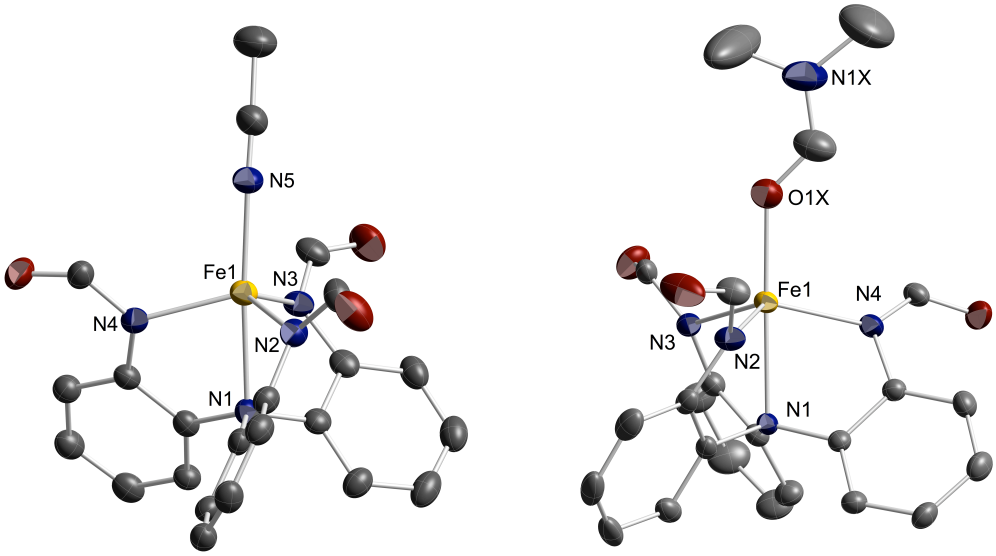

Figure 3-3: Solid-state structure of (left) $Ph_4P[Fe(NCCH_3)L^{Ph}]$ and (right) $Ph_4P[Fe(DMF)L^{Ph}]$. Thermal ellipsoids drawn at 40% probability. Hydrogen atoms, phenyl substituents, and countercations omitted for clarity.

Table 3-1: Selected bond lengths and angles for $Ph_4P[Fe(NCCH_3)L^{Ph}]$ (middle) and $Ph_4P[Fe(DMF)L^{Ph}]$ (right).

Bond Lengths (Å) and Angles (°)		
Fe1 – solv	2.089(5)	2.0025(16)
Fe1 – N1	2.229(4)	2.2456(16)
Ave. Fe1 – N_{eq}	2.089(3)	2.088(9)
Fe1 – Eq. Plane	0.491	0.506
N5 – Fe1 – N1	174.29(18)	178.24(6)
Ave. N_{eq} – Fe – N_{eq}	114.65(17)	114.09(4)
Ave. N_{eq} – Fe – N1	76.42(17)	75.72(3)

$Ph_4P[Fe(DMF)L^{Ph}]$ gives rise to a paramagnetically-shifted ^1H NMR spectrum that contains seven paramagnetic signals. These results suggest that the complex maintains an overall C_3-symmetric structure in solution. The solution-state magnetic moment was measured and indicates a μ_{eff} of 5.14 μ_B (the method of Evans, CD_2Cl_2, 25 °C), consistent with the assignment of a high-spin (S = 2) Fe(II) center. The electrochemical properties of $Ph_4P[Fe(NCCH_3)L^{Ph}]$ and its cyanide adduct have been investigated by cyclic voltammetry experiments.[35] The acetonitrile adduct does not display any significant or reversible electrochemical events within the DMF electrochemical solvent window, but the addition of cyanide ion to $Ph_4P[Fe(NCCH_3)L^{Ph}]$ gave rise to a reversible oxidation event centered at $E_{1/2}$ = -507 mV (ΔE_p = 81 mV V; i_{pc}/i_{pa} = 0.85) vs. Fc/Fc^+. This shift to more positive potentials relative to that observed for the cyanide adduct of $K(Ph_4P)[Fe(L^{iPr})]_2$ (-774 mV vs. Fc/Fc^+) is consistent with the change in acyl substituents from electron donating isopropyl groups to less electron donating phenyl groups. Also as expected, this oxidation potential is also shifted -197 mV from the cyanide adduct of $K[Fe(NCCH_3)L^{F5}]$.

When $Ph_4P[Fe(NCCH_3)L^{Ph}]$ is reacted with a stoichiometric amount PhIO in DMF at room temperature, an immediate color change from bright yellow to dark brown takes place over a short time period. The ESI mass spectrum of the reaction product exhibits a parent peak with m/z = 743.2 along with smaller peaks at m/z = 601.3 and 655.2, which correspond to the ligand and the starting iron complex, respectively (Figure 3-4). Single crystals were obtained in low yield (32.4%) from the reaction by diffusion of diethyl ether into a DMF solution of the dark brown product. The solid-state structure of the product reveals a trigonal bipyramidal iron complex, and the fifth coordination site

is occupied by a molecule that is the product of *N*-methyl C-H bond oxidation of DMF, (*N*-methylformamido)methanolate ((OMMF)$^-$). This ligand is disordered by rotation about the N5-C bond over two positions, with a distribution of 70:30. The complex, Ph_4P[Fe(OMMF)L^{Ph}], features an Fe1-O1 bond length of 1.844(10) Å, equatorial N-Fe1 distances that are slightly shorter than those in the starting material, and a slightly elongated Fe-N_{axial} distance, which is expected, as Fe1 sits further above the plane formed by the equatorial nitrogen atoms (Table 3-2).

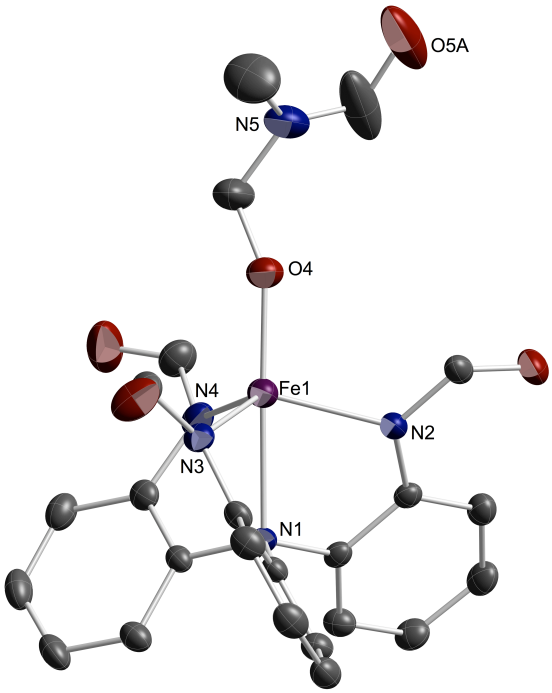

Figure 3-4. Molecular structure of Ph_4P[Fe(OMMF)L^{Ph}]. Thermal ellipsoids drawn at 40%. Hydrogen atoms, phenyl substituents, and the countercation are excluded for clarity.

Table 3-2. Selected bond lengths and angles for $Ph_4P[Fe(OMMF)L^{Ph}]$.

Bond Lengths (Å) and Angles (°)			
Fe1 – O1	1.844(10)	Ave. O1 – Fe – N_{eq}	104.7(9)
Fe1 – N1	2.251(2)	Ave. N_{eq} – Fe – N_{eq}	113.74(2)
Ave. Fe1 – N_{eq}	2.064(1)	Ave. N_{eq} – Fe – N_{ax}	75.24(8)
Fe1 – Eq. Plane	0.526	O1 – Fe – N1	177.6(3)

Due to the disorder and instability of the axial, hemiaminate ligand, the oxidation state of the metal ion was ambiguous. Magnetic susceptibility measurements of the complex were consistent with an high-spin iron(II) complex, but a solution of the complex exhibited a shoulder in the UV-visible absorption spectrum that was consistent with an iron(III) complex.[31] Due to this ambiguity in the oxidation state of the iron ion, an alternative method of synthesis was sought. Addition of *N*-hydroxymethyl-*N*-methylformamide (HMMF) to a solution of FeL^{Ph} resulted in decomposition of the transition metal complex, likely via protonation of the ligand. However, addition of LiOMMF to a solution of FeL^{Ph} followed by *in situ* chemical oxidation with one equivalent of $FcBF_4$ yielded a product with an m/z = 743.2, as shown in Figure 3-5B, and a similar UV-visible absorption spectrum (Figure 3-6), indicating that the product is $Ph_4P[Fe^{III}(OMMF)L^{Ph}]$.

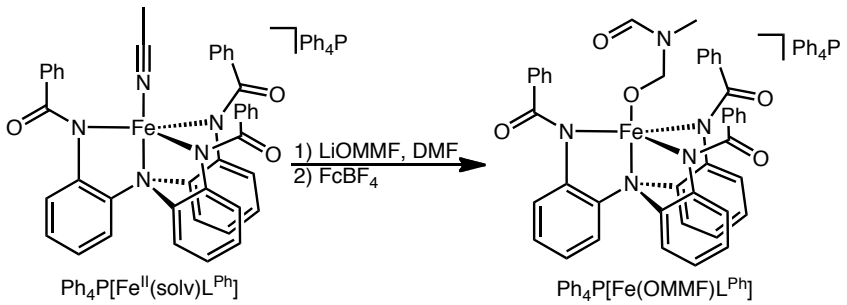

Scheme 3-9. Synthesis of $Ph_4P[Fe^{III}(OMMF)L^{Ph}]$ by *in situ* oxidation of $Li(Ph_4P)[Fe^{II}(OMMF)L^{Ph}]$ with $FcBF_4$.

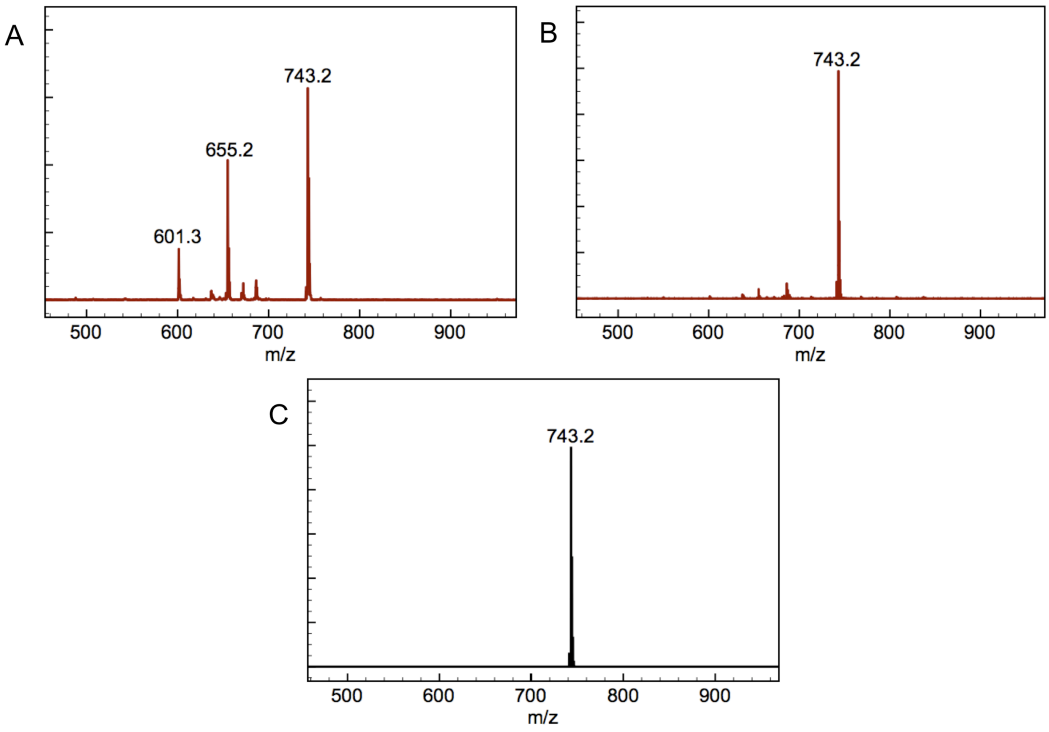

Figure 3-5. ESI-MS spectra of $Ph_4P[Fe(OMMF)L^{Ph}]$ prepared by (A) $Ph_4P[Fe(OMMF)L^{Ph}]$ prepared from oxidation of DMF with PhIO and (B) *in situ* oxidation of $(Ph_4P)_2[Fe^{II}(OMMF)L^{Ph}]$ with $FcBF_4$ and (C) calculated using mMass.[42,43]

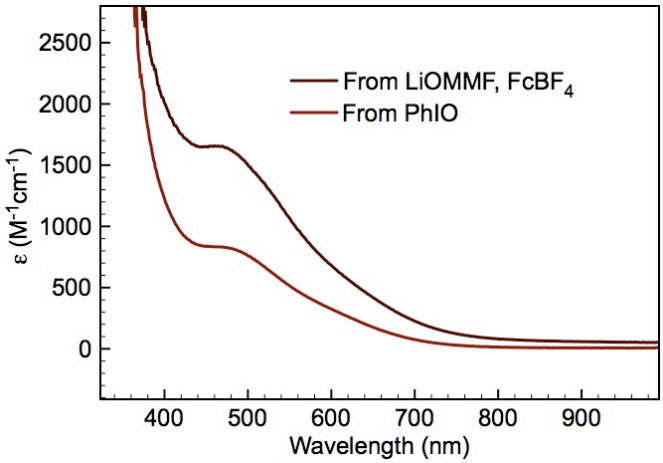

Figure 3-6. UV-visible absorption spectra of $Ph_4P[Fe(OMMF)L^{Ph}]$ prepared from oxidation of DMF with PhIO and *in situ* oxidation of $(Ph_4P)_2[Fe^{II}(OMMF)L^{Ph}]$ with $FcBF_4$.

Hemiaminals are implicated as intermediates in the reaction of amines and aldehydes yielding Schiff bases and in demethylation reactions in nature. Though unstable, there have been reports of trapping hemiaminals for structural characterization in macromolecules,[44] porous networks,[45] and enzymes.[46-49] Structurally characterized hemiaminals that are bound to transition metals are more common, where the hemiaminal is typically part of a chelating[50-52] or macrocyclic[53,54] ligand and is stabilized by chelation of the nitrogen atom to the transition metal. In contrast to the number of examples of chelating hemiaminal ligands, there is only one example of an unsupported hemiaminate bound to a transition metal ion. The complex, $W_2[OC(CF_3)_2NMe_2]_2(NMe_2)_4$, is a trapped intermediate in the aldol condensation of hexafluoroacetone with dimethylamine.[55]

In synthetic chemistry, DMF is commonly employed as a reagent in organometallic carbonylation reactions.[56-58] While detailed mechanistic studies of carbonylation reactions with DMF have not yet been carried out, these reactions are

proposed to proceed via initial activation of the aldehydic C-H bond to yield a carbamoyl intermediate followed by C-N bond breakage.[59] Support for this postulated pathway is provided by several crystal structures in which DMF activation at the aldehydic position has been observed.[60-62]

For example, when the monohydride, dihydrogen ruthenium complex $Ru(H)Cl(H_2)(P^iPr_3)_2$ was reacted with DMF at 80 °C over three hours, an isolable, seven-coordinate ruthenium carbamoyl species, $Ru(H)_2(\eta^2\text{-}C(O)NMe_2)Cl(P^iPr_3)_2$, was isolated and characterized by single crystal X-ray diffraction studies.[62] This reactivity profile is not unexpected, as adehydic C-H bond activation is commonly observed in the decarbonylation of aldehydes.[63] Because aldehydic bond activation is facile and reversible at transition metal centers, molecules containing aldehydic C-H bonds are unlikely to undergo C-H activation processes at other sites within the substrate.

Only recently has a C-H activation at an *N*-methyl group of DMF been observed. In 2009, Bercaw and co-workers reported the C-H activation of an *N*-methyl group in DMF by an iridium complex.[64] The C-H activated product was characterized by single X-ray diffraction studies. This unusual species was trapped by coordination to an iridium(III) center.

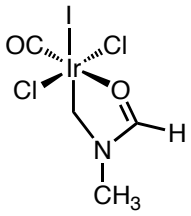

Figure 3-7. $[Ir(CO)\eta^2\text{-}CH_2N(CH_3)CHO)Cl_2I]^{1-}$ prepared by Bercaw and co-workers.[64]

The iridium complex, $[Ir(CO)(\eta^2\text{-}CH_2N(CH_3)CHO)Cl_2I]^{1-}$, (Figure 3-7) was isolated as a trace impurity during the synthesis of $[AsPh_4][Ir(CO)_2I_3Me]$ from the decarbonylation of DMF by $IrCl_3 \cdot 3H_2O$ in the presence of NaI. While the origin of the *N*-methyl activated product is a mystery, the authors speculate that the impurity must arise from trace impurities of DMF.

N-alkyl oxidation is an important type of reactivity for a number of biological systems. For example, *N*-alkyl oxidation has been proposed in the metabolic break down of DMF by cytochrome P_{450} in both humans and rats. The function of most cytochrome P_{450} enzymes is to catalyze the oxidation of organic substrates using dioxygen and electrons from either NADPH or NADH. A schematic of the proposed mechanism for this process is shown in Scheme 3-10.

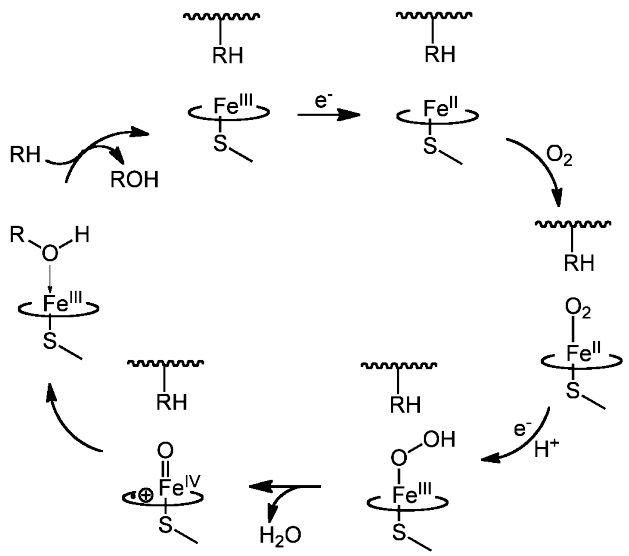

Scheme 3-10. Catalytic cycle for oxygen activation and hydroxylation of C-H bonds by cytochrome P_{450}.[15]

Dioxygen binds to the Fe(II) center of cytochrome P_{450}. It is reduced to the peroxide, then loses water to form the active ferryl-oxo unit with a ligand-based radical. This can

then perform hydrogen atom abstraction followed by radical rebound, generating an Fe(III) species. The alcohol is lost, and the catalyst is regenerated.

One class of cytochromes P450 does this regio- and stereoselectively, oxidizing compounds like steroids or fatty acids for their synthesis or degradation. Another class of cytochromes P_{450} is less selective, catalyzing the oxidation of foreign organic molecules, like those from solvents or drugs, which are then further broken down for excretion.[65] When humans and other mammals are exposed to DMF, it is believed that it is broken down in the liver as shown in Scheme 3-11.[66-69]

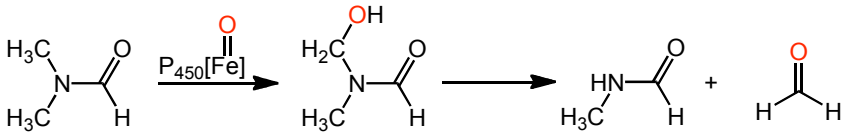

Scheme 3-11. Metabolites of DMF breakdown by cytochrome P_{450}.

The DMF molecule is first hydroxylated by cytochrome P_{450} to form *N*-hydroxymethyl-*N*-methylformamide (HMMF). This molecule is unstable and loses formaldehyde to form *N*-methylformamide (NMF). Both HMMF and NMF are seen in urine after human exposure. Another metabolite of DMF is *N*-acetyl-*S*-(*N*-methylcarbamoyl)cysteine (AMCC). AMCC is likely produced upon oxidation of NMF to methylisocyanate and subsequent reaction with glutathione. Despite the fact that these species have been quantified in urine by liquid and gas chromatography and by ^{1}H NMR, there have been no reports that verify the structure of the initial oxidation reaction—that of DMF being hydroxylated by cytochrome P_{450}.[70-74]

N-alkyl oxidation is also an important reaction carried out by DNA repair enzymes. The alkylation of nucleic acids can be mutagenic and cytotoxic. This process

occurs when exogenous or endogenous reagents cause an S_N2 alkylation at the N1 position of adenine and guanine or the N3 position of thymine or cytosine. In *Escherichia coli*, the enzyme responsible for repair of this damage to DNA is AlkB (in humans, the homologues are ABH2 and ABH3), an iron-containing dioxygenase. The consensus mechanism (Scheme 3-12) begins with Fe(II) binding α-ketoglutarate, followed by oxidative addition of dioxygen. The dioxygen is cleaved, releasing CO_2, resulting in a ferryl-oxo species. This reactive intermediate abstracts a proton from the alkyl residue followed by radical rebound, to generate an Fe(II)-succinate species and the hydroxylated nucleic acid. The latter, a hemiaminal, is unstable, and it spontaneously loses formaldehyde, yielding the repaired nucleic acid.[75]

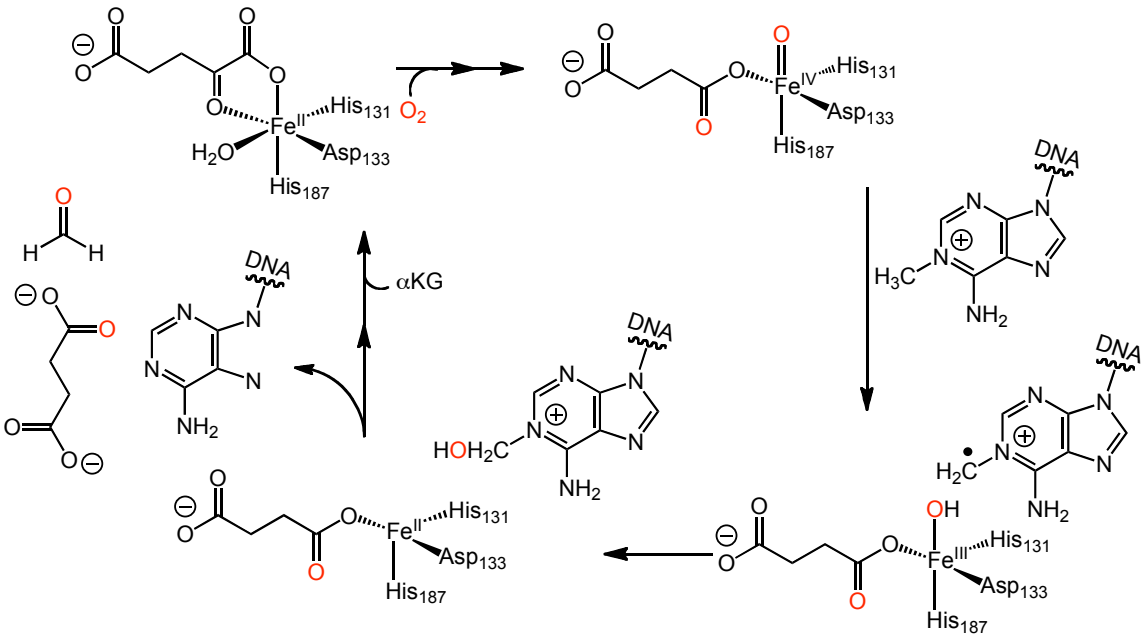

Scheme 3-12. Catalytic cycle for α-ketoglutarate-dependent enzyme AlkB.

Though several structures of AlkB, both bound to DNA and substrate, exist[75-80], it was only recently that Yi et al. reported crystal structures of AlkB with the active

intermediate, the hemiaminal, present in the active site.[46] These structures were obtained through *in situ* exposure of crystalline enzyme, substrate, and α-ketoglutarate to dioxygen. Their results indicate that a zwitteranionic hemiaminal is formed prior to loss of formaldehyde.

A number of groups have attempted to mimic the activity of iron-containing enzymes like cyctochrome P_{450} and AlkB, since both of these enzymes are known to catalyze the oxidation of amides at the alpha position of nitrogen to yield the corresponding hemiaminal. However, examples of these types of oxidations in synthetic chemistry are far less common. Murahashi and co-workers have explored the oxidation of tertiary amines and cyclic amides with ruthenium complexes using alkyl peroxides as the terminal oxidant.[81,82] In a subsequent study, this group showed that they could use peracids, generated *in situ* for the reaction of aldehydes with molecular oxygen, to carry out the oxidation of β-lactams. This catalytic method is currently used industrially (ca. 100 tons per year) to produce key intermediates in the synthesis of carbapenem antibiotics. When tertiary amines are used as substrates, Murahashi has demonstrated that the iminium ion intermediates formed in these reactions can be trapped with carbon pronucleophiles such as cyanide to form the corresponding α-substituted nucleophiles (Scheme 3-13).[83]

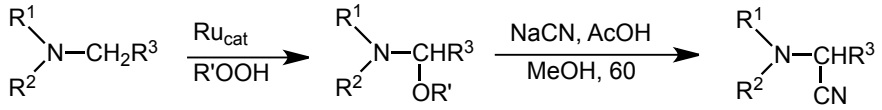

Scheme 3-13. Formation of α-substituted nucleophiles from tertiary amines.

When the oxidation of $Ph_4P[Fe(NCCH_3)L^{Ph}]$ is carried out in DMF under catalytic conditions (i.e. excess oxidant) HMMF and its decomposition product, *N*-

methylformamide, are detected spectrometrically (LC-MS), and the yields of HMMF are consistent with catalytic turnover (TON = 9 mol HMMF/mol catalyst). The catalytic oxidation of DMF by $Ph_4P[Fe(NCCH_3)L^{Ph}]$ represents an unprecedented transformation in synthetic chemistry.

To probe the mechanism of the catalytic reaction, we performed non-competitive, intermolecular, isotopic labeling studies. The catalytic reaction was performed in side-by-side reactions using DMF and DMF-d_7. The [HMMF] in the samples was determined by analyzing for NMF using gas chromatography, as HMMF converts to NMF at the high temperature of the inlet (230 °C). These studies yielded a kinetic deuterium isotope effect (KDIE = k_H/k_D) of 4.4. This value is higher than the non-competitive, intermolecular KDIE's exhibited by cytochrome P_{450} but within the known range of KDIE's for the cytochrome P_{450}-catalyzed *N*-demethylation of amides (KDIE = 2-7)[84] and similar to that observed for cytochrome P_{450}-catalyzed *N*-methyl oxidation of DMF (KDIE = 4-6).[85] The large value of the non-competitive, intermolecular KDIE indicates that the mechanism involves hydrogen atom abstraction from the *N*-methyl fragment of DMF.[86] Furthermore, the fact that this transformation occurs by hydrogen atom abstraction lends evidence for a high-valent iron-oxo intermediate, which abstracts the hydrogen, followed by radical rebound to form HMMF. This may occur through an intramolecular or an intermolecular mechanism. The proposed mechanisms for the catalytic hydroxylation of an *N*-methyl C-H bond of DMF are shown in Scheme 3-14.

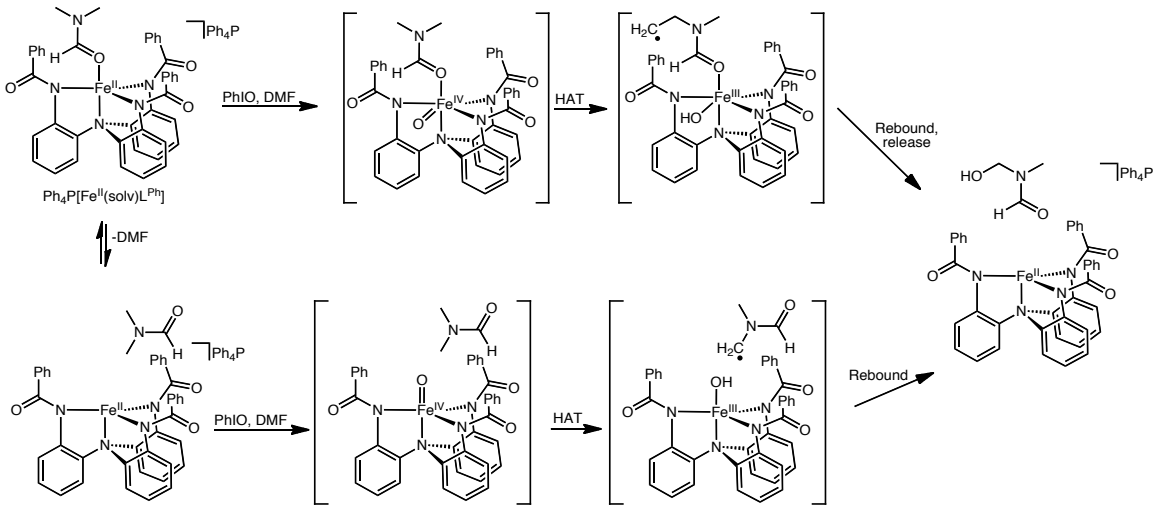

Scheme 3-14. Proposed mechanisms for intermolecular *N*-alkyl C-H bond activation of DMF catalyzed by $Ph_4P[Fe(NCCH_3)L^{Ph}]$.

The first step of the proposed intramolecular mechanism and second step of the proposed intermolecular mechanism includes the formation of a high-valent iron-oxo complex. The oxygen may coordinate either in an equatorial position, while the DMF remains bound, or the DMF may dissociate, and the oxygen binds in the open apical position. The reactive oxo ligand would then abstract a hydrogen atom from DMF. Radical rebound would yield HMMF and regenerate the catalyst. Notably, this also implies that $Ph_4P[Fe(OMMF)L^{Ph}]$ is only a byproduct of the reaction, which explains the consistently low yield of this species from the reaction with iodosobenzene.

To probe the effect of varying the electronic character of the catalyst on the TON of the catalytic reaction, the iron(II) complexes, $Ph_4P[Fe(NCCH_3)L^{OMe}]$ and $Ph_4P[Fe(NCCH_3)L^{F2}]$ (L^{OMe} = $[N(o\text{-}PhNC(O)(p\text{-}OMePh))_3]^{3-}$ and L^{F2} = $[N(o\text{-}PhNC(O)(3,5\text{-}C_6H_3F_2))_3]^{3-}$), were prepared. These complexes could both be prepared in a similar manner to $Ph_4P[Fe(NCCH_3)L^{Ph}]$ in 59% and 63% yield, respectively.

$Ph_4P[Fe(NCCH_3)L^{OMe}]$ gives rise to 8 paramagnetically shifted peaks in the ^1H NMR (CD_3CN, 400 MHz), indicating that the complex is C_3-symmetric in solution. A peak at 2.06 ppm indicates that the complex is the $NCCH_3$ solvento adduct. This is confirmed by an FT-IR (KBr) stretch at 2253 cm^{-1}, which is consistent with bound $NCCH_3$. A μ_{eff} = 5.57 μ_B (the method of Evans, CD_3CN, 400 MHz) indicates that the iron(II) ion is high spin (S = 2). The ESI-mass spectrum of the complex in the negative mode displays a parent peak with m/z = 745.6, which is consistent with $(FeL^{OMe})^-$. The electrochemical properties of $Ph_4P[Fe(NCCH_3)L^{OMe}]$ were explored by cyclic voltammetry. This complex exhibits an oxidation event centered at $E_{1/2}$ = -581 mV (ΔE_P = 79 mV; i_{pc}/i_{pa} = 1.58) vs. Fc/Fc^+, as well as an irreversible, cathodic event at -725 mV.

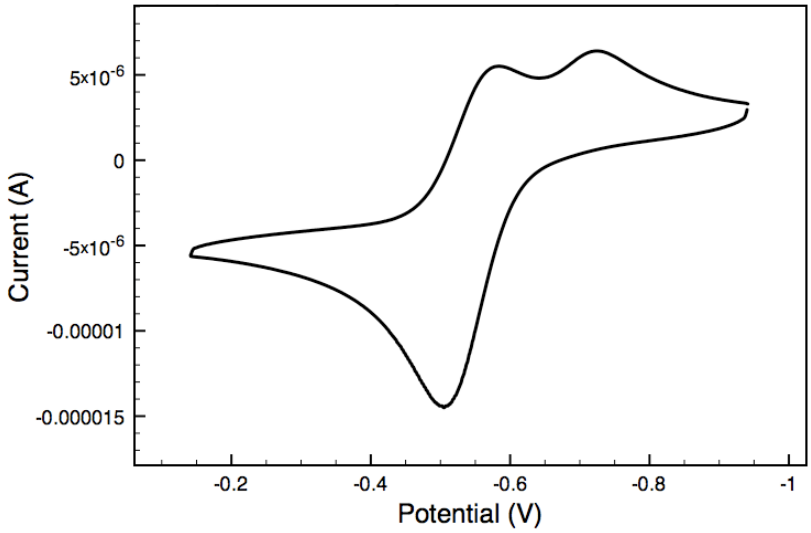

Figure 3-8. Cyclic voltammogram of $Ph_4P[Fe(solv)L^{OMe}]$. In DMF at a scan rate of 50 mV/s with 0.15 M $TBAPF_6$ as the supporting electrolyte, a glassy carbon working electrode, and Ag/Ag^+ as the reference electrode.

Crystallization by diffusion of diethyl ether into an $NCCH_3$ solution of the complex yields single crystals that are suitable for X-ray diffraction. The molecular structure of $Ph_4P[Fe(NCCH_3)L^{OMe}]$ is shown in Figure 3-9.

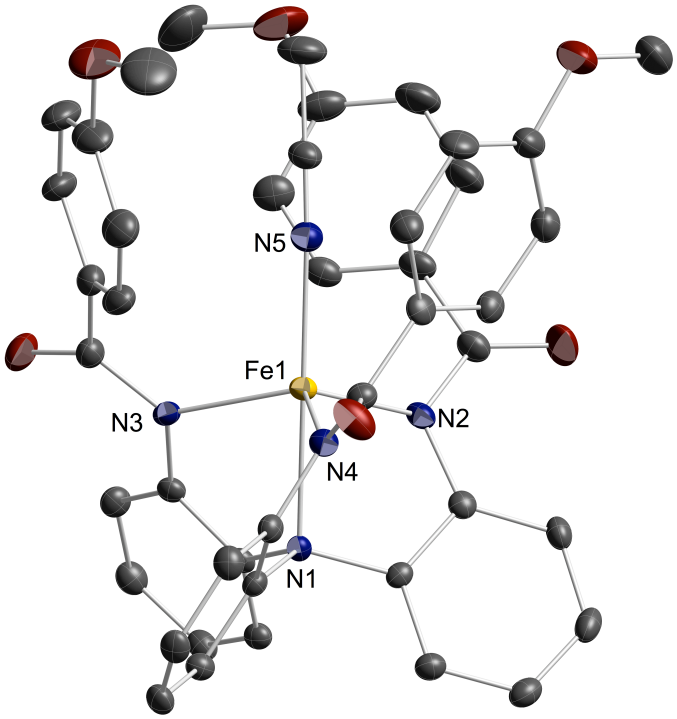

Figure 3-9. Molecular structure of $Ph_4P[Fe(NCCH_3)L^{OMe}]$. Thermal ellipsoids drawn at 40%. Hydrogen atoms and the countercation are excluded for clarity.

Table 3-3. Selected bond lengths and angles for $Ph_4P[Fe(NCCH_3)L^{OMe}]$.

Bond Lengths (Å) and Angles (°)			
Fe1 – N1	2.240(2)	Ave. N1 – Fe – N_{eq}	76.36(5)
Ave. Fe1 – N_{eq}	2.097(2)	Ave. N_{eq} – Fe – N_{eq}	114.61(6)
Fe1 – N5	2.116(3)	N1 – Fe1 – N5	177.29(9)
Fe1 – Eq. Plane	0.495		

$Ph_4P[Fe(NCCH_3)L^{OMe}]$ has slightly longer Fe1-N_{eq} bond lengths than the phenyl substituted analoges. The Fe-N1 distance as well as the distance that the iron sits above the plane formed by the equatorial nitrogen atoms fall in between those reported for $Ph_4P[Fe(NCCH_3)L^{Ph}]$ and $Ph_4P[Fe(DMF)L^{Ph}]$. This is likely because $Ph_4P[Fe(NCCH_3)L^{OMe}]$ has a more electron rich metal center, that can interact more with the $NCCH_3$ ligand through π-backbonding, resulting in a shorter bond length to the $NCCH_3$ than in $Ph_4P[Fe(NCCH_3)(L^{Ph})]$.

To determine if the TON could be increased using a more electron-rich iron complex, the catalytic reaction was carried out using $Ph_4P[Fe(NCCH_3)L^{OMe}]$ as the catalyst. This does not increase the TON of the reaction (TON = 7). The slight decrease in TON for $Ph_4P[Fe(NCCH_3)L^{OMe}]$ when compared to $Ph_4P[Fe(NCCH_3)L^{Ph}]$ indicates that $Ph_4P[Fe(NCCH_3)L^{OMe}]$ may be subject to decomposition via protonation of the ligand faster than $Ph_4P[Fe(NCCH_3)L^{Ph}]$.

The negative mode ESI-mass spectrum of $Ph_4P[Fe(NCCH_3)L^{F2}]$ exhibits a parent peak with m/z = 763.4, which is consistent with the formulation $(FeL^{F2})^-$. The peak at the stretching frequency 2250 cm^{-1} in the FT-IR spectrum (KBr) indicates that the complex, like $Ph_4P[Fe(NCCH_3)L^{OMe}]$ and $Ph_4P[Fe(NCCH_3)L^{Ph}]$ is the $NCCH_3$ adduct. The ^1H NMR spectrum (CD_3CN, 400 MHz) displays 5 paramagnetically shifted peaks, which indicates that $Ph_4P[Fe(NCCH_3)L^{F2}]$ is C_3-symmetric in solution. This is further evidenced by the ^{19}F NMR spectrum (CD_3CN, 400 MHz), which contains only 1 peak. The μ_{eff} = 4.97 μ_B (the method of Evans, CD_3CN, 400 MHz), which is consistent with an high spin (S = 2), iron(II) center. The electrochemical properties of this species were also explored using cyclic voltammetry. Unlike $Ph_4P[Fe(NCCH_3)L^{OMe}]$, $Ph_4P[Fe(NCCH_3)L^{F2}]$ does not

display any reversible events within the DMF solvent window. However, addition of excess tetraethylammonium cyanide to the solution of $Ph_4P[Fe(NCCH_3)L^{F2}]$ yields a cyclic voltammogram that does exhibit a reversible oxidation event centered at $E_{1/2}$ = -524 mV (ΔE_p = 94 mV; i_{pc}/i_{pa} = 1.14) vs. Fc/Fc^+, as shown in Figure 3-10.

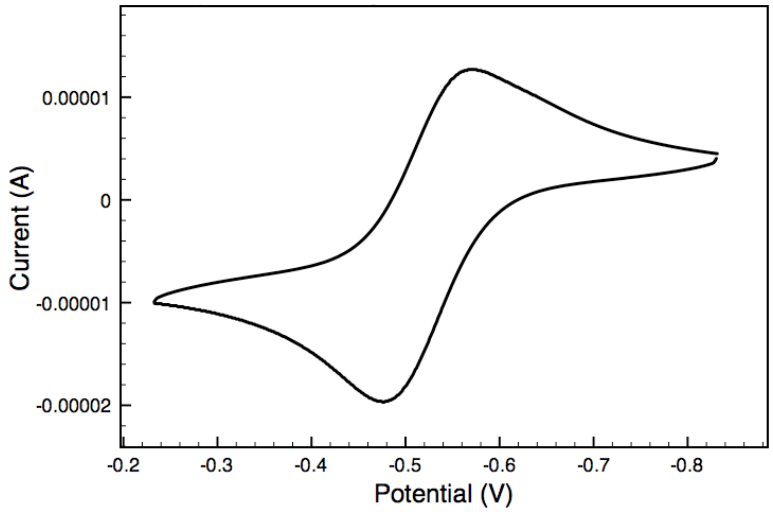

Figure 3-10. Cyclic voltammogram of $Ph_4P(Et_4N)[Fe(CN)L^{F2}]$. In DMF at a scan rate of 50 mV/s with 0.15 M $TBAPF_6$ as the supporting electrolyte, a glassy carbon working electrode, and Ag/Ag^+ as the reference electrode.

Single crystals of $Ph_4P[Fe(NCCH_3)L^{F2}]$ suitable for X-ray diffraction were grown by diffusion of diethyl ether into a 1:1 DMF:$NCCH_3$ solution of the complex. The molecular structure, as determined by X-ray diffraction, of $Ph_4P[Fe(NCCH_3)L^{F2}]$ is shown in Figure 3-11.

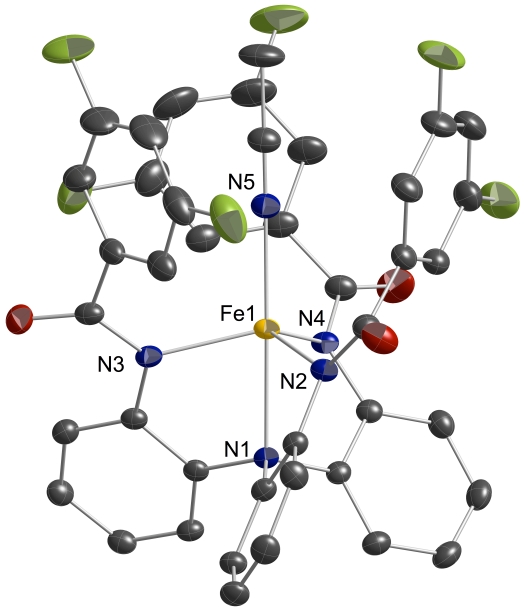

Figure 3-11. Molecular structure of $Ph_4P[Fe(NCCH_3)L^{F2}]$. Thermal ellipsoids drawn at 40%. Hydrogen atoms, the residual diethyl ether solvent molecule, and the countercation are excluded for clarity.

Table 3-4: Selected bond lengths and angles for $Ph_4P[Fe(NCCH_3)L^{F2}]$.

Bond Lengths (Å) and Angles (°)			
Fe1 – N1	2.2428(14)	Ave. N1 – Fe – N_{eq}	76.90(3)
Ave. Fe1 – N_{eq}	2.0915(9)	Ave. N_{eq} – Fe – N_{eq}	115.01(3)
Fe1 – N5	2.1303(16)	N1 – Fe1 – N5	176.99(6)
Fe1 – Eq. Plane	0.474		

In the solid-state, $Ph_4P[Fe(NCCH_3)L^{F2}]$ exhibits slightly distorted trigonal bipyramidal geometry (τ_5 = 0.99).[87] The iron - equatorial nitrogen distances average 2.0915(9) Å, which is slightly shorter than the complex' electron-rich analogues, and cause the iron to sit nearer the plane formed by the equatorial nitrogen atoms. The iron – apical nitrogen distances are, in turn, slightly longer than in the electron-rich analogues.

Due to the fact that $Ph_4P[Fe(NCCH_3)L^{Ph}]$ decomposes via protonation of the ligand by HMMF, it was hypothesized that the decrease in pK_a supplied by $Ph_4P[Fe(NCCH_3)L^{F2}]$ may discourage deprotonation of HMMF and allow for a higher TON. However, the change in the electronic nature of the iron center makes the intermediate iron oxo less electrophilic and, therefore, less reactive towards H-atom abstraction, resulting in fewer turnovers (TON = 4).[36]

To probe the effect of decreasing the steric bulk of the catalyst on the TON, the iron(II) complexes $Ph_4P[Fe(DMF)L^{CF3}]$ and $Ph_4P[Fe(L^{Me})]$ were prepared.[88]

$Ph_4P[Fe(DMF)L^{CF3}]$ is prepared by a similar procedure to the iron(II) complexes previously described and the previously described $[K(DMA)][Fe(DMA)L^{CF3}]$ (DMA = *N*,*N*-dimethylacetamide) and $[K(NCCH_3)][Fe(NCCH_3)L^{CF3}]$.[40] Recrystallization by diffusion of diethyl ether into an $NCCH_3$ solution of the product affords X-ray quality crystals in 64% yield. This complex exhibits an *m*/*z* in the negative mode of it's mass spectrum of 631.0, which is consistent with the formation of the monoanionic $[Fe(L^{CF3})]^-$. The ^1H NMR spectrum (CD_3CN) displays only two broad singles in the paramagnetic region, two broad singlets in the diagmagnetic region at 3.05 and 3.22 ppm, corresponding to the bound DMF, and two peaks corresponding to tetraphenylphosphonium. There is only one singlet in the ^{19}F NMR spectrum, indicating that this complex is C_3-symmetric in solution. The electrochemical properties of $Ph_4P[Fe(DMF)L^{CF3}]$ were investigated by cyclic voltammetry. As shown in Figure 3-12, this complex gives rise to a quasi-reversible oxidation event centered at $E_{1/2}$ = -56 mV (ΔE_p = 135 mV; i_{pc}/i_{pa}^{-1} = 1.40) vs. Fc/Fc^+.

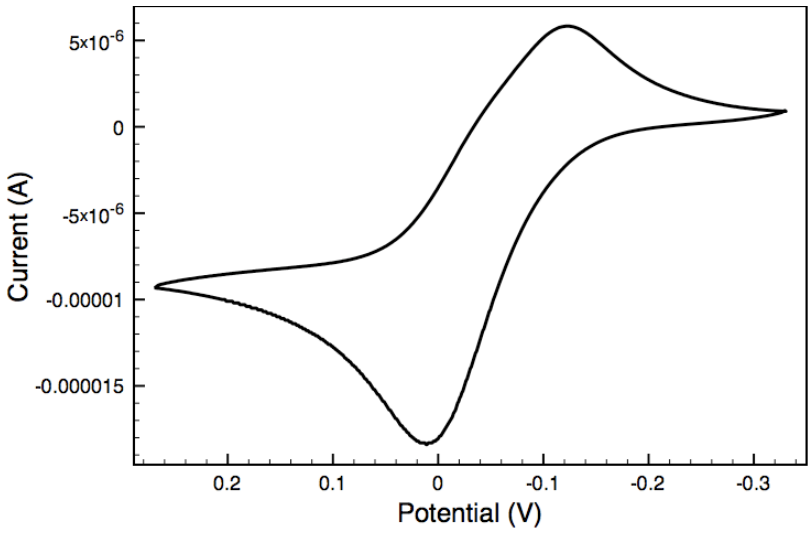

Figure 3-12. Cyclic voltammogram of $Ph_4P[Fe(solv)L^{CF3}]$. In DMF at a scan rate of 10 mV/s with 0.15 M $TBAPF_6$ as the supporting electrolyte, a glassy carbon working electrode, and Ag/Ag^+ as the reference electrode.

This oxidation potential is the highest of the iron(II) oxidation potentials discussed herein, which is expected, as $(L^{CF3})^{3-}$ is the most electron-withdrawing of the ligands utilized for this study. The fact that a reversible electrochemical event was observed for this species was somewhat surprising, as the analogous complexes, $[K(DMA)][Fe(DMA)L^{CF3}]$ and $[K(NCCH_3)][Fe(NCCH_3)L^{CF3}]$, did not exhibit reversible electrochemical events in DMA and DMF, respectively.[40] These complexes did, however, exhibit irreversible, anodic events at E_{pa} = 13 and 17 mV, respectively, which is similar to the anodic feature at E_{pa} = 12 mV exhibited by $Ph_4P[Fe(DMF)L^{CF3}]$ in DMF.

A single crystal of $Ph_4P[Fe(DMF)L^{CF3}]$ was analyzed by XRD, and the solid-state structure is shown in Figure 3-13.

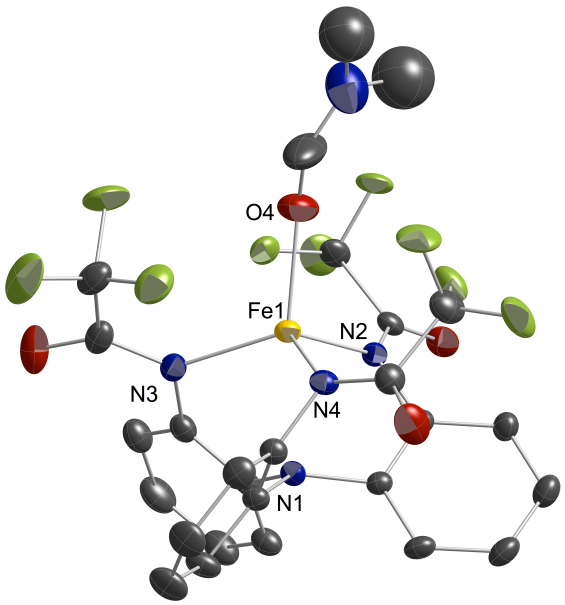

Figure 3-13. Molecular structure of $Ph_4P[Fe(DMF)L^{CF3}]$. Except for the *N*-methyl carbon atoms of the bound solvent, which were refined isotropically, thermal ellipsoids drawn at 40%. Hydrogen atoms, -CF_3 disorder, and the countercation are excluded for clarity.

Table 3-5. Selected bond lengths and angles for $Ph_4P[Fe(DMF)L^{CF3}]$.

Bond Lengths (Å) and Angles (°)			
Fe1•••N1	2.3557(19)	Ave. N1 – Fe – N_{eq}	73.00(4)
Ave. Fe1 – N_{eq}	2.112(1)	Ave. N_{eq} – Fe – N_{eq}	111.79(4)
Fe1 – N5	2.058(2)	N1•••Fe1 – N5	172.93(8)
Fe1 – Eq. Plane	0.618		

The solid-state structure of $Ph_4P[Fe(DMF)L^{CF3}]$ reveals a trigonal pyramidal geometry about the iron center ($\tau_4 = 0.92$).[89] The bound DMF molecule exhibits disorder in the *N*-methyl moieties that was not refined. The *N*-methyl carbon atoms were, therefore, left isotropic. Fe1 interacts with the apical nitrogen atom from a distance of

2.3557(19) Å, which is 0.1 Å longer than the Fe1-N1 bond in the related complex, $Ph_4P[Fe(DMF)L^{Ph}]$. The Fe1-O4 bond length is also longer than the Fe1-O1S bond in $Ph_4P[Fe(DMF)L^{Ph}]$. Finally, the equatorial nitrogen atoms bind Fe1 with an average length which is longer than the average Fe1-N_{eq} bond length in $Ph_4P[Fe(DMF)L^{Ph}]$.

Use of $Ph_4P[Fe(DMF)L^{CF3}]$ as the catalyst does not increase the TON. Rather, the TON matches that of $Ph_4P[Fe(NCCH_3)L^{F2}]$ (TON = 4). Conversely, the TON obtained when $Ph_4P[Fe(L^{Me})]$ is used as the catalyst matches that of $Ph_4P[Fe(NCCH_3)L^{Ph}]$ (TON = 9).

Single crystals of $Ph_4P[Fe(L^{Me})]$ were not obtained. However, the FT-IR spectrum of this complex does not match that of the ligand precursor. Though the symmetric and asymmetric N-H stretches of the ligand (i.e. 3425 and 3314 cm^{-1}) are no longer present, there are less intense peaks at lower frequency in the N-H stretching region (i.e. 3238 and 3181 cm^{-1}) that may indicate the presence of some incompletely deprotonated ligand. The ^1H NMR spectrum of the crude material in CD_3CN shows 23 signals in the range of -8 – 58 ppm that do not correspond to starting material, countercation, or residual solvent. This indicates that the reaction product does not exhibit C_3 symmetry in solution and, furthermore, may exist in equilibrium between the possible coordination isomers shown in Figure 3-14, which is similar to what has been observed before in cobalt(II), nickel(II), and zinc(II) complexes of this ligand.[88,90]

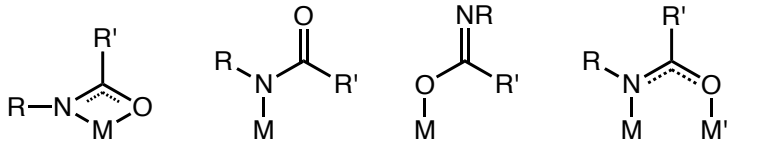

Figure 3-14. Possible coordination modes of amidate donors.

The electrochemical properties of the cyano adduct of the Fe(II) complex were explored by cyclic voltammetry. Though the reaction product does not exhibit any reversible oxidation events in the DMF solvent window, the cyclic voltammogram of crude cyano adduct displays a reversible oxidation event, as shown in Figure 3-15, with $E_{1/2}$ = -746 mV (ΔE_p = 50 mV; i_{pc}/i_{pa}^{-1} = 1.36) vs. Fc/Fc^+. This oxidation potential is, as expected, slightly higher than that of $Ph_4P(Et_4N)[Fe(CN)L^{iPr}]$ and more negative than that of all the other complexes previously discussed.

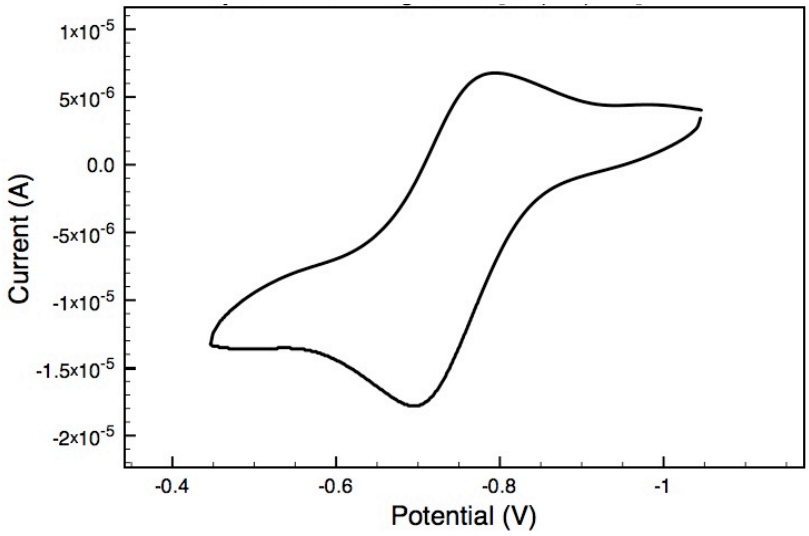

Figure 3-15. Cyclic voltammogram of $Et_4N(Ph_4P)[Fe(CN)L^{Me}]$. In DMF at a scan rate of 50 mV/s with 0.15 M $TBAPF_6$ as the supporting electrolyte, a glassy carbon working electrode, and Ag/Ag^+ as the reference electrode.

The ESI mass spectrum of the product of the reaction between H_3L^{Me}, KH, and $Fe(OAc)_2$ in DMF does not show the calculated parent ion peak. However, if a solution of the crude complex is exposed to air, the resulting negative mode ESI mass spectrum (Figure 3-17A) displays peaks with *m/z* = 955.2 and 1293.3, which are consistent with what is expected for the $[M+1]^-$ and $[M+Ph_4P]^-$ peaks, respectively, of an oxo-bridged,

Fe(III):Fe(III) dimer. This spectrum also displays a peak at m/z = 477.6, which is consistent with an hydroxo-bridged, Fe(III):Fe(II) dimer, as well as a peak with an m/z = 496.6, which is consistent with the potassium salt of an oxo-bridged, Fe(III):Fe(II) dimer, both with an overall charge of -2.

The *in situ* reaction of H_3L^{Me} with 3.1 equivalents KH, 1 eq. $Fe(OAc)_2$, 1 eq. Ph_4PBr and 1 eq. O_2, followed by filtration and recrystallization from diffusion of diethyl ether into a DMF solution of the dark brown product yielded crystals suitable for X-ray diffraction. The solid state structure of the product, as shown in Figure 3-16, reveals an oxo-bridged, Fe(III):Fe(III) dimer, $(Ph_4P)_2[(FeL^{Me})_2\mu\text{-}O]$.

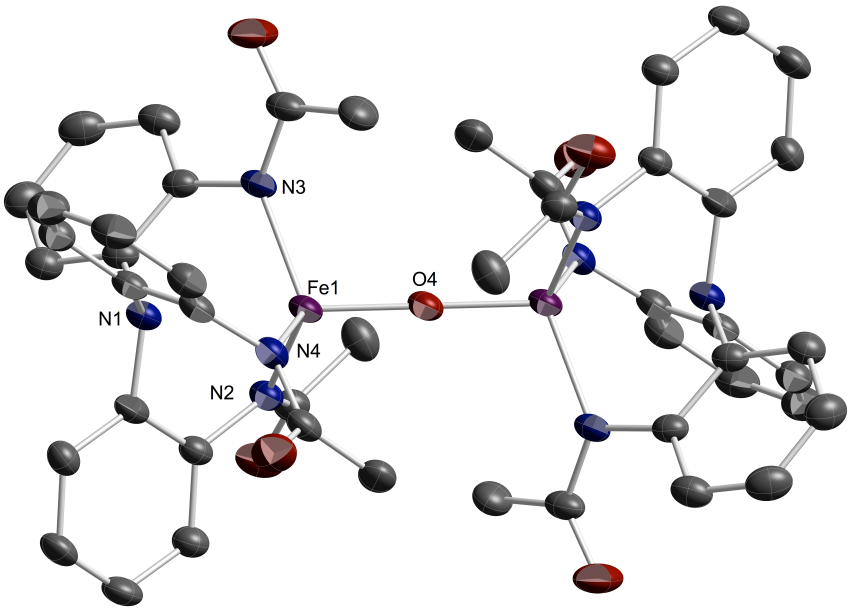

Figure 3-16. Molecular structure of $(Ph_4P)_2[(FeL^{Me})_2\mu\text{-}O]$. Thermal ellipsoids drawn at 40%. Hydrogen atoms and the countercation are excluded for clarity.

Table 3-6. Selected bond lengths and angles for $(Ph_4P)_2[(FeL^{Me})_2\mu\text{-}O]$.

Bond Lengths (Å) and Angles (°)			
Fe1•••N1	2.431(3)	Ave. O1 – Fe – N_{eq}	107.25(4)
Ave. Fe1 – N_{eq}	2.022(2)	Ave. N_{eq} – Fe – N_{eq}	111.59(6)
Fe1 – O4	1.7992(6)	Fe1 – O4 – Fe1	180
Fe1 – Eq. Plane	0.600		

$(Ph_4P)_2[(FeL^{Me})_2\mu\text{-}O]$ crystallizes in the space group P-1, with O4 as the inversion center of the two symmetry-equivalent FeL^{Me} fragments. The complex has four-coordinate, distorted tetrahedral (τ_4 = 0.97) geometry,[89] and the iron sits 0.600 Å out of the plane formed by the equatorial nitrogen atoms. The apical nitrogen, N1, interacts with the iron(III) center from a distance of 2.431(3) Å. The equatorial nitrogen atoms bind the iron center with distances shorter than those in $Ph_4P[(Fe(OMMF)L^{Ph}]$. The Fe1-O4 distance Å is shorter than the Fe-alkoxide oxygen in $Ph_4P[(Fe(OMMF)L^{Ph}]$, and, due to its position on a center of symmetry, the Fe1-O4-Fe1 angle is 180°.

This species displays an *m/z* = 477.1 (negative mode ESI-MS, Figure 3-17B), corresponding to the molecular weight divided by the charge, -2. This spectrum also contains the aforementioned peaks at *m/z* = 955.2 and 1293.3, which correspond to $[M+1]^-$ and $[M+Ph_4P]^-$, respectively. This indicates that exposure of a solution of the putative $[FeL^{Me}]^-$ to O_2 results in the formation of the $[(Fe^{III}L^{Me})_2\mu\text{-}O]^{2-}$, and exposure to water (from air) yields the mixed valent, $[(Fe^{III}L^{Me})(\mu\text{-}OH)(Fe^{II}L^{Me})]^{2-}$.

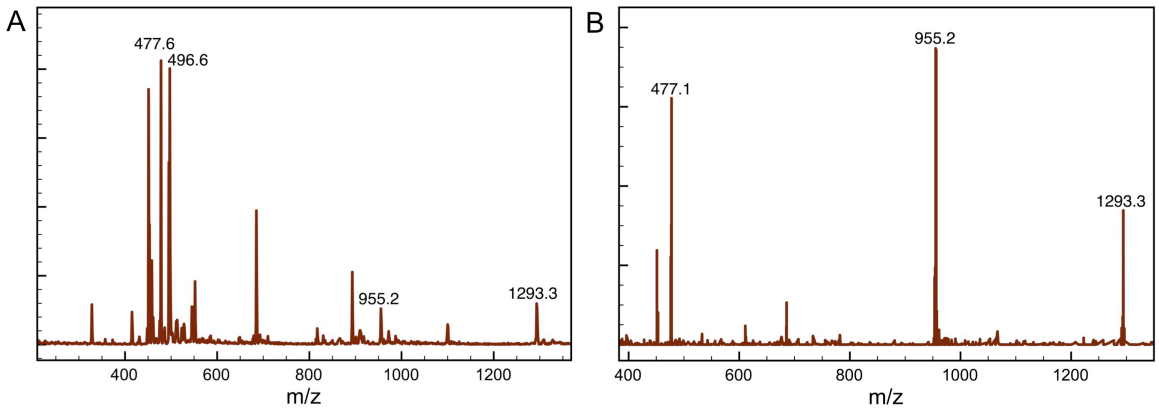

Figure 3-17. Negative mode ESI-MS spectra for (A) a DMF solution of the crude reaction product from mixing H_3L^{Me} with 3.1 eq. KH, 1 eq. $Fe(OAc)_2$, and 1 eq. Ph_4PBr that has been exposed to air and (B) a DMF solution of crystalline $(Ph_4P)_2[(FeL^{Me})_2\mu\text{-}O]$.

The ^1H NMR spectrum contains peaks that are in the diamagnetic region but significantly broadened, which is consistent with a high-spin, Fe(III) complex that is strongly antiferromagnetically coupled.[91,92] Magnetic susceptibility measurements (μ_{eff} = 1.7 μ_B/Fe; the method of Evans) and UV-visible absorbtion spectroscopy confirm this assignment. The UV-visible absorption spectrum of $(Ph_4P)_2[(FeL^{Me})_2\mu\text{-}O]$ displays absorption maxima corresponding to the O → Fe charge transfer at 378 and 469 nm (ε = 5157 and 5378 $M^{-1}cm^{-1}$, respectively). This spectrum is similar to previously reported, high-spin, LFe^{III} - O - $Fe^{III}L$ complexes.[93]

In situ preparation of the iron(II) precursor followed by oxidation with 0.5 eq PhIO and recrystallization from diffusion of diethyl ether into a DMF solution of the dark brown product yields material in 82% yield that has identical UV-visible absorption maxima (Figure 3-18) and FT-IR spectra to the product obtained by oxidation with O_2, indicating that $(Ph_4P)_2[(FeL^{Me})_2\mu\text{-}O]$ is the product of oxidation by O_2 or PhIO.

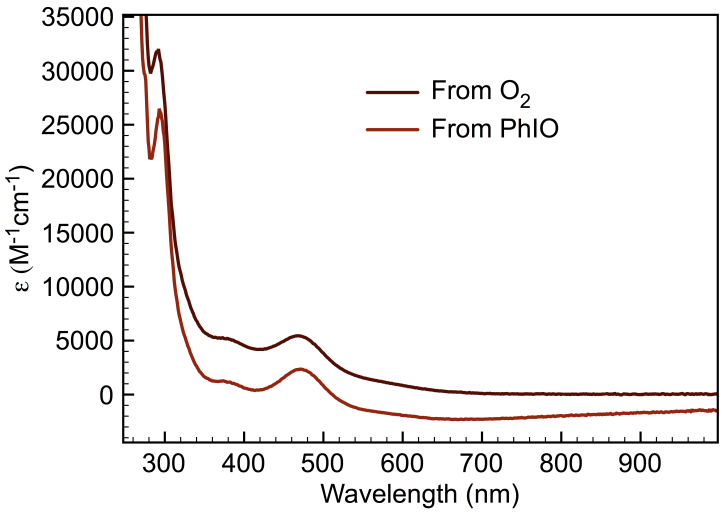

Figure 3-18. UV-visible absorption spectra of $(Ph_4P)_2[(FeL^{Me})_2\mu\text{-}O]$ prepared *in situ* from O_2 and PhIO.

Lastly, to confirm that $(Ph_4P)_2[(FeL^{Me})_2\mu\text{-}O]$ was not a product of the deprotonation of water by unreacted KH, the product of the reaction between H_3L^{Me}, KH, $Fe(OAc)_2$ and Ph_4PBr was isolated as a crude, tan powder, then reacted with 0.5 equivalents PhIO or O_2. The products were recrystallized and isolated in the same manner as the *in situ* reaction products. Their UV-visible absorption spectra matched those of the *in situ* products, indicating that water was not the oxygen source.

Despite the fact that these two methods yield the same isolable product, addition of excess O_2 does not result in catalytic formation of HMMF as the addition of excess PhIO does. This result is consistent with the fact that addition of excess O_2 to a solution of $Ph_4P[Fe(NCCH_3)L^{Ph}]$ does not result in formation of HMMF.

To determine the substrate scope of *N*-alkyl C-H oxidation that is catalyzed by $Ph_4P[Fe(NCCH_3)L^{Ph}]$, the reaction was explored with various substrates. Addition of PhIO and 0.04 eq $Ph_4P[Fe(NCCH_3)L^{Ph}]$ (relative to PhIO) to 5 mL *N*,*N*-diethylformamide

yields a product that has a t_{ret} = 1.68 and *m/z* = 118.1 (LC-MS), consistent with the formulation *N*-ethyl-*N*-(1-hydroxyethyl)formamide. The LC-MS of the reaction product also indicates the presence of *N*-ethylformamide (t_{ret} = 0.753, *m/z* = 74.2), the result of decomposition of *N*-ethyl-*N*-(1-hydroxyethyl)formamide by loss of acetaldehyde. The result of hydroxylation of a methyl C-H bond, *N*-ethyl-*N*-(2-hydroxyethyl)formamide (t_{ret} = 1.14 min), was not present in the LC-MS.

Addition of PhIO and 0.04 eq. $Ph_4P[Fe(NCCH_3)L^{Ph}]$ (relative to PhIO) to a 9:1 cyclohexane: *N*-methyl-2-piperidone solution results in formation of an hydroxylated product (*m/z* = 130) that does not have the same retention time (t_{ret} = 1.32 min) as the anticipated *N*-hydroxymethyl-2-piperidone (t_{ret} = 1.93 min) or the demethylated, 2-piperidone (t_{ret} = 1.78 min) (LC-MS). Therefore, the likely product of the oxidation is *N*-methyl-6-hydroxy-2-piperidone.

To determine if this catalyst could hydroxylate larger molecules, caffeine was explored as a substrate. Mixture of caffeine, PhIO, and 0.04 or 0.1 eq $Ph_4P[Fe(NCCH_3)L^{Ph}]$ in dichloromethane or acetonitrile does not result in oxidation of caffeine, as evidenced by the lack of change in the ^1H NMR spectrum of the reaction products after removal of solvent. The substrate 9,10-dihydroanthracene was also tested under similar conditions. The ^1H NMR spectrum of the reaction products after solvent removal also showed no change. This may support the hypothesis that pre-association of the substrate may be necessary for the catalytic reaction to proceed.

Section 3-3. Conclusion

The results presented herein demonstrate the isolation of a stable transition metal-hemiaminate species and the catalytic hydroxylation of DMF in the N-alkyl position by a non-heme iron complex. Isotope labelling studies indicate that the mechanism of this reaction is similar to that of the N-demethylation of amides and the N-methyl oxidation of DMF by cytochrome P_{450}, both of which are believed to involve hydrogen atom abstraction from the N-methyl moiety as the rate-limiting step. These results demonstrate that by tuning the electronic character of the carboxamide substituent of the ligand and removing nearby oxidizeable C-H bonds, a catalyst capable of intermolecular C-H bond activation was obtained. The position of C-H bond activation on small substrates (i.e. DEF, *N*-methyl-2-piperidone) and the lack of reaction with larger substrates (i.e. caffeine, 9,10-dihydroanthracene) indicates that this may be directed C-H bond activation.

Section 3-4. Experimental Section

General Considerations and Materials

All manipulations were carried out using standard Schlenk techniques or conducted in an MBraun Labmaster 130 drybox under a nitrogen atmosphere. All reagents used were purchased from commercial vendors and used as received unless otherwise noted. Anhydrous solvents were purchased from Sigma-Aldrich and further purified by sparging with Ar gas followed by passage through activated alumina columns. *N*-methylformamide (NMF) was purchased from Sigma-Aldrich, dried over molecular sieves, and distilled under reduced pressure prior to use. Deuterated NMR solvents were purchased from Cambridge Isotope Laboratories, Inc. and degassed and

dried according to standard procedures prior to use.[94] Elemental analyses were performed either by Midwest Microlab, LLC, Indianapolis, IN or Atlantic Microlab, Inc., Norcross, GA. ^{1}H and ^{13}C NMR spectra were recorded on either an Inova 400 MHz or a Varian Mercury 300 MHz spectrometers at ambient temperature. Chemical shifts were referenced to residual solvent peaks. Infrared spectra were recorded as KBr pellets on a Varian Scimitar 800 Series FT-IR spectrometer. Solution-state magnetic moments were measured using the the method of Evans.[95,96] Mass spectra were recorded in the Mass Spectrometry Center at Emory University on a JEOL JMS-SX102/SX102A/E mass spectrometer. LC-MS experiments were performed on an Agilent Technology 1200 Series LC-MS. For LC-MS determination of HMMF formation a 150 mm C18 Agilent XDB column and a mobile phase of 0.1% formic acid in water were used. The products of the catalytic reactions with *N*,*N*-diethylformamide and *N*-methyl-2-piperidone were analyzed using a 50 mm C18 Agilent XDB column with a mobile phase gradient of 10-95% methanol over 3 minutes. Gas chromatograph determination of [NMF] was performed on a Shimadzu GC-2014 with a 30 m x 0.25 mm x 0.25 μm ZB-WAX column connected to a flame ionization detector heated to 250 °C. The injector injector temperature was 230 °C. The column was heated to 60 °C for 1 min then 30 °C/min to 120 °C for 1 min then 20 °C/min to 220 °C and held for 5 mins, with a constant total flow of He carrier gas of 2.1 mL/min and split ratio of 1. All samples were diluted with dichloromethane containing an internal standard of *N*,*N*-diethylformamide. All samples containing catalyst were passed through a silica plug after dilution with the internal standard solution. The ligand, N(*o*-PhNHC(O)Ph)$_3$ (H_3L^{Ph}) was prepared using a previously published procedure.[29] *N*-hydroxymethyl-*N*-methylformamide (HMMF), *N*-(1-

hydroxyethyl)-*N*-ethyl formamide, *N*-(2-hydroxyethyl)-*N*-ethyl formamide, and *N*-hydroxymethyl-2-piperidone were prepared by published literature procedures.[97-100]

Syntheses

2,2',2''-Trismethylamidotriphenylamine (H_3L^{Me}). A suspension of N(*o*-$PhNH_2$)$_3$ (1.70 g, 5.85 mmol) in dichloromethane (DCM, 150 mL) was lowered to 0 °C under an atmosphere of N_2. Triethylamine (2.90 mL, 21.1 mmol) was then added to the suspension, followed by acetyl chloride (1.40 mL, 19.3 mmol). The mixture was stirred for 30 minutes, allowed to warm to room temperature, and stirred overnight. The resulting yellow solution was washed with saturated sodium bicarbonate solution (3 x 50 mL) and distilled water (3 x 50 mL), dried over magnesium sulfate, filtered, and concentrated *in vacuo*. The resulting white powder was collected and rinsed with hexanes. Crystals of the product were obtained by layering pentane onto a concentrated DCM solution and cooling to -40 °C (1.30 g, 53%). ^{1}H NMR (δ, $CDCl_3$, 400 MHz): 8.12 (br s, 3H, NH), 7.69 (br s, 3H), 7.12 (t, 3H, *J* = 7.2 Hz, ArH), 7.05 (td, 3H, *J* = 8.0, 1.6 Hz, ArH), 6.82 (d, 3H, *J* = 8.0 Hz, ArH), 1.75 (s, 9H, MeH). ^{13}C NMR (δ, $CDCl_3$, 400 MHz): 169.27, 138.57, 131.45, 126.57, 125.85, 125.35, 124.73, 23.51. HRESI-MS: $C_{24}H_{24}O_3N_4Na$ m/z $[M+Na]^+$ Calcd. 439.17540 Found 439.17434. FTIR (KBr, cm^{-1}): ν(NH) 3425, 3314, ν(CO) 1692; 3111, 3062, 2937, 1672, 1594, 1534, 1490, 1443, 1368, 1308, 1232, 1044, 1016, 763, 592, 471.

$Ph_4P[Fe^{II}(DMF)L^{Ph}]$. To a solution of H_3L^{Ph} (143.7 mg, 0.238 mmol) in dimethylformamide (DMF, 5 mL), potassium hydride (31.6 mg, 0.787 mmol) was added

as a solid. After stirring 2.75 hrs, $Fe(OAc)_2$ (41.4 mg, 0.238 mmol) was added to the yellow solution as a solid followed by Ph_4PBr (102.3 mg, 0.244 mmol). After stirring the mixture for one additional hour, DMF was removed *in vacuo* to yield a yellow solid. This solid was dissolved in dichloromethane (CH_2Cl_2, 10 mL), yielding a yellow solution and colorless precipitate (KBr and KOAc). The mixture was filtered to remove the precipitate (67.1 mg, 88.5%). The filtrate was then concentrated to dryness *in vacuo*. The product was recrystallized by the slow diffusion of diethyl ether into a DMF solution, yielding yellow blocks of the desired product (146.7 mg, 57.6%). ^{1}H NMR (δ, CD_2Cl_2, 400 MHz): 113.72, 57.89, 34.53, 17.81, 13.50, 11.71, 10.13, 7.45 (s), 7.20 (s), 6.99 (s). UV-vis (CH_2Cl_2): λ_{max}, nm (ε, M^{-1} cm^{-1}): 231 (55565), 269 (25976), 296 (20292). ESI-MS (*m/z*) for $[Fe(L^{Ph})]^{1-}$ ($C_{39}H_{27}FeN_4O_3$) calcd 655.1; found 655.3. FTIR (KBr, cm^{-1}): ν(CO) 1659; 3058, 2973, 2931, 2869, 1596, 1556, 1474, 1442, 1349, 1238, 1108, 1041, 997, 929, 755, 723, 690, 527. μ_{eff} = 5.14 μ_B (the method of Evans, CD_2Cl_2, 400 MHz). (Anal. Calcd (found) for $Ph_4P[Fe(DMF)L^{Ph}]\bullet Et_2O$: C, 73.61 (73.58); H, 5.65 (5.76); N, 6.13 (6.26).

$Ph_4P[Fe^{II}(NCCH_3)L^{OMe}]$. To a solution of H_3L^{OMe} (303.2 mg, 0.438 mmol) in dimethylformamide (DMF, 6 mL), KH (54.6 mg, 1.361 mmol) was added as a solid. After stirring 1.5 hrs, $Fe(OAc)_2$ (76.3 mg, 0.439 mmol) was added to the yellow solution as a solid followed by Ph_4PBr (185.5 mg, 0.442 mmol). DMF was removed *in vacuo* to yield a yellow solid. This solid was dissolved in $NCCH_3$ (20 mL), yielding a yellow solution and colorless precipitate (KBr and KOAc). The mixture was filtered, and the filtrate was concentrated by half *in vacuo*. The product was crystallized by the slow

diffusion of diethyl ether into this $NCCH_3$ solution, yielding yellow blocks of the desired product (291.2 mg, 59%). ^{1}H NMR (δ, CD_3CN, 400 MHz): 28.68, 14.39, 14.00, 7.86 (s, Ph_4P), 7.70 (s, Ph_4P), 5.91, 5.76, 5.51, 4.93, 2.06. Negative mode ESI-MS (*m/z*) for $[Fe(L^{OMe})]^{1-}$ $(C_{42}H_{33}FeN_4O_6)^-$ calcd 745.2; found 745.6. FTIR (KBr, cm^{-1}): ν(CO) 1604; 3057, 2835, 2253, 1604, 1558, 1507, 1474, 1442, 1343, 1246, 1168, 1108, 1028, 920, 845, 773, 753, 724, 689, 527. μ_{eff} = 5.57 μ_B (the method of Evans, CD_3CN, 400 MHz).

$Ph_4P[Fe^{II}(NCCH_3)L^{F2}]$. To a solution of H_3L^{F2} (377.1 mg, 0.531 mmol) in dimethylformamide (DMF, 5 mL), KH (66.7 mg, 1.663 mmol) was added as a solid. After stirring 1 hr, $Fe(OAc)_2$ (92.0 mg, 0.529 mmol) was added to the yellow solution as a solid followed by Ph_4PBr (223.5 mg, 0.533 mmol). DMF was removed *in vacuo* to yield a yellow solid. This solid was dissolved in $NCCH_3$ (20 mL), yielding a yellow solution and colorless precipitate (KBr and KOAc). The mixture was filtered, and the filtarate was concentrated by half *in vacuo*. The product was crystallized by the slow diffusion of diethyl ether into this $NCCH_3$ solution, yielding yellow needles of the desired product (381.8 mg, 63%). ^{1}H NMR (δ, CD_3CN, 400 MHz): 28.31, 13.51 7.83 (s, Ph_4P), 7.65 (s, Ph_4P), 6.24, 5.60. ^{19}F NMR (δ, CD_3CN, 400 MHz): -102.95. Negative mode ESI-MS (*m/z*) for $[Fe(L^{F2})]^{1-}$ $(C_{39}H_{21}F_6FeN_4O_3)$ calcd 763.1; found 763.4. FTIR (KBr, cm^{-1}): ν(CO) 1620; 3060, 2980, 2255, 2206, 1590, 1576, 1475, 1442, 1343, 1111, 986, 867, 773, 754, 724, 690, 527. μ_{eff} = 5.57 μ_B (the method of Evans, CD_3CN, 400 MHz).

$Ph_4P[Fe(L^{Me})]$. To a solution of H_3L^{Me} (34.0 mg, 0.082 mmol) in DMF (4 mL) KH (11.0 mg, 0.274 mmol) was added as a solid. A colorless precipitate formed over one hour. To the mixture was added $Fe(OAc)_2$ (15.2 mg, 0.087 mmol) followed by Ph_4PBr (34.3 mg, 0.082 mmol). DMF was removed *in vacuo*. The resulting solid was dissolved in DCM (5.0 mL) and filtered. The DCM was removed from the filtrate *in vacuo* to yield a tan-yellow solid. The crude product was isolated and rinsed with diethyl ether to yield 55.5 mg (84%). FTIR (KBr, cm^{-1}): ν(CO) 1672; 3238, 3181, 3056, 2925, 2205, 1597, 1535, 1479, 1439, 1372, 1328, 1255, 1109, 1037, 997, 754, 724, 691, 527. ^1H NMR (δ, CD_3CN, 400 MHz): 58.17, 30.76, 28.38, 20.38, 18.76, 16.81, 15.59, 14.73, 12.78, 10.91, 9.91, 8.95, 8.56, 7.89 (Ph_4P), 7.67 (Ph_4P), 5.76, 3.65, 1.48, -0.08, -3.22, -5.36, -6.24, -6.73, -7.92.

$Ph_4P[Fe(DMF)L^{CF3}]$. To a solution of H_3L^{CF3} (203.5 mg, 0.352 mmol) in DMF (3 mL) KH (43.6 mg, 1.087 mmol) was added as a solid. The solution was stirred for four hours. To the solution was added $Fe(OAc)_2$ (60.4 mg, 0.345 mmol). After stirring for two hours, to the solution was added Ph_4PBr (147.8 mg, 0.353 mmol). The clear, yellow solution was stirred overnight. DMF was removed *in vacuo*. The resulting solid was dissolved in $NCCH_3$ (10.0 mL) and filtered. The $NCCH_3$ was removed from the filtrate *in vacuo*, to yield a crude powder. The product was recrystallized by slow diffusion of diethyl ether into a concentrated $NCCH_3$ solution of the product to yield pale peach crystals (204.8 mg, 60%). FTIR (KBr, cm^{-1}): ν(CO) 1650; 3061, 2972, 2929, 2871, 1718, 1484, 1439, 1253, 1163, 1110, 938, 724, 690, 528. ^1H NMR (δ, CD_3CN, 400 MHz):

20.50, 11.14, 7.89 (Ph_4P), 7.71 (Ph_4P), 3.22, 3.06. ^{19}F NMR (δ, CD_3CN, 400 MHz): -70.36. ESI-MS negative mode (*m/z*) for $C_{24}H_{12}F_9FeN_4O_3^-$ calcd 631.01; found 631.02.

Lithium (*N*-methylformamido)methanolate, LiOMMF. To a solution of HMMF (169.6 g, 1.904 mmol) in dichloromethane (CH_2Cl_2, 3 mL) was added a CH_2Cl_2 solution (10 mL) of lithium hexamethyldisilazide (316.8 mg, 1.893 mmol). Colorless precipitate formed immediately. The mixture was stirred overnight. The crude, white powder was collected by filtration on a sintered glass frit and washed with an additional 10 mL CH_2Cl_2 (173.5 mg, 95.9%). The product of this reaction is very insoluble in all of the solvents we tested (e.g., DMSO, DMF, THF, CH_2Cl_2). ^1H NMR (δ, DMSO-d_6, 300 MHz), two rotamers (E_{major} and Z_{minor}) are observed for this product in an approximate ~15:1 (major:minor) ratio. ^1H NMR (δ, DMSO-d_6, 400 MHz): major[minor] 8.00[7.96] (s, 1H, -C(O)*H*), 4.86[4.93] (br s, 2H, -CH_2-OH), 2.69[2.81] (s, 3H, -NCH_3). FTIR (KBr, cm^{-1}): ν(CO) 1665; 2928, 2873, 2840, 1439, 1408, 1268, 1228, 1168, 1116, 1078, 1030, 866, 714.

$Ph_4P[Fe^{III}(OMMF)L^{Ph}]$. *Method A- from reaction of $Ph_4P[Fe^{II}(NCCH_3)L^{Ph}]$ with PhIO:* To a solution of $Ph_4P[Fe^{II}(NCCH_3)L^{Ph}]$ (159.1 mg, 0.154 mmol) in DMF (6 mL), PhIO (35.4 mg, 0.161 mmol) was added as a solid. The solution immediately turned reddish-brown. The reaction mixture was stirred for 22 hours at room temperature. DMF was removed *in vacuo*. The resulting solid was dissolved in acetonitrile (CH_3CN, 5.0 mL) and filtered. The acetonitrile was removed *in vacuo* to yield a reddish-brown solid. The solid was extracted back into DMF and recrystallized by slow diffusion of diethyl ether

into a concentrated DMF solution of the product to yield a small number of reddish blocks that were analyzed by X-ray diffraction studies and starting material. FTIR (KBr, cm^{-1}): ν(CO) 1662; 3057, 2930, 1598, 1561, 1549, 1527, 1475, 1439, 1341, 1272, 1109, 1042, 997, 925, 754, 723, 690, 527 (*m/z*) for $[Fe(L^{Ph})(HMMF)]^{1-}$ ($C_{42}H_{34}FeN_5O_5$) calcd 743.183; found 743.184. μ_{eff} = 5.23 μ_B (the method of Evans, CD_2Cl_2, 400 MHz). Anal. Calcd (found) for $Ph_4P[Fe(OMMF)L^{Ph}]$: C, 73.13 (73.26); H, 5.02 (5.21); N, 6.46 (6.68).

Method B- from LiOMMF: To a solution of $Ph_4P[Fe^{II}(NCCH_3)L^{Ph}]$ (54.9 mg, 0.0530 mmol) in DMF (1 mL), LiOMMF (5.6 mg, 0.059 mmol) was added as a solid. The solution was stirred for 2 hours. To the resulting homogeneous orange solution, $FcBF_4$ (16.0 mg, 0.0586 mmol) was added dropwise as a DMF solution. DMF was removed *in vacuo* to yield a reddish solid. The resulting solid was dissolved in dichloromethane (CH_2Cl_2, 5.0 mL) and filtered. The CH_2Cl_2 was removed *in vacuo* to yield a reddish-brown solid. The crude material was isolated and washed with diethyl ether (~20 mL) to yield a brown powder (41.9 mg, 73.0%). FTIR (KBr, cm^{-1}): ν(CO) 1664; 3284, 3060, 2932, 1587, 1527, 1483, 1400, 1314, 1258, 1194, 1109, 1057, 999, 931, 902, 756, 724, 691, 527. UV-vis (CH_2Cl_2) λ_{max}, nm (ε, $M^{-1}\,cm^{-1}$): shoulder 469 (1655), ESI-MS (m/z) for $[Fe(L^{Ph})(HMMF)]^{1-}$ ($C_{42}H_{34}FeN_5O_5$) m/z calcd 743.183; found 743.186.

$(Ph_4P)_2[(Fe^{III}L^{Me})\mu\text{-}O]$. To a solution of H_3L^{Me} (38.6 mg, 0.093 mmol) in DMF (3 mL) KH (12.5 mg, 0.312 mmol) was added as a solid. A colorless precipitate formed over one hour. To the mixture was added $Fe(OAc)_2$ (16.2 mg, 0.093 mmol) followed by Ph_4PBr (41.2 mg, 0.098 mmol). The clear, yellow solution was stirred for 20 minutes at room

temperature. The headspace of the flask was evacuated, and the flask was removed from the glovebox. O_2 (g) (2.3 mL, 0.094 mmol) was added via gas-tight syringe. The reaction mixture was stirred for 15 minutes at room temperature. The solution turned dark orange-red. The headspace of the flask was evacuated, and the flask was returned to the glovebox. DMF was removed *in vacuo*. The resulting solid was dissolved in $NCCH_3$ (5.0 mL) and filtered. The $NCCH_3$ was removed *in vacuo* to yield a reddish-brown solid. The product was recrystallized by slow diffusion of diethyl ether into a concentrated DMF solution of the product to yield dark red-brown, X-ray quality crystals. FTIR (KBr, cm^{-1}): ν(CO) 1670; 3061, 2922, 2851, 1610, 1582, 1479, 1448, 1370, 1322, 1252, 1104, 985, 760, 724, 692, 529. ^{1}H NMR (δ, CD_3CN, 400 MHz): 10.70, 7.89 (Ph_4P), 7.71 (Ph_4P). μ_{eff} = 1.68 μ_B/Fe (the method of Evans, CD_2Cl_2, 400 MHz). ESI-MS negative mode (*m/z*) for $(Ph_4P)_2[(Fe^{III}L^{Me})\mu\text{-}O]$ $(C_{48}H_{42}Fe_2N_8O_7)^{2-}$ calcd 477.09; found 477.09 $(M/2)^-$; calcd 955.20; found 955.18 $(M+1)^-$.

Catalytic Studies

LC-MS Calibration and Yield Determination. Calibration curves were constructed for concentration determination of both NMF and HMMF over the concentration ranges 7.5 x 10^{-6} – 3 x 10^{-4} M and 4.6 x 10^{-6} – 1.8 x 10^{-4} M, respectively, with a constant concentration of internal standard (*N*-methylacetamide, NMA, 1 x 10^{-4} M). Each solution was injected twice. The M + 1 ion areas of NMF (A_{NMF}) (60.1, t_{Ret} = 2.1 min.) and HMMF ($A_{analyte}$) (90.1, t_{Ret} = 2.6 min.) were extracted. The average of the two areas of the extracted ion peaks were plotted vs. concentration. The slopes of the resultant trendlines were used to establish response ratios (r_s):

$$r_s = \frac{A_{analyte} * [analyte]}{A_{NMA} * [NMA]}$$

The response ratios from these calibration curves were subsequently used to determine HMMF and NMF concentrations in subsequent reactions. Yields reported are the average of three trials.

Sample reaction: Ph4P[$Fe^{II}(NCCH_3)L^{Ph}$] (7.0 mg, 6.8 μmol) was dissolved in 10 mL of anhydrous DMF. PhIO (37.1 mg, 0.169 mmol) was added to the reaction mixture as a solid. The mixture was stirred for 24 hrs at room temperature. From the resulting solution a 0.50 mL aliquot was withdrawn. This aliquot was diluted to 1.5 mL with 0.1% formic acid in water. Fifty microliters of the resultant solution was again diluted to 1.5 mL, using 0.50 mL of a 0.3 mM NMA, 0.1% formic acid solution and 0.950 mL of 0.1% formic acid solution. This solution was used for LC-MS (5 μL injections). Two injections were taken from each sample. The areas of the extracted ion peak of HMMF were (*vide supra*) converted to [HMMF] in the sample by the equation:

$$[HMMF] = \frac{[NMA] * A_{HMMF}}{r_s * A_{NMA}} .$$

[HMMF] in the bulk solution and the turnover number (TON, moles product/moles catalyst) was then calculated (average [HMMF] in aliquot = 6.91 x 10^{-5} M, [HMMF] in reaction = 6.22 x 10^{-3} M, TON = 9.2, yield based on oxidant (PhIO) = 37%).

A control reaction of PhIO in anhydrous DMF (stirred for 24 hours) did not produce HMMF in appreciable quantities (< 5% conversion based on PhIO).

Substrate Scope Sample Reactions

Reaction with N,N-diethylformamide (DEF): $Ph_4P[Fe(NCCH_3)L^{Ph}]$ (7.1 mg, 6.9 μmol) was dissolved in 5 mL of anhydrous DEF. PhIO (30.4 mg, 0.138 mmol) was added to the reaction mixture as a solid. The mixture was stirred for 24 hrs at room temperature. From the resulting solution a 0.050 mL aliquot was withdrawn. This aliquot was diluted to 1.5 mL with 0.1% formic acid in water. This solution was used for LC-MS (5 μL injections). T_{ret} (m/z = 118) = 1.672 min, T_{ret} (m/z = 74) = 0.753 min.

Reaction with N-methyl-2-piperidone: $Ph_4P[Fe(NCCH_3)L^{Ph}]$ (5.5 mg, 5.3 μmol) was dissolved in 0.5 mL of anhydrous *N*-methyl-2-piperidone and 4.5 mL cyclohexane. PhIO (28.7 mg, 0.130 mmol) was added to the reaction mixture as a solid. The mixture was stirred for 24 hrs at room temperature. From the resulting solution a 0.050 mL aliquot was withdrawn. This aliquot was diluted to 1.5 mL with methanol. This solution was used for LC-MS (5 μL injections). T_{ret} (m/z = 129) = 1.319 min.

Reaction with caffeine: $Ph_4P[Fe(NCCH_3)L^{Ph}]$ (10.8 mg, 0.010 mmol) was dissolved in 5 mL of anhydrous $NCCH_3$. Caffeine (20.4 mg, 0.110 mmol) was added followed by PhIO (23.2 mg, 0.105 mmol). The mixture was stirred for 4 days at room temperature. Solvent was removed from the mixture *in vacuo*. The resulting solid was dissolved in $CDCl_3$. The ^1H NMR spectrum indicated no change to the caffeine.

Reaction with 9,10-dihydroanthracene: $Ph_4P[Fe(NCCH_3)L^{Ph}]$ (6.3 mg, 6.1 μmol) was dissolved in 5 mL of anhydrous $NCCH_3$. 9,10-dihydroanthracene (11.7 mg, 0.065 mmol) was added followed by PhIO (14.3 mg, 0.065 mmol). The mixture was stirred for 2 days

at room temperature. The reaction mixture was filtered to remove unreacted PhIO, and solvent was removed from the yellow filtrate *in vacuo*. The resulting solid was dissolved in $CDCl_3$. The ^1H NMR spectrum indicated no significant change to the 9,10-dihydroanthracene.

GC Calibration Curve and Kinetic Studies

A calibration curve was constructed for concentration determination NMF over the concentration range 4.6 x 10^{-5} – 1.1 x 10^{-2} M with a constant concentration of internal standard (*N*,*N*-diethylformamide, 1 x 10^{-4} M). Each solution was injected twice. The average of the two areas were plotted vs. concentration. The slopes of the resultant trendlines were used to establish a response ratio and used as described above.

Determination of KDIE by GC: Two trials separate trials were performed on different days to determine the KDIE of the catalytic reaction. The reactions were run as described above except in 1 mL DMF or DMF-d_7. The protio- and deutero-solvated reactions were run side-by-side in each trial. Aliquots (0.100 mL) were removed from each after 4, 8, and 24 hours, diluted to 1.5 mL with the internal standard solution, passed through a plug of silica, and analyzed by GC. Each solution was injected twice, and the averages of the areas of the peaks were used to calculate the [NMF] in the solution and corresponding TON as described above. The rates of catalyst turnover were then used to determine k_H/k_D, which was the same for both trials (4.4).

Crystallographic Data

For each complex, crystals were coated with Paratone N oil, and suitable crystals were suspended in small fiber loops. They were mounted in a cooled nitrogen gas stream at 173 K on a Bruker D8 APEX II CCD sealed tube diffractometer with graphite monochromated Mo Kα (0.71073 Å) radiation. Data was collected using a series of phi and omega scans with 10s frame exposures and 0.5° frame widths. The structures were solved using direct methods and difference Fourier techniques (Shelxtl, V6.12).[101] Hydrogen atoms were added with the HFIX command. These were included in the final cycles of least squares refinement, with isotropic Uij's that were determined by the riding model. Structure solution, refinement, and generation of publication materials were performed by using SHELX, V6.12 software for $Ph_4P[Fe(DMF)L^{Ph}]$ and $Ph_4P[Fe(DMF)L^{CF3}]$ and Olex2, V1.5c for $Ph_4P[Fe(OMMF)L^{Ph}]$, $Ph_4P[Fe(NCCH_3)L^{OMe}]$, $Ph_4P[Fe(NCCH_3)L^{F2}]$, and $(Ph_4P)_2[(FeL^{Me})_2(\mu\text{-}O)]$.[101,102]

$Ph_4P[Fe(DMF)L^{Ph}]$, $Ph_4P[Fe(NCCH_3)L^{OMe}]$, $Ph_4P[Fe(NCCH_3)L^{F2}]$, and $(Ph_4P)_2[(FeL^{Me})_2(\mu\text{-}O)]$ crystallize in the space group P-1, with R1 = 0.055, 0.0678, 0.0607, and 0.0455, respectively. All atoms were refined anisotropically. One of the distal phenyl groups in $Ph_4P[Fe(DMF)L^{Ph}]$ was disordered over two positions in a ratio of 0.47:0.53. The unit cells of both $Ph_4P[Fe(DMF)L^{Ph}]$ and $Ph_4P[Fe(NCCH_3)L^{F2}]$ contain a molecule of residual diethyl ether, which was used in recrystallization. These molecules were refined anisotropically at full occupancy. $Ph_4P[Fe(DMF)L^{CF3}]$ crystallized in the space group $P2_1/n$, with R1 = 0.0628. All atoms were refined anisotropically, except the *N*-methyl carbons of the bound DMF and those belonging to the residual solvent molecule, diethyl ether. The diethyl ether molecule was refined isotropically at 50%

occupancy. The $-CF_3$ substituents exhibited disorder, which was refined over two positions. $Ph_4P[Fe(OMMF)L^{Ph}]$ crystallizes in the space group $P2_1/c$, and has been refined to an R1 = 0.062. All molecules were refined anistropically. The bound $(OMMF)^-$ fragment is disordered over its two rotamers with a ratio of 0.67:0.33. There was disordered DMF solvent in the unit cell that could not be refined. These electron density peaks were omitted using the SQUEEZE function in Platon, resulting in 4 solvent accessible voids, corresponding to 36 electrons each.[103]

Table 3-7. Crystal data and structure refinement parameters for $PPh_4[Fe(DMF)L^{Ph}]\bullet Et_2O$, $PPh_4[Fe(OMMF)L^{Ph}]$, and $PPh_4[Fe(NCCH_3)L^{OMe}]$.

	$PPh_4[Fe(DMF)L^{Ph}]\bullet Et_2O$	**$PPh_4[Fe(OMMF)L^{Ph}]$**	**$PPh_4[Fe(NCCH_3)L^{OMe}]$**
Formula	$C_{70}H_{65}FeN_5O_5P$	$C_{66}H_{47}FeN_5O_5P$	$C_{72}\ H_{62}\ Fe\ N_7\ O_6\ P$
Crystal size (mm^3)	0.77 × 0.27 × 0.14	0.54 × 0.38 × 0.20	-
Form. wt. (g/mol)	1143.09	1076.96	1208.11
Space group	P-1	$P2_1/c$	P -1
a (Å)	14.3316 (12)	11.0775(10)	10.9384(14)
b (Å)	14.6928 (12)	26.172(2)	13.9225(18)
c (Å)	16.1605 (13)	19.6484(17)	20.669(3)
α (deg)	89.2790 (10)	90	92.700(2)
β (deg)	75.6880 (10)	91.011(1)	92.161(2)
γ (deg)	63.9930 (10)	90	102.736(3)
V ($Å^3$)	2945.5 (4)	5695.6(9)	3063.1(7)
Z	2	4	2
T (K)	173(2)	173(2)	173(2)
ϱ, calcd (g/cm)	1.289	1.256	1.310
Reflns collected	59862	78641	52121
Unique reflns	17783	10054	14010
Par/restr.	812/0	715/96	790/0
μ Kα (mm^{-1})	0.34	0.348	0.333
GOF[b]	1.156	1.045	1.035
Final *R* indices [$I > 2\sigma(I)$][b]	$R_1 = 0.055$	$R_1 = 0.062$	$R_1 = 0.0678$
All data	$wR_2 = 0.170$	$wR_2 = 0.186$	$wR_2 = 0.1987$

Table 3-8. Crystal data and structure refinement parameters for $Ph_4P[Fe(DMF)(L^{CF3})]$•0.5 Et_2O, $(Ph_4P)_2[(FeL^{Me})_2\mu\text{-}O]$, and $PPh_4[Fe(NCCH_3)L^{F2}])]$•$Et_2O$

	$PPh_4[Fe(DMF)(L^{CF3})]$• 0.5 Et_2O	**$(Ph_4P)_2[Fe(L^{Ph})(OMMF)]$**	**$PPh_4[Fe(NCCH_3)L^{F2}]$ •Et_2O**
Formula	$C_{53}\ H_{42.50}\ F_9\ Fe\ N_5\ O_{4.50}\ P$	$C_{108}\ H_{110}\ Fe_2\ N_{12}\ O_{11}\ P_2$	$C_{69}\ H_{54}\ F_6\ Fe\ N_5\ O_4\ P$
Crystal size (mm^3)	0.39 × 0.32 × 0.27	0.609 x 0.336 x 0.26	0.419 x 0.328 x 0.3
Form. wt. (g/mol)	1079.24	1925.72	1217.99
Space group	$P2_1/n$	P-1	P -1
a (Å)	18.397(8)	12.4054(17)	10.8233(4)
b (Å)	9.847(4)	12.7421(18)	13.6229(5)
c (Å)	30.034(13)	17.033(2)	21.4234(7)
α (deg)	90	94.343(2)	99.647(2)
β (deg)	104.973(7)	102.470(2)	102.888(2)
γ (deg)	90	111.401(2)	102.249(2)
V ($Å^3$)	5256(4)	2412.0(6)	2931.53(18)
Z	4	2	2
T (K)	173(2)	173(2)	173(2)
ϱ, calcd (g/cm)	1.364	1.326	1.380
Reflns collected	97530	28056	31633
Unique reflns	15330	9854	12772
Par/restr.	698/0	655/0	778/0
μ Kα (mm^{-1})	0.399	0.402	0.359
GOF[b]	1.006	1.033	1.034
Final *R* indices [I > $2\sigma(I)$][b]	R_1 = 0.0628	R_1 = 0.0607	R_1 = 0.0455
All data	wR_2 = 0.2472	wR_2 = 0.1884	wR_2 = 0.1294

References

(1) Labinger, J. A.; Bercaw, J. E. *Nature* **2002**, *417*, 507.

(2) Labinger, J. A. *J. Mol. Catal. A: Chem.* **2004**, *220*, 27.

(3) Crabtree, R. H. *J. Chem. Soc., Dalton Trans.* **2001**, 2437.

(4) Dick, A. R.; Sanford, M. S. *Tetrahedron* **2006**, *62*, 2439.

(5) Periana, R. A.; Taube, D. J.; Gamble, S.; Taube, H.; Satoh, T.; Fujii, H. *Science* **1998**, *280*, 560.

(6) Kao, L. C.; Sen, A. *J. Chem. Soc., Chem. Commun.* **1991**, 1242.

(7) Dick, A. R.; Kampf, J. W.; Sanford, M. S. *Organometallics* **2005**, *24*, 482.

(8) Dick, A. R.; Hull, K. L.; Sanford, M. S. *J. Am. Chem. Soc.* **2004**, *126*, 2300.

(9) Kalyani, D.; Sanford, M. S. *Org. Lett.* **2005**, *7*, 4149.

(10) Dolphin, D.; Traylor, T. G.; Xie, L. Y. *Acc. Chem. Res.* **1997**, *30*, 251.

(11) Groves, J. T.; Viski, P. *J. Am. Chem. Soc.* **1989**, *111*, 8537.

(12) Groves, J. T.; Viski, P. *J. Org. Chem.* **1990**, *55*, 3628.

(13) Das, S.; Incarvito, C. D.; Crabtree, R. H.; Brudvig, G. W. *Science* **2006**, *312*, 1941.

(14) Bigi, M. A.; Reed, S. A.; White, M. C. *Nat. Chem.* **2011**, *3*, 216.

(15) Groves, J. T. *Proc. Natl. Acad. Sci. U. S. A.* **2003**, *100*, 3569.

(16) Li, C.; Wu, W.; Kumar, D.; Shaik, S. *J. Am. Chem. Soc.* **2006**, *128*, 394.

(17) Wang, Y.; Li, D.; Han, K.; Shaik, S. *J. Phys. Chem. B* **2010**, *114*, 2964.

(18) Dinnocenzo, J. P.; Karki, S. B.; Jones, J. P. *J. Am. Chem. Soc.* **1993**, *115*, 7111.

(19) Eser, B. E.; Barr, E. W.; Frantom, P. A.; Saleh, L.; Bollinger, J. M.; Krebs, C.; Fitzpatrick, P. F. *J. Am. Chem. Soc.* **2007**, *129*, 11334.

(20) Krebs, C.; Galonić Fujimori, D.; Walsh, C. T.; Bollinger, J. M. *Acc. Chem. Res.* **2007**, *40*, 484.

(21) Panay, A. J.; Lee, M.; Krebs, C.; Bollinger, J. M.; Fitzpatrick, P. F. *Biochemistry* **2011**, *50*, 1928.

(22) Sinnecker, S.; Svensen, N.; Barr, E. W.; Ye, S.; Bollinger, J. M., Jr.; Neese, F.; Krebs, C. *J. Am. Chem. Soc.* **2007**, *129*, 6168.

(23) Hoffart, L. M.; Barr, E. W.; Guyer, R. B.; Bollinger, J. M., Jr.; Krebs, C. *Proc. Natl. Acad. Sci. U. S. A.* **2006**, *103*, 14738.

(24) Que, L. *Acc. Chem. Res.* **2007**, *40*, 493.

(25) Srnec, M.; Wong, S. D.; England, J.; Que, L., Jr.; Solomon, E. I. *Proc. Natl. Acad. Sci. U. S. A.* **2012**, 1.

(26) England, J.; Martinho, M.; Farquhar, E. R.; Frisch, J. R.; Bominaar, E. L.; Münck, E.; Que, L. *Angew. Chem., Int. Ed.* **2009**, *48*, 3622.

(27) Jones, M. B.; Hardcastle, K. I.; MacBeth, C. E. *Polyhedron* **2010**, *29*, 116.

(28) Jones, M. B.; MacBeth, C. E. *Inorg. Chem.* **2007**, *46*, 8117.

(29) Jones, M. B.; Newell, B. S.; Hoffert, W. A.; Hardcastle, K. I.; Shores, M. P.; MacBeth, C. E. *Dalton Trans.* **2010**, *39*, 401.

(30) Jones, M. B.; Newell, B. S.; Hoffert, W. A.; Hardcastle, K. I.; Shores, M. P.; MacBeth, C. E. *Dalton Trans.* **2010**, *39*, 401.

(31) Jones, M. B.; Hardcastle, K. I.; Hagen, K. S.; MacBeth, C. E. *Inorg. Chem.* **2011**, *50*, 6402.

(32) Reinaud, O. M.; Theopold, K. H. *J. Am. Chem. Soc.* **1994**, *116*, 6979.

(33) Mahapatra, S.; Halfen, J. A.; Wilkinson, E. C.; Que, L., Jr.; Tolman, W. B. *J. Am. Chem. Soc.* **1994**, *116*, 9785.

(34) Allen, W. E.; Sorrell, T. N. *Inorg. Chem.* **1997**, *36*, 1732.

(35) Jones, M. B. Ph.D. Dissertation, Emory University, 2010.

(36) Kang, Y.; Chen, H.; Jeong, Y. J.; Lai, W.; Bae, E. H.; Shaik, S.; Nam, W. *Chem.--Eur. J.* **2009**, *15*, 10039.

(37) Paraskevopoulou, P.; Ai, L.; Wang, Q.; Pinnapareddy, D.; Acharyya, R.; Dinda, R.; Das, P.; Celenligil-Cetin, R.; Floros, G.; Sanakis, Y.; Choudhury, A.; Rath, N. P.; Stavropoulos, P. *Inorg. Chem.* **2009**, *49*, 108.

(38) Jones, M. B.; Newell, B. S.; Hoffert, W. A.; Hardcastle, K. I.; Shores, M. P.; MacBeth, C. E. *Dalton Transactions* **2010**, *39*, 401.

(39) Jones, M. B.; MacBeth, C. E. *Inorg. Chem.* **2007**, *46*, 8117.

(40) Paraskevopoulou, P.; Ai, L.; Wang, Q.; Pinnapareddy, D.; Acharyya, R.; Dinda, R.; Das, P.; CÃßelenligil-CÃßetin, R.; Floros, G.; Sanakis, Y.; Choudhury, A.; Rath, N. P.; Stavropoulos, P. *Inorg. Chem.* **2010**, *49*, 108.

(41) Addison, A. W.; Rao, T. N.; Reedijk, J.; Van Rijn, J.; Verschoor, G. C. *J. Chem. Soc., Dalton Trans.* **1984**, 1349.

(42) Strohalm, M.; Hassman, M.; Košata, B.; Kodíček, M. *Rapid Commun. Mass Spectrom.* **2008**, *22*, 905.

(43) Strohalm, M.; Kavan, D.; Novák, P.; Volný, M.; Havlíček, V. *Anal. Chem.* **2010**, *82*, 4648.

(44) Iwasawa, T.; Hooley, R. J.; Jr., J. R. *Science* **2007**, *317*, 493.

(45) Kawamichi, T.; Haneda, T.; Kawano, M.; Fujita, M. *Nature* **2009**, *461*, 633.

(46) Yi, C.; Jia, G.; Hou, G.; Dai, Q.; Zhang, W.; Zheng, G.; Jian, X.; Yang, C.-G.; Cui, Q.; He, C. *Nature* **2010**, *468*, 330.

(47) Lorentzen, E.; Siebers, B.; Hensel, R.; Pohl, E. *Biochemistry* **2005**, *44*, 4222.

(48) Heine, A.; DeSantis, G.; Luz, J. G.; Mitchell, M.; Wong, C.-H.; Wilson, I. A. *Science* **2001**, *294*, 369.

(49) Thorell, S.; Schürmann, M.; Spregner, G. A.; Schneider, G. *J. Mol. Biol.* **2002**, *319*, 161.

(50) You, L.; Long, S. R.; Lynch, V. M.; Anslyn, E. V. *Chem. Eur. J.* **2011**, *17*, 11017.

(51) Alegria, E. C. B.; Martins, L. M. D. R. S.; Haukka, M.; Pombeiro, A. J. L. *Dalton Trans.* **2006**, 4954.

(52) Maiti, D.; Lee, D.-H.; Gaoutchenova, K.; Würtele, C.; Holthausen, M. C.; Narducci Sarjeant, A. A.; Sundermeyer, J.; Schindler, S.; Karlin, K. D. *Angew. Chem., Int. Ed.* **2008**, *47*, 82.

(53) Adams, H.; Bailey, N. A.; Bertrand, P.; Collinson, S. R.; Fenton, D. E.; Kitchen, S. J. *J. Chem. Soc., Dalton Trans.*, 1181.

(54) Herrera, A. M.; Kalayda, G. V.; Disch, J. S.; Wikstrom, J. P.; Korendovych, I. V.; Staples, R. J.; Campana, C. F.; Nazarenko, A. Y.; Haas, T. E.; Rybak-Akimova, E. V. *Dalton Trans.* **2003**, 4482.

(55) Roesky, H. W.; Bertel, N.; Edelmann, F.; Herbst, R.; Egert, E.; Sheldrick, G. M. *Z. Naturforsch., B Anorg. Chem., Org. Chem.* **1986**, *41B*, 1506.

(56) Mizobe, Y.; Ishida, T.; Egawa, Y.; Ochi, K.; Tanase, T.; Hidai, M. *J. Coord. Chem.* **1991**, *23*, 57.

(57) Rusina, A.; Vlcek, A. A. *Nature* **1965**, *206*, 295.

(58) Serp, P.; Hernandez, M.; Richard, B.; Kalck, P. *Eur. J. Inorg. Chem.* **2001**, 2327.

(59) Gómez-Benı´tez, V.; Olvera-Mancilla, J.; Hernández-Ortega, S.; Morales-Morales, D. *J. Mol. Struct.* **2004**, *689*, 137.

(60) Ishida, T.; Mizobe, Y.; Tanase, T.; Hidai, M. *Chem. Lett.* **1988**, 441.

(61) Ishida, T.; Mizobe, Y.; Tanase, T.; Hidai, M. *J. Organomet. Chem.* **1991**, *409*, 355.

(62) Coalter, J. N., III; Huffman, J. C.; Caulton, K. G. *Organometallics* **2000**, *19*, 3569.

(63) Alaimo, P. J.; Arndtsen, B. A.; Bergman, R. G. *Organometallics* **2000**, *19*, 2130.

(64) Scott, V. J.; Henling, L. M.; Day, M. W.; Bercaw, J. E.; Labinger, J. A. *Organometallics* **2009**, *28*, 4229.

(65) *Bioinorganic Catalysis*; Second ed.; Reedijk, J.; Bouwman, E., Eds.; Marcel Dekker, Inc.: New York, NY, 1999.

(66) Mraz, J.; Jheeta, P.; Gescher, A.; Hyland, R.; Thummel, K.; Threadgill, M. D. *Chem. Res. Toxicol.* **1993**, *6*, 197.

(67) Van, d. B. M.; Rosseel, M. T.; Wijnants, P.; Buylaert, W.; Belpaire, F. M. *Arch. Toxicol.* **1994**, *68*, 291.

(68) Kafferlein, H. U.; Goen, T.; Muller, J.; Wrbitzky, R.; Angerer, J. *Int. Arch. Occup. Environ. Health* **2000**, *73*, 113.

(69) Kafferlein, H. U.; Angerer, J. *J. Chromatogr., B: Biomed. Sci. Appl.* **1999**, *734*, 285.

(70) Imbriani, M.; Maestri, L.; Marraccini, P.; Saretto, G.; Alessio, A.; Negri, S.; Ghittori, S. *Int. Arch. Occup. Environ. Health* **2002**, *75*, 445.

(71) Kaefferlein, H. U.; Mraz, J.; Ferstl, C.; Angerer, J. *Int. Arch. Occup. Environ. Health* **2004**, *77*, 427.

(72) Kestell, P.; Gill, M. H.; Threadgill, M. D.; Gescher, A.; Howarth, O. W.; Curzon, E. H. *Life Sci.* **1986**, *38*, 719.

(73) Sakai, T.; Kageyama, H.; Araki, T.; Yosida, T.; Kuribayashi, T.; Masuyama, Y. *Int. Arch. Occup. Environ. Health* **1995**, *67*, 125.

(74) Sohn, J. H.; Han, M. J.; Lee, M. Y.; Kang, S.-K.; Yang, J. S. *J. Pharm. Biomed. Anal.* **2005**, *37*, 165.

(75) Yu, B.; Edstrom, W. C.; Benach, J.; Hamuro, Y.; Weber, P. C.; Gibney, B. R.; Hunt, J. F. *Nature* **2006**, *439*, 879.

(76) Yang, C.-G.; Yi, C.; Duguid, E. M.; Sullivan, C. T.; Jian, X.; Rice, P. A.; He, C. *Nature* **2008**, *452*, 961.

(77) Holland, P. J.; Hollis, T. *PLoS ONE* **2010**, *5*, e8680.

(78) Lu, L.; Yi, C.; Jian, X.; Zheng, G.; He, C. *Nucleic Acids Res.* **2010**, *38*, 4415.

(79) Yu, B.; Hunt, J. F. *Proc. Natl. Acad. Sci. U. S. A.* **2009**, *106*, 14315.

(80) Sundheim, O.; Vagbo, C. B.; Bjoras, M.; Sousa, M. M. L.; Talstad, V.; Aas, P. A.; Drablos, F.; Krokan, H. E.; Tainer, J. A.; Slupphaug, G. *EMBO J.* **2006**, *25*, 3389.

(81) Murahashi, S.; Naota, T.; Kuwabara, T.; Saito, T.; Kumobayashi, H.; Akutagawa, S. *J. Am. Chem. Soc.* **1990**, *112*, 7820.

(82) Murahashi, S.; Naota, T.; Yonemura, K. *J. Am. Chem. Soc.* **1988**, *110*, 8256.

(83) Murahashi, S.-I.; Nakae, T.; Terai, H.; Komiya, N. *J. Am. Chem. Soc.* **2008**, *130*, 11005.

(84) Hall, L. R.; Hanzlik, R. P. *J. Biol. Chem.* **1990**, *265*, 12349.

(85) Mra´z, J.; Jheeta, P.; Gescher, A.; Hyland, R.; Thummel, K.; Threadgill, M. D. *Chem. Res. Toxicol.* **1993**, *6*, 197.

(86) Shilov, A. E.; Shul'pin, G. B. *Chem. Rev.* **1997**, *97*, 2879.

(87) Addison, A. W.; Rao, T. N.; Reedijk, J.; Rijn, J. v.; Verschoor, G. C. *J. Chem. Soc., Dalton Trans.* **1984**, 1349.

(88) Mouat, A. R., Emory University, 2009.

(89) Yang, L.; Powell, D. R.; Houser, R. P. *Dalton Trans.* **2007**, 955.

(90) Lee, A. V.; Schafer, L. L. *Eur. J. Inorg. Chem.* **2007**, 2243.

(91) Wu, F. J.; Kurtz, D. M. *J. Am. Chem. Soc.* **1989**, *111*, 6563.

(92) Norman, R. E.; Yan, S.; Que, L.; Backes, G.; Ling, J.; Sanders-Loehr, J.; Zhang, J. H.; O'Connor, C. J. *J. Am. Chem. Soc.* **1990**, *112*, 1554.

(93) Reem, R. C.; McCormick, J. M.; Richardson, D. E.; Devlin, F. J.; Stephens, P. J.; Musselman, R. L.; Solomon, E. I. *J. Am. Chem. Soc.* **1989**, *111*, 4688.

(94) Armarego, W. L. F.; Chai, C. L. L. *Purification of Laboratory Chemicals*; 5th ed.; Butterworth-Heinemann: New York, 2003.

(95) Evans, D. F. *J. Chem. Soc.* **1959**, 2003.

(96) Sur, S. K. *J. Magn. Reson.* **1989**, *82*.

(97) Santoni, G.; Bavazzano, P.; Perico, A.; Colzi, A.; Benassi, S.; Medica, A.; La, M. R.; Giuliano, G. *J. Chromatogr., Biomed. Appl.* **1992**, *581*, 287.

(98) Leister, N. A. In *United States Patent*; Office, U. S. P., Ed.; Rohm and Haas Company: United States of America, 1971; Vol. 3,585,194.

(99) Ohta, K.; Nagamatsu, S.; Ishii, T. In *European Patent Register*; Patent, E., Ed. 2010; Vol. EP2386538.

(100) Nishimura, K.; Kitahaba, T.; Ikemoto, U.; Fujita, T. *Pestic. Biochem. Physiol.* **1988**, *31*, 155.

(101) Sheldrick, G. M. *Acta Crystallogr., Sect. A: Found. Crystallogr.* **2008**, *A64*.

(102) Dolomanov, O. V.; Bourhis, L. J.; Gildea, R. J.; Howard, J. A. K.; Puschmann, H. *J. Appl. Crystallogr.* **2009**, *42*, 339.

(103) Sluis, P. v. d.; Spek, A. L. *Acta Crystallogr., Sect. A: Found. Crystallogr.* **1990**, *A46*, 194.

Chapter 4: Use of a Neutral, Tridentate Ligand for Stabilization of Low Coordinate Transition Metal Complexes

Section 4-1. Introduction

Low coordinate transition metal complexes, or transition metal complexes with coordination numbers less than or equal to four, tend to be very reactive, especially for metals with d-electron counts less than ten. This is due to the fact that low coordinate complexes have open sites for reactivity. In cases where the d-electron count is less than ten, not only are there open sites for reactivity, but the transition metal also has unfilled d-orbitals and an electron count less than the ideal eighteen, thereby increasing its potential to react.

This added reactivity is demonstrated by four coordinate complexes prepared by the Peters and Smith groups. The Peters group utilized the monoanionic ligand [$PhB(PPh_2)_3$] to prepare the isolable cobalt and iron imido complexes, [$PhB(PPh_2)_3$][$Co^{III}N$(*p*-tolyl)] and [$PhB(PPh_2)_3$][$Fe^{III}N$(*p*-tolyl)] starting from the Co(I)- and Fe(I)-PR_3 complexes.[1,2] Furthermore, they found that the imido functionality could be transferred to CO, forming the isocyanide, O=C=N(*p*-tolyl), with this transformation occurring rapidly at room temperature for the Fe complex. Using a similar quaternary borate-centered, *N*-heterocyclic carbene ligand, phenyltris(1-*tert*-butylimidazol-2-ylidene)borate (L^{tBu}), Scepaniak et al. prepared a terminal Fe(IV)-nitrido complex by irradiation of the starting $L^{tBu}Fe^{II}N_3$.[3] This complex reacts with triphenylphosphine to slowly form the phosphiniminato complex, $L^{tBu}Fe^{II}$-N=PPh_3, the product of nitrogen atom transfer.

In the same year, Vogel et al., also using a ligand with N-heterocyclic carbene functionalities, tris[2-(3-mesityl-imidazol-2-ylide-ne)ethyl]imine ($TIMEN^{mes}$), prepared and structurally characterized an Fe(IV) nitrido complex by photolysis of the starting $[(Fe^{II}N_3)(TIMEN^{mes})]BPh_4$.[4] The Fe(III)-imido complex and the Fe(IV)-nitrido complexes are shown in Figure 4-1.

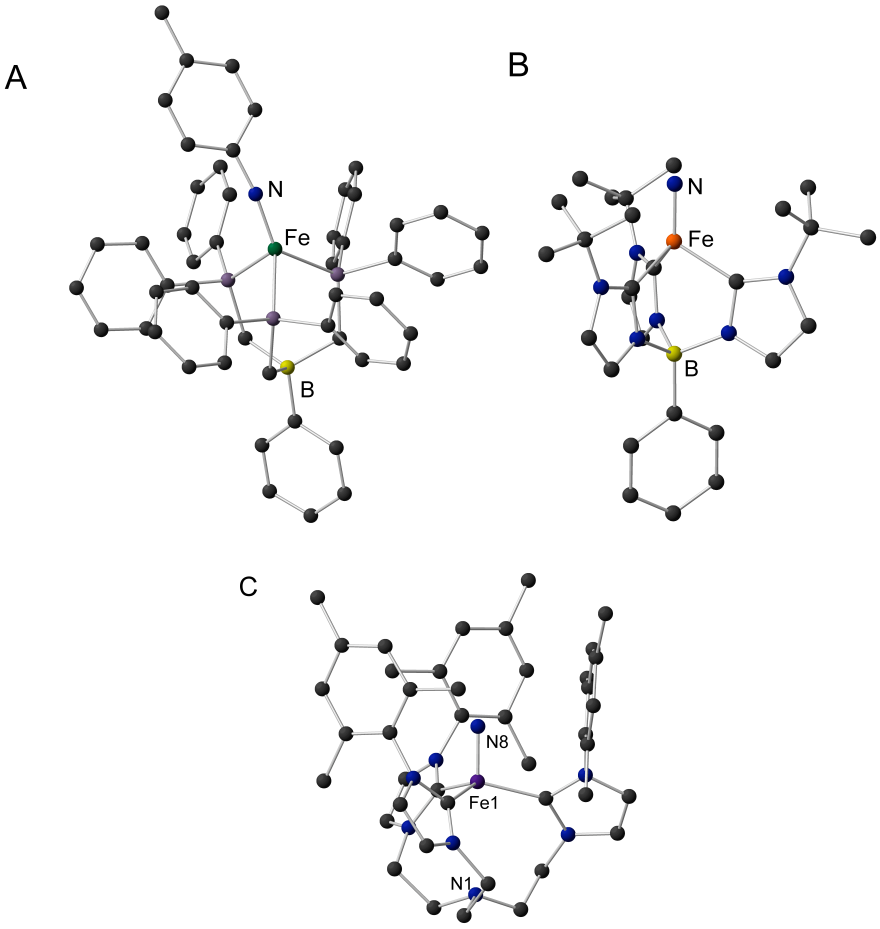

Figure 4-1. Solid-state structures of (A) $[PhB(PPh_2)_3][Fe^{III}N(p\text{-tolyl})]$,[2] (B) $L^{tBu}Fe^{IV}N$,[3] and (C) $[(Fe^{IV}N)(TIMEN^{mes})]BPh_4$,[4] with the counterion omitted for clarity. Hydrogen atoms have been omitted from the structures for clarity.

Three-coordinate complexes exhibit similar reactivity. For example, Cowley et al. reported a three-coordinate Fe(I) complex of a sterically demanding β-diketiminate ligand (2,2,6,6-tetramethyl-3,5-bis(diisopropylphenylimido)-hept-4-yl, L^{ket}) that exhibits similar nitrogen atom transfer activity.[5] Addition of 2 eq. 1-azidoadamantane (N_3Ad) to $L^{ket}Fe^{I}$-N=N-$Fe^{I}L^{ket}$ results in the formation of an imidoiron(III) complex that reacts at room temperature with CO, *tert*-butylisocyanide (^{t}BuNC), and PMe_3 to form AdN=C=O, AdN=C=N^{t}Bu, and AdN=PMe_3, respectively, as shown in Scheme 4-1.

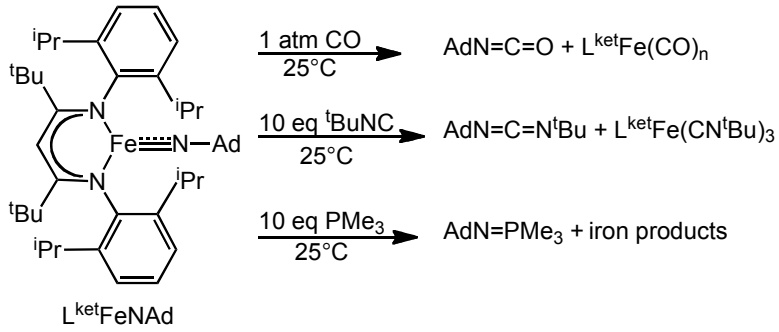

Scheme 4-1. Insertion reactions of 3-coordinate $L^{ket}Fe^{III}N$.[5]

Similar insertion products (ArN=C=N^{t}Bu and ArN=PMe_3, Ar = 3,5-$Me_2C_6H_3$) result when a dicopper nitrene of a variation of the β-diketiminate ligand is used.[6]

Use of the 2-coordinate ligand 1,2-bis(di-*tert*-butylphosphine)ethane (dtbpe) allows for isolation of a unique, 3-coordinate Ni-carbene complex.[7] This complex is very reactive, as addition of CO_2, CO, SO_2, and other small molecules result in insertion products, yielding the metalladicarboxylate, diphenylketene and [(dtbpe)Ni$(CO)_2$], and the metallasulfone, respectively (Scheme 4-2).

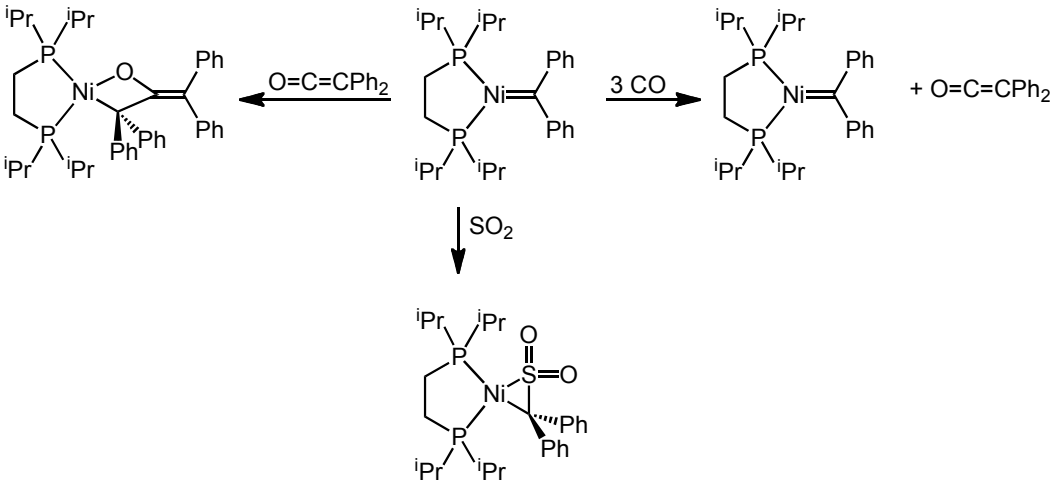

Scheme 4-2: Insertion reactions of 3-coordinate [(dtbpe)Ni=C(Ph)$_2$].[7]

Given the reactivity of 3- and 4-coordinate complexes, it is expected that the isolation of 2-coordinate transition metal complexes would be rare. In fact, the first homoleptic, 2-coordinate monomer was not structurally characterized until 1995.[8,9] This was made possible by utilizing very bulky ligands that deter binding and dimerization. Two-coordinate transition metal complexes of Mn, Fe, and Co have been prepared, using the ligand –N(SiMe$_3$)$_2$.[9,10] These complexes are reactive to Lewis bases and protic reagents, reacting in such a way that increases the coordination number or forms dinuclear complexes.

Use of the bulky terphenyl ligand, 2,6-bis(2,6-diisopropylphenyl)phenyl (dippPh), allows for the isolation and structural characterization of the 2-coordinate complexes Mn(dippPh)$_2$, Fe(dippPh)$_2$, and Co(dippPh)$_2$.[11-13] The iron and manganese complexes exhibit interesting activity (Scheme 4-3). For instance, carbon monoxide and dioxygen are inserted into the Fe-Ar bonds, yielding the η^2-acyl complex and the Fe-aryloxide, respectively. Both the iron and the

manganese complexes react with ammonia to yield the N-H cleavage products, $[(dippPh)Fe(\mu\text{-}NH_2)]_2$ and $[(dippPh)Mn(\mu\text{-}NH_2)(NH_3)]_2$.

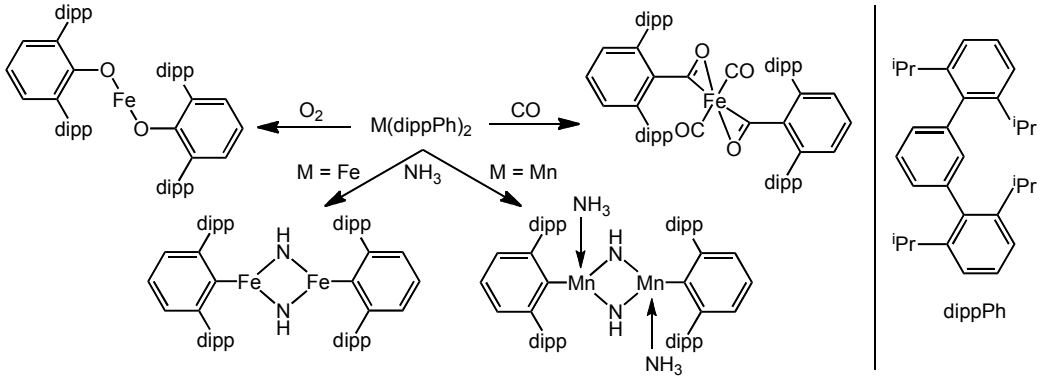

Scheme 4-3. Insertion reactions of 2-coordinate $Mn(dippPh)_2$ and $Fe(dippPh)_2$.[12,13]

Many of the reactions here described involve two-electron reductions of substrate with a concomitant two-electron oxidation of the transition metal mediating the process. For this reason, the generation of low-valent transition metal complexes has been necessary, as high-valent, mid to late 3d transition metal complexes are unstable and strongly oxidizing. Though early 3d or second and third row transition metals are generally more amenable to multi-electron transfer reactions, there are several advantages to using the later first row transition metals for this type of reactivity. Mid to late, first row transition metals (Mn – Cu) are naturally abundant and, therefore, inexpensive. Furthermore, the later 3d metals tend to form weaker metal-ligand bonds than 4d and 5d metals, which suggests that this type of complex might be more reactive.[14]

Another approach to achieving two-electron reactivity in mid to late 3d transition metal complexes is through the use of redox-active ligands. For

example, Smith et al. recently reported a Co(III) complex of the noninnocent ligand, 2,4-di-*tert*-butyl-6-(2,6-diisopropylphenylamido)phenolate ($Na[Co^{III}(ap^{Ph})_2]$), that catalyzes the cross-coupling of alkyl halides and organozinc reagents.[15] The mechanism by which this reaction occurs involves 2-electron oxidative addition of the alkyl halide and 2-electron reductive elimination of the product. In this example, Smith et al. showed that the oxidation state of the metal did not change during the reaction; rather, the electrons came from the redox-active ligand (Scheme 4-4).

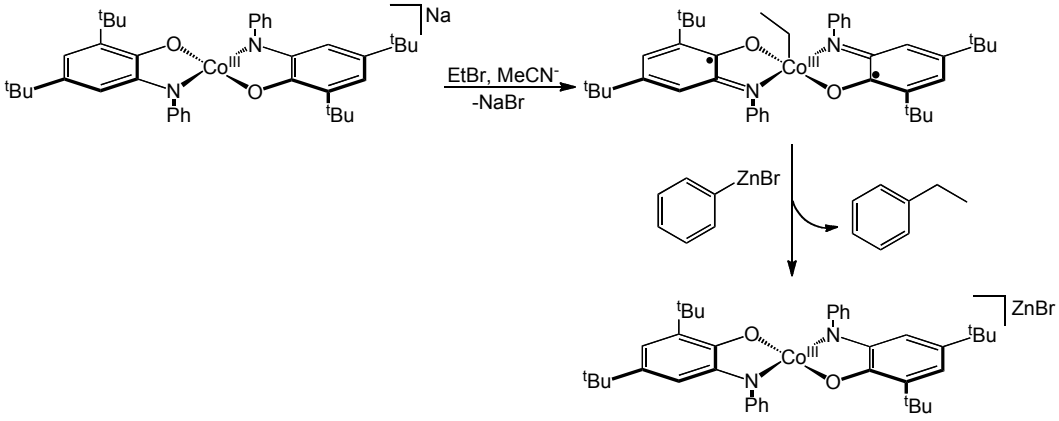

Scheme 4-4. Cross-coupling chemistry mediated by $Na[Co^{III}(ap^{Ph})_2]$. Electrons are transferred from the aminophenolate ligand; the Co(III) ion remains in the same oxidation state throughout the reaction.[15]

Similarly, Chaudhuri et al. reported Cu(II) and Zn(II) complexes of *N*,*N*-bis(3,5-di-tert-butyl-2-hydroxyphenyl)-1,2-phenylenediamine that catalyze the aerobic oxidation of alcohols to form aldehydes, a net 2-electron process, wherein the electrons are taken from the ligand, not the metal.[16]

Our group has recently been exploring the preparation and properties of

redox-active ligands. In Chapters 2-3 tripodal, tetradentate, carboxamide ligands were described. Removal of one (*o*-PhNC(O)R) moiety yields HN(*o*-PhNC(O)R)$_2$ (R = iPr,), a tridentate, carboxamide ligand with the potential to be redox-active.[17] The mononuclear and dinuclear complexes, $(Et_4N)_2[Co^{II}(N\text{-}\kappa N(o\text{-}PhNC(O)^iPr\text{-}\kappa N)\text{-}(o\text{-}PhNHC(O)^iPr))_2]_2$ and $(Et_4N)_2[(Co^{II}(\mu_2\text{-}N(o\text{-}PhNC(O)^iPr\text{-}\kappa N)_2))_2]_2$, display multiple oxidation events in their cyclic voltammagrams. Furthermore, they catalytically activate dioxygen and, in the presence of PPh_3, transfer the oxygen to form $O{=}PPh_3$. These results, along with work currently being carried out by Omar Villanueva et al., indicate that this ligand is redox-active.

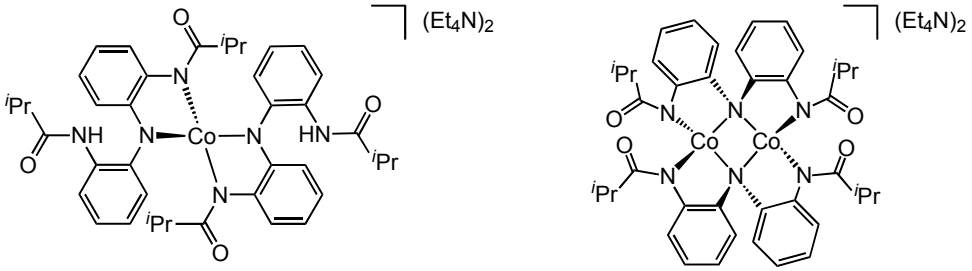

$(Et_4N)_2[Co^{II}(N\text{-}\kappa N(o\text{-}PhNC(O)^iPr\text{-}\kappa N)\text{-}(o\text{-}PhNHC(O)^iPr))_2]_2$ $(Et_4N)_2[\{Co^{II}(\mu_2\text{-}N(o\text{-}PhNC(O)^iPr\text{-}\kappa N)_2)\}_2]_2$

Figure 4-2. Cobalt(II) complexes of a redox-active dicarboxamidate ligand prepared by Sharma et al.[17]

Given the ability to form complexes with overall higher oxidation states, we then sought an analogous ligand framework that could stabilize low valent transition metals. Whereas transition metals in higher oxidation states (hard acids) are stabilized by anionic ligands (hard bases), low valent transition metals (softer acids) are better stabilized by neutral ligands (softer bases).

Section 4-2. Results and Discussion

We hypothesized that the incorporation of imine substituents into our established NNN (tridentate with nitrogen donors) pincer-type ligand framework may allow for the isolation of low-valent, coordinatively unsaturated transition metal complexes while maintaining the redox-activity of the ligand, itself. This may, in turn, allow for us to effect the types of transformations previously discussed for low-valent, coordinatively unsaturated transition metal complexes. Therefore, the ligand HN(*o*-PhN=C(H)Ph)$_2$ (Figure 4-3) was sought.

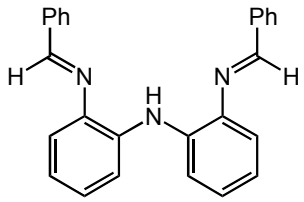

Figure 4-3. The desired ligand, N(*o*-PhN=C(H)Ph)$_2$.

Addition of benzaldehyde and a catalytic amount of formic acid to a benzene solution of HN(*o*-PhNH$_2$)$_2$, followed by reflux and concomitant azeotropic distillation, results in a product in moderate yield (58%) that has the expected parent peak in its mass spectrum, (positive mode ESI-MS, *m/z* = 376.2) and peaks in its FT-IR spectrum that are consistent with the expected N-H and C=N stretches (KBr, υ_{NH} = 3429, 3275 cm^{-1} and υ_{CN} = 1607, 1580 cm^{-1}). However, both the ^{1}H and ^{13}C NMR spectra provide evidence for the formation of an asymmetric species. This is not uncommon for this type of ligand, as it has been shown that the alkyl analog, (*7E*)-N^1-benzylidene-N^2-[(*E*)-2-(benzylideneamino)ethyl]ethane-1,2-diamine, exists in an equilibrium between

the diimine and the monoaminal (Figure 4-4A).[18] It has also been demonstrated that metallation of these species results in the formation of the metallated diimine exclusively.[18-20]

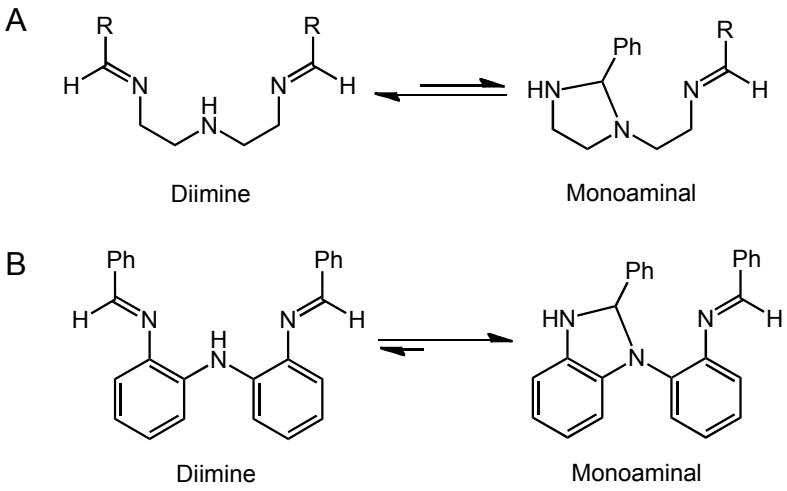

Figure 4-4. (A) Equilibrium between the diimine and monoaminal of analogous ligand, (*7E*)-N^1-benzylidene-N^2-[(*E*)-2-(benzylideneamino)-ethyl]ethane-1,2-diamine and (B) the equilibrium between the desired ligand, N(*o*-PhN=C(H)Ph)$_2$ and the asymmetric monoaminal that forms.[18]

Though this previous work was promising, the NMR spectra of HN(*o*-PhN=C(H)Ph)$_2$ did not indicate that there was an equilibrium between the two species in solution, and attempts to metallate with and without deprotonating were unsuccessful.

To prevent the cyclization of the ligand, a methyl group was installed, to make a tertiary central amine. The precursor amine, MeN(*o*-PhNH$_2$)$_2$ was prepared by a modified published procedure developed by Omar Villanueva.[21] Addition of benzaldehyde and 3 drops HCl to a toluene solution of MeN(*o*-

$PhNH_2)_2$, followed by reflux/azeotropic distillation yielded the desired product, N(*o*-PhN=C(H)Ph)$_2$ (L^{im}), in good yield (90%).

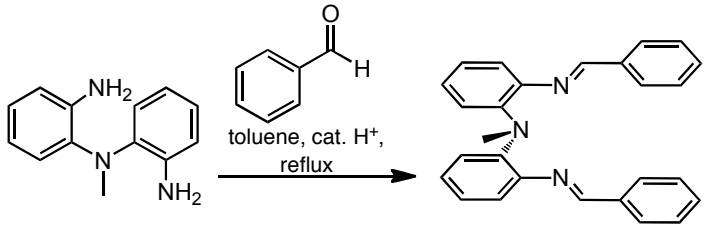

Scheme 4-5. Synthesis of ligand described herein, L^{im}.

The solution-state, two-fold symmetry of this ligand is confirmed by both its ^{1}H and ^{13}C NMR spectra. The mass spectrum (positive mode ESI-MS) confirms the structural assignment, as the parent peak exhibits an *m/z* = 390.3 ($[M+1]^+$). The protonation state of the nitrogen atoms is confirmed by the integration of the ^{1}H NMR spectrum and the lack of N-H stretches in its FT-IR spectrum. The CN stretching frequencies (υ_{CN} = 1625, 1576 cm^{-1}) are consistent with the formation of the imino functionality. Metallation with $M^{II}Br_2$ salts (M = Co, Zn) results in the formation of the neutral complexes, $[M^{II}(L^{im})(Br)_2]$.

$[Co(L^{im})(Br)_2]$ can be prepared as green, crystalline material in good yield (77%) by addition of one equivalent $CoBr_2$ to a solution of L^{im}, as shown in Scheme 4-6.

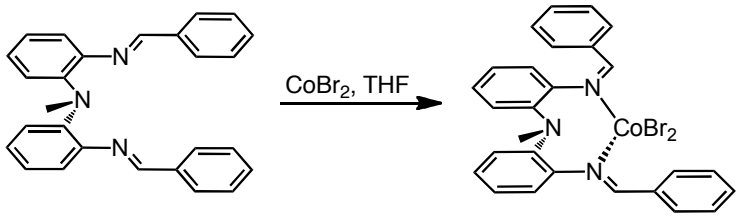

Scheme 4-6. Synthesis of $[Co(L^{im})(Br)_2]$.

Upon metallation, there is a shift in the CN stretching frequencies, consistent with the changing of the bonding environment of the nitrogen (υ_{CN} = 1610, 1582 cm^{-1}). The positive mode ESI-MS spectrum of this complex shows *m/z* = 527.0 and 529.0 (~1:1 distribution). This value is consistent with the loss of one bromide upon ionization, and the isotope distribution is consistent with one bound bromide ion. The solid-state structure of this complex is shown in Figure 4-5.

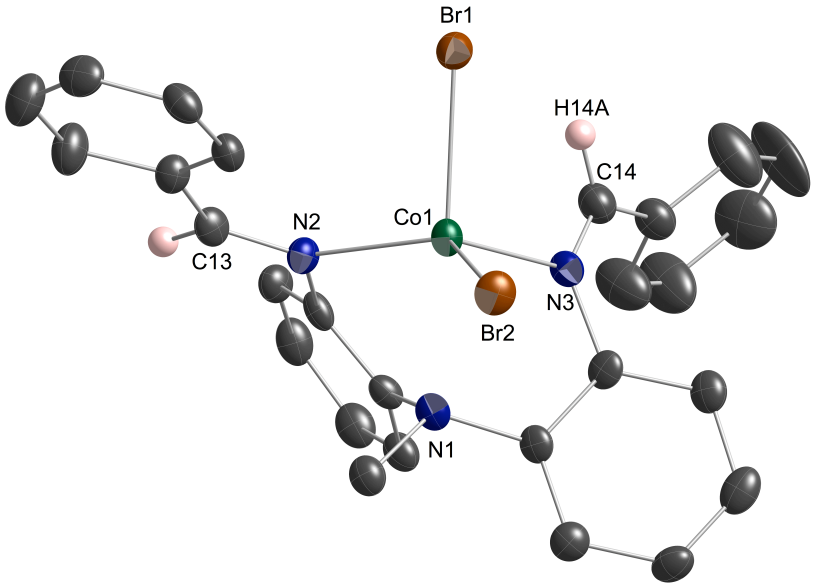

Figure 4-5. Molecular structure of $[Co(L^{im})(Br)_2]$. Thermal ellipsoids drawn at 40%. Except H13A and H14A, hydrogen atoms are excluded for clarity.

Table 4-1. Selected bond lengths and angles for $[Co(L^{im})(Br)_2]$.

Bond Lengths (Å) and Angles (°)			
Co1••N1	2.410(4)	N2 – Co1 – N3	113.67(15)
Co1 – N2	2.093(4)	Br1 – Co1 – Br2	107.48(3)
Co1 – N3	2.084(4)	Ave. N – Co1 – Br1	98.89(8)
Co1 – Br1	2.4557(10)	Ave. N – Co1 – Br2	116.91(8)
Co1 – Br2	2.3851(9)		
Ave. N=C	1.277(4)		
Ave. N-C_{Ar}	1.431(4)		

$[Co(L^{im})(Br)_2]$ crystallizes with trigonal pyramidal geometry (τ_4 = 0.85)[22] about the 4-coordinate cobalt(II) center. One of the phenylmethanimine substituents is inverted, yielding the *E*-isomer. This may be enforced by a weak hydrogen bond between Br1 and H14A (Br1 – C14 distance = 3.471 Å) as well as the unfavorable interaction between the phenyl substituent and the bound bromide. This lack of symmetry in the solid-state is consistent with the corresponding solution-state data. The ^{1}H NMR of this complex contains 12 signals, indicating that the ligand does not exhibit C_2 symmetry in solution.

To determine the electrochemical properties of this complex, cyclic voltammetry experiments were performed. $[Co(L^{im})(Br)_2]$ did not exhibit any reversible or irreversible events within the THF solvent window. This is consistent with the fact that attempts to chemically reduce the complex were unsuccessful. It was hypothesized that removal of one or both bromide ligands may allow for reduction of the cobalt by removing the possibility of halide radical formation.[23]

Synthesis of $[Co(L^{im})(Br)_2]$ followed by addition of a halogen abstracting reagent ($TlPF_6$) results in the loss of one equivalent of TlBr and formation of the monocationic $[Co(L^{im})(Br)]^+$ in good yield (70%) (Scheme 4-7).

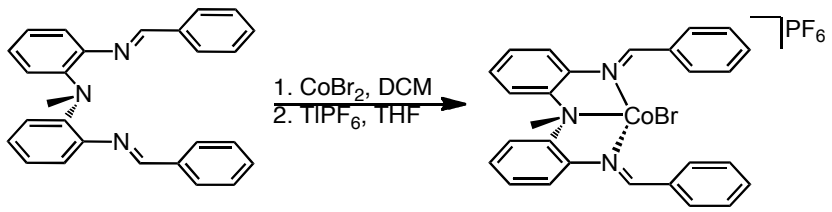

Scheme 4-7. Synthesis of $[Co(L^{im})(Br)]PF_6$.

This complex is less soluble in non-coordinating solvents than its neutral counterpart. It also exhibits fewer signals in its ^1H NMR spectrum, indicating that it is of higher symmetry in solution. A decrease in the frequencies of the CN stretching frequencies in the FT-IR (KBr) is indicative of greater N-donation to the metal center. The solid-state structure of $[Co(L^{im})(Br)]PF_6$ is shown in Figure 4-6.

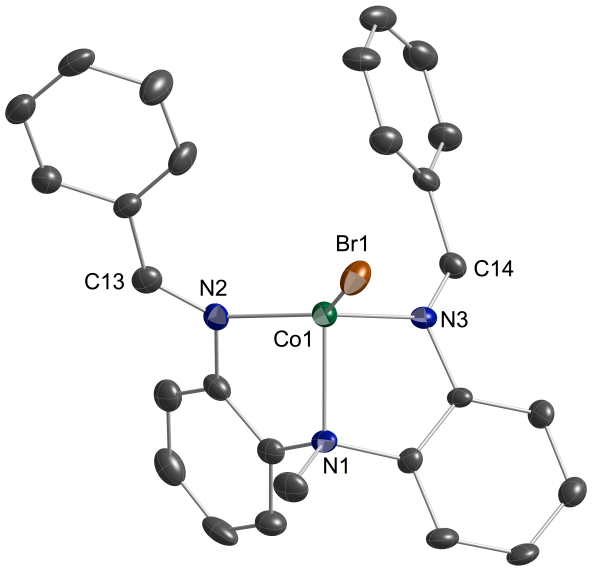

Figure 4-6. Molecular structure of $[Co(L^{im})(Br)]PF_6$. Thermal ellipsoids drawn at 40%. The counterion and hydrogen atoms are excluded for clarity.

Table 4-2. Selected bond lengths and angles for $[Co(L^{im})(Br)]^+$.

Bond Lengths (Å) and Angles (°)			
Co1 – N1	2.102(4)	Ave. N=C	1.281(5)
Co1 – N2	2.016(5)	Ave. N-C_{Ar}	1.435(5)
Co1 – N3	2.025(4)	N2 – Co1 – N3	114.43(18)
Co1 – Br1	2.3271(10)	Ave. N_{im} – Co1 – Br1	121.91(9)

As indicated by the ^{1}H NMR spectrum, this complex exhibits higher symmetry in the solid-state than $[Co(L^{im})(Br)_2]$. Loss of the bromide *trans* to N1 removes both the potential hydrogen bonding interaction and the repulsive interaction between the bromide and the electron-rich phenyl groups. As a result, both imine substituents are in the *Z* conformation. As indicated by the FT-IR spectrum, the imine NC bonds are elongated with respect to $[Co(L^{im})(Br)_2]$. However, the

differences are within the error of the measurement. Loss of the bromide ion also causes the contraction of the Co-N2 and Co-N3 bonds, such that the cobalt ion is now bonding N1, forming a distorted trigonal pyramid (τ_4 = 0.82)[22]. This structure resembles that of the recently reported, 4-coordinate Ru(II) complex shown in Figure 4-7 ([Cy-PSiP)RuN($SiMe_3$)$_2$] (Cy-PSiP = [κ^3-(2-$Cy_2PC_6H_4$)$_2$SiMe]).[24] This complex is a rare example of a 14-electron Ru(II) complex in slightly distorted trigonal pyramidal geometry.

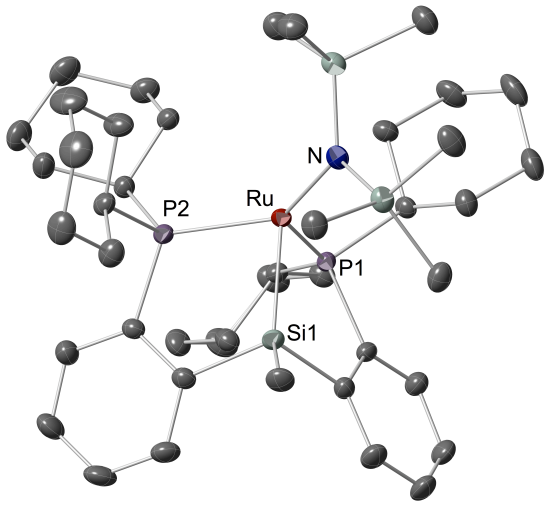

Figure 4-7. Molecular structure of [Cy-PSiP)RuN($SiMe_3$)$_2$].[24] Hydrogen atoms are excluded for clarity.

To determine the electrochemical properties of this complex, cyclic voltammetry experiments were performed. Like [Co(L^{im})($Br)_2$], [Co(L^{im})(Br)]PF_6 did not exhibit any reversible events within the DCM or $NCCH_3$ solvent window.

The zinc(II) complex was prepared concurrently with the cobalt complexes. Addition of one equivalent of $ZnBr_2$ to a THF solution of L^{im}

followed by precipitation of the crude, yellow solid with diethyl ether results in the isolation of crude $[Zn(L^{im})(Br)_2]$ (Scheme 4-8)

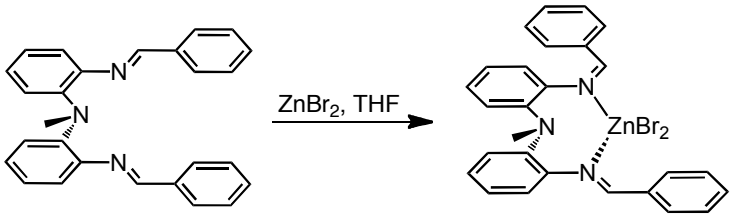

Scheme 4-8. Synthesis of $[Zn(L^{im})(Br)_2]$.

This product displays two peaks in the positive mode ESI-MS spectrum with an isotopic distribution and *m/z* (532.0 and 534.0) that are consistent with $[Zn(L^{im})(Br)]^+$. The NC stretching frequencies, as determined by FT-IR spectroscopy, are identical within error to those exhibited by $[Co(L^{im})(Br)_2]$. Also, like $[Co(L^{im})(Br)_2]$, this complex displays a number of signals in its ^1H NMR spectrum, indicating that it is not C_2 symmetric in solution. Recrystallization of $[Zn(L^{im})(Br)_2]$ by diffusion of diethyl ether into an MeOH and DCM solution of the product yields X-ray quality material. The solid-state structure is shown in Figure 4-8.

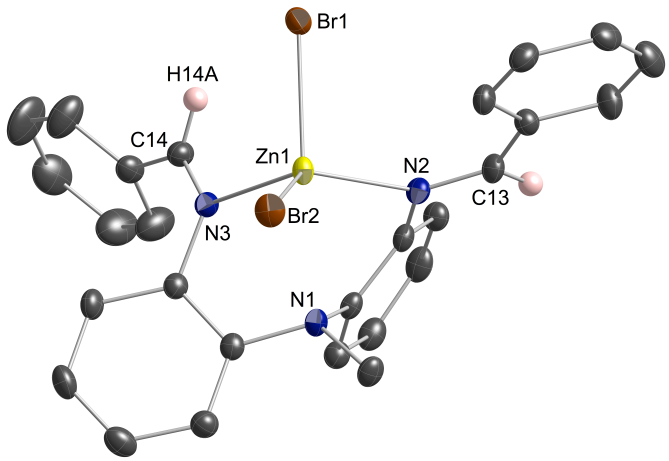

Figure 4-8. Molecular structure of $[Zn(L^{im})(Br)_2]$. Thermal ellipsoids drawn at 40%. Except H13A and H14A, hydrogen atoms are excluded for clarity.

Table 4-3. Selected bond lengths and angles for $[Zn(L^{im})(Br)_2]$.

Bond Lengths (Å) and Angles (°)			
Zn1••N1	2.581	N2 – Zn1 – N3	110.51(11)
Zn1 – N2	2.117(3)	Br1 – Zn1 – Br2	110.857(19)
Zn1 – N3	2.106(3)	Ave. N – Zn1 – Br1	99.14(5)
Zn1 – Br1	2.4484(8)	Ave. N – Zn1 – Br2	117.00(5)
Zn1 – Br2	2.3598(7)		
Ave. N=C	1.283(3)		
Ave. N-C_{Ar}	1.428(3)		

$[Zn(L^{im})(Br)_2]$ crystallizes in slightly distorted trigonal pyramidal geometry (τ_4 = 0.88).[22] The Zn-N distances are longer than the Co-N distances in the analogous cobalt complex, but the Zn-Br distances are similar to those in the cobalt complex. This may be due to the decreased polarizability of Zn(II) making the interaction with the neutral ligand less favorable. Like the cobalt complex, the

imine arms of $[Zn(L^{im})(Br)_2]$ are in opposite configurations, one having the *E* configuration and the other the *Z* configuration in the solid state as well as in solution. The zinc complex also does not exhibit any electrochemical events within the solvent window. This indicates that the ligand is not redox-active.

To determine if L^{im} would stabilize a low-valent transition metal complex, a transition metal salt that was stable in its low-valent oxidation state was sought. Addition of one equivalent of CuCl to a THF solution of L^{im} results in the formation of an orange solution. Upon removal of solvent, a red product can be isolated. This product exhibits CN stretching frequencies (FT-IR, KBr) that are very similar to those of $[Co(L^{im})(Br)]PF_6$ (1608 and 1571 cm^{-1}). The ^1H and ^{13}C NMR of the complex indicate that the species is C_2-symmetric in solution. The positive mode mass spectrum (ESI-MS) exhibits a parent peak with m/z = 452.3 and a smaller peak with m/z = 940.8, which are consistent with $[Cu(L^{im})]^+$ and $[(Cu(L^{im}))_2Cl] + 1$, respectively. The product can be recrystallized by diffusion of diethyl ether into a THF/MeOH solution to yield red needles in good yield (70.2%). As identified by X-ray crystallography, the product is $[(Cu(L^{im}))_2(\mu\text{-}Cl)]CuCl_2$. The solid-state structure of this complex is shown in Figure 4-9.

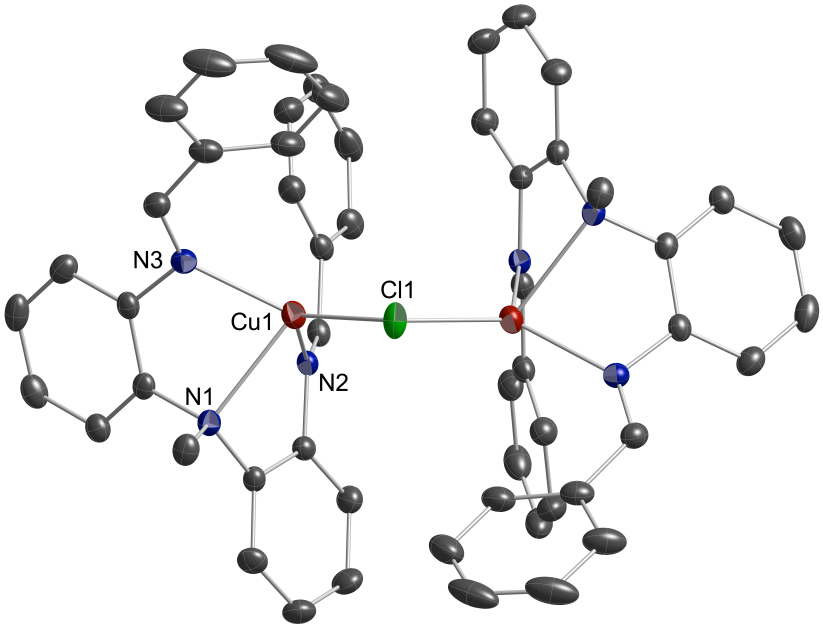

Figure 4-9. Molecular structure of $[(Cu(L^{im}))_2(\mu\text{-}Cl)]CuCl_2$. Thermal ellipsoids drawn at 40%. The counterion and hydrogen atoms are excluded for clarity.

Table 4-4. Selected bond lengths and angles for $[(Cu(L^{im}))_2(\mu\text{-}Cl)]^+$

Bond Lengths (Å) and Angles (°)			
Cu1 – N1	2.3018(19)	N2 – Cu1 – N3	112.84(7)
Cu1 – N2	2.0921(19)	Ave. N_{im} – Cu1 – Cl1	123.55(4)
Cu1 – N3	2.071(2)	N1 – Cu1 – Cl1	116.63(5)
Cu1 – Cl1	2.2248(7)	Cu1 – Cl1 – Cu1	111.22(4)
Ave. N=C	1.287(2)		
Ave. N-C_{Ar}	1.436(2)		

The complex crystallizes in the space group C2/c with Z' = 0.5 and exhibits distorted trigonal pyramidal geometry about the copper ion ($\tau_4 = 0.80$).[22] Both of the imine arms are in the *Z* conformation, as it is in solution. As indicated by the

FT-IR spectrum, the Cu-N_{im} and $N_{im}C$ distances are similar to those found in $[Co(L^{im})(Br)]PF_6$, whereas the Cu-N1 distance is 0.2 Å longer. This may be due to the fact that Cl^- is more *cis*-labilizing than Br^-.

To determine the electrochemical properties of this complex, cyclic voltammetry experiments were performed. Like $[Co(L^{im})(Br)_2]$ and $[Co(L^{im})(Br)]PF_6$, $[(Cu(L^{im}))_2(\mu\text{-}Cl)]CuCl_2$ did not exhibit any reversible events within the THF or DCM solvent window.

$[(Cu(L^{im}))_2(\mu\text{-}Cl)]CuCl_2$ does not react with organic azides, as evidenced by the FT-IR spectrum, in which only free azide was observed. The complex does react with the inorganic azide, NaN_3, to form $[Cu(L^{im})(N_3)]$. However, it is unlikely that this complex would extrude N_2, as the previously synthesized imido complexes incorporate a bridging, organic imide.[6] Therefore, it is no surprise that heating a solution of this species results in demetallation, as the ^1H NMR spectrum of the product only displays peaks corresponding to free ligand. $[(Cu(L^{im}))_2(\mu\text{-}Cl)]CuCl_2$ is also unreactive towards O_2.

To prepare an hypothetically more reactive Cu(I) complex without the halide ligand, $[Cu(NCCH_3)_4]PF_6$ was utilized as the metal salt. As shown in Scheme 4-9, addition of one equivalent of $[Cu(NCCH_3)_4]PF_6$ to a solution of of L^{im} followed by precipitation with diethyl ether yields a yellow powder in 77% yield.

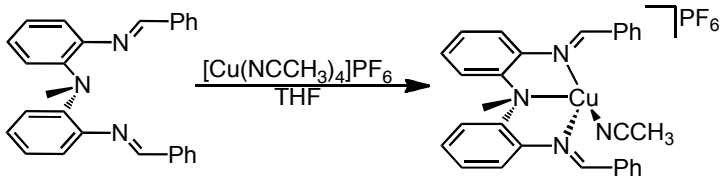

Scheme 4- 9. Synthesis of $[Cu(NCCH_3)(L^{im})]PF_6$.

This product is C_2-symmetric in solution, as indicated by its ^1H and ^{13}C NMR spectra. The CN stretching frequencies of 1608 and 1572 cm^{-1} (FT-IR, KBr) are similar to those of $[(Cu(L^{im}))_2(\mu\text{-}Cl)]CuCl_2$. Another peak seen in the FT-IR at 2253 cm^{-1} indicates that a molecule of $NCCH_3$ is bound to the metal center. A parent peak with m/z = 452.3 in the positive mode mass spectrum (ESI-MS) is consistent with $[Cu(L^{im})]^+$. Recrystallization by diffusion of diethyl ether into a THF solution of the product yields X-ray quality crystals. The solid-state structure is shown in Figure 4-10.

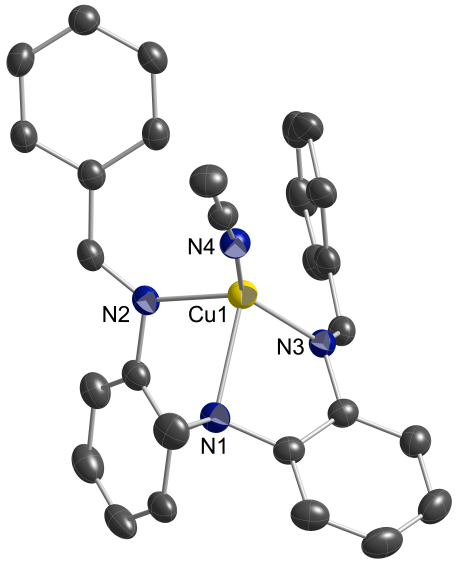

Figure 4-10. Molecular structure of $[Cu(NCCH_3)(L^{im})]PF_6$. Thermal ellipsoids drawn at 40%. The counterion and hydrogen atoms are excluded for clarity.

Table 4-5. Selected bond lengths and angles for $[Cu(NCCH_3)(L^{im})]^+$

Bond Lengths (Å) and Angles (°)			
Cu1 – N1	2.266(3)	N2 – Cu1 – N3	105.53(12)
Cu1 – N2	2.057(3)	Ave. N_{im} – Cu1 – N1	79.50(9)
Cu1 – N3	2.013(3)	Ave. N_{im} – Cu1 – N4	127.18(10)
Cu1 – N4	1.885(3)	N1 – Cu1 – N4	110.37(13)
Ave. N=C	1.283(4)		
Ave. N-C_{Ar}	1.430(4)		

The geometry about the copper ion is intermediate between trigonal pyramidal and seesaw ($\tau_4 = 0.75$).[22] Despite the difference in geometry, the bond lengths are similar to those found in $[(Cu(L^{im}))_2(\mu\text{-}Cl)]CuCl_2$, indicating that the change in ligand, from bridging chloride to acetonitrile, did not strongly affect the ligand-metal interaction. As in solution, in the solid-state both imine arms are in *Z* configuration.

The reactivity of this complex was explored with dioxygen. Copper(I) complexes tend to react readily with O_2 to ultimately form dimeric species that bind the two-electron reduced O_2^{2-}, forming the Cu(II):Cu(II) μ-1,2-peroxo, the Cu(II):Cu(II) μ-η^2:η^2-peroxo, or the Cu(III):Cu(III) bis-μ-oxo.[25] However, no reaction occurs upon addition of O_2 to a solution of $[Cu(NCCH_3)(L^{im})]PF_6$, as evidenced by the ^{1}H NMR spectrum of the product. The electrochemical properties of $[Cu(NCCH_3)(L^{im})]PF_6$ were explored by cyclic voltammetry (0.2 M $TBAPF_6$ in DCM, referenced vs. Fc/Fc^+, with a Ag/Ag^+ reference electrode and

glassy carbon working electrode). The resulting, reversible electrochemical event is shown in Figure 4-11.

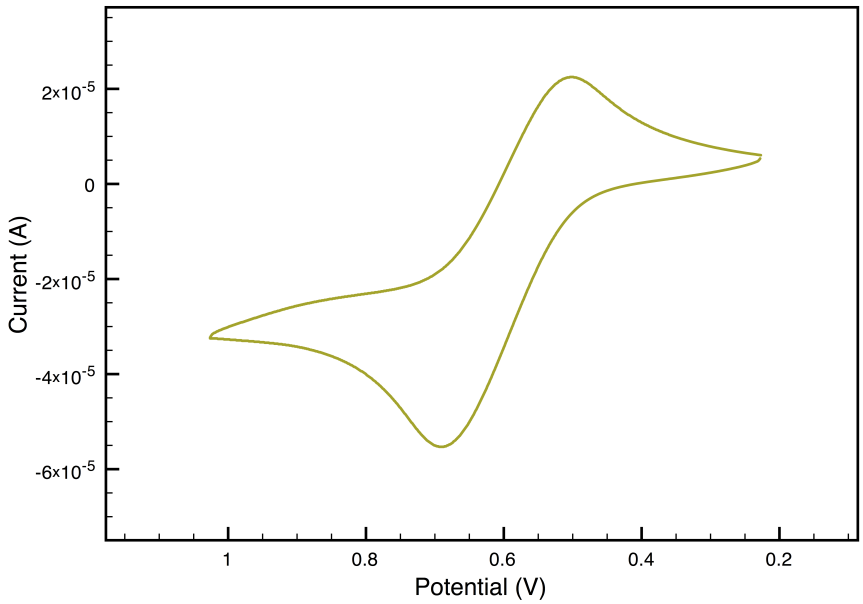

Figure 4-11. Cyclic voltammogram of $[Cu(NCCH_3)(L^{im})]PF_6$ (50 mV/s, $E_{1/2}$ = +597 mV) with 0.2 M $TBAPF_6$ in DCM, referenced vs. Fc/Fc^+, Ag/Ag^+ reference electrode, glassy carbon working electrode.

$[Cu(NCCH_3)(L^{im})]PF_6$ displays a reversible $Cu^{I/II}$ couple at +597 mV vs. Fc/Fc^+, which is equal to 784 mV vs. SCE.[26] This value is considerably higher than the $Cu^{I/II}$ oxidation potentials of the four coordinate, Cu(I) complexes, $[Cu(solv)(TMPA)]^+$, $[Cu(solv)(^{TMB}TMPA)]^+$, $[Cu(solv)(^{Bz}TMPA)]^+$, and $[Cu(solv)(^{MOB}TMPA]^+$, discussed in Chapter 1. This value is also considerably higher than the reduction potential of dioxygen (-0.79 V vs. SCE).[27]

Addition of neutral donor ligands PPh_3, CO, and ^{t}BuNC to a solution of $[Cu(NCCH_3)(L^{im})]PF_6$ results in the formation of the complexes $[Cu(PPh_3)(L^{im})]PF_6$, $[Cu(CO)(L^{im})]PF_6$, and $[Cu(CN^tBu)(L^{im})]PF_6$, as evidenced by

the resulting ^{1}H and ^{31}P spectra for $[Cu(PPh_3)(L^{im})]PF_6$ and the FT-IR spectra of $[Cu(CO)(L^{im})]PF_6$ and $[Cu(CN^{t}Bu)(L^{im})]PF_6$. The CO stretching frequency of 2111 cm^{-1} (free CO υ = 2143 cm^{-1}) in the FT-IR spectrum (KBr) of $[Cu(CO)(L^{im})]PF_6$ is high compared to many of those known for 4-coordinate Cu(I) complexes, indicating that there is minimal contribution to the π^*-orbitals of the CO ligand.[28,29]

Section 4-3. Conclusion

In summary, a series of late, first-row transition metal complexes were prepared with the novel, neutral, pincer-type ligand, L^{im}. These complexes exist in the relatively rare trigonal pyramidal geometry. The tertiary amino nitrogen only binds the metal ion when there is no ligand *trans* to it. The geometry about the imine CN bond is also dependent upon the ligand *trans* to the tertiary amine, which is likely due to hydrogen bonding and repulsive π interactions.

The zinc and copper complexes have the ideal 18-electron metal center. However, both cobalt(II) complexes contain unstable, 15-electron metal centers. Except for $[Cu(NCCH_3)(L^{im})]PF_6$, solutions of the complexes do not exhibit any electrochemical events within the solvent window studied. Clearly, the ligand is not redox-active, which may be due to the tertiary nature of the amine nitrogen, preventing movement of electrons through the ligand backbone. Furthermore, the desired cobalt(I) complexes were not accessible. The copper(I) complexes are relatively unreactive with dioxygen and azides. However, they do form complexes with the neutral ligands CO, PPh_3, and $CN^{t}Bu$.

Section 4-4. Experimental Section

General Considerations and Materials

All manipulations were carried out using standard Schlenk techniques or conducted in an MBraun Labmaster 130 drybox under a nitrogen atmosphere. All reagents used were purchased from commercial vendors and used as received unless otherwise noted. Anhydrous solvents were purchased from Sigma-Aldrich and further purified by sparging with Ar gas followed by passage through activated alumina columns. Deuterated NMR solvents were purchased from Cambridge Isotope Laboratories, Inc. and degassed and dried according to standard procedures prior to use.[30] Elemental analyses were performed either by Midwest Microlab, LLC, Indianapolis, IN or Atlantic Microlab, Inc., Norcross, GA. ^{1}H and ^{13}C NMR spectra were recorded on either an Inova 400 MHz or a Varian Mercury 300 MHz spectrometers at ambient temperature. Chemical shifts were referenced to residual solvent peaks. Infrared spectra were recorded as KBr pellets on a Varian Scimitar 800 Series FT-IR spectrometer. Solution-state magnetic moments were measured using the method of Evans.[31,32] Mass spectra were recorded in the Mass Spectrometry Center at Emory University on a JEOL JMS-SX102/SX102A/E mass spectrometer.

Syntheses

L^{im}. To a solution of MeN(*o*-$PhNH_2$)$_2$ (2.08 g, 9.75 mmol) in toluene (DCM, 125 mL) was added benzaldehyde (2.10 mL, 20.8 mmol) followed by 3 drops HCl. A green precipitate formed in the orange solution. The mixture was equipped with a

Dean-Stark apparatus and heated to reflux under N_2 overnight. The brown solution was cooled to room temperature, filtered, and concentrated in vacuo to yield a brown oil. The product was crystallized by layering hexanes over a diethyl ether solution thereof and storing at -35 °C. The resulting brown crystals were collected by filtration (3.41 g, 90%). ^{1}H NMR (δ, $CDCl_3$, 400 MHz): 8.13 (s, 2H, =CH), 7.57 (dd, 4H, *J* = 8.4, 2.0 Hz, ArH), 7.40 (m, 6H, ArH), 7.14 (m, 4H, ArH), 6.95 (m, 2H, ArH), 6.79 (dd, 2H, *J* = 7.6, 0.8 Hz, ArH), 3.45 (s, 3H, MeH). ^{13}C NMR (δ, $CDCl_3$, 400 MHz): 159.16, 145.78, 143.64, 136.62, 130.97, 128.72, 128.43, 126.14, 122.71, 122.11, 119.49, 40.72. Positive mode ESI-MS: $C_{27}H_{24}N_3$ *m/z* $[M+1]^+$ Calcd. 390.3 Found 390.3. FTIR (KBr, cm^{-1}): 3057, 3022, 2869, 2811, 1625, 1576, 1483, 1447, 1344, 1282, 1242, 1188, 1134, 1105, 1047, 960, 875, 848, 761, 692, 534, 506, 464.

[Co(L^{im})(Br_2)]. To a solution of L^{im} (141.4 mg, 0.363 mmol) in THF (3 mL) was added $CoBr_2$ (76.0 mg, 0.347 mmol) as a solid. After stirring for 3 hours, diethyl ether was added (10 mL) as the green solution was stirred vigorously. The crude powder was collected by filtration. Diffusion of diethyl ether into a 3:2 MeOH: DCM solution yielded the crystalline, green product (162.7 mg, 77.4%). ^{1}H NMR (δ, CD_2Cl_2, 300 MHz): 74.08, 15.46, 12.97, 11.50, 10.51, 7.56, 5.95, 4.71, 4.15, 1.47, 1.27, -0.87, -5.79. UV-vis (CH_2Cl_2): λ_{max}, nm (ε, M^{-1} cm^{-1}): 648 (264), 624 (265). Positive mode ESI-MS (*m/z*) for $[Co(L^{im})(Br)]^+$ $(C_{27}H_{23}BrCoN_3)^+$ calcd 527.0 and 529.0; found 527.0 and 529.0. FTIR (KBr, cm^{-1}): 3063, 3003, 2933, 1610, 1582, 1575, 1484, 1452, 1403, 1305, 1259, 1219, 1180, 1112, 1097, 1032,

988, 887, 768, 727, 685, 562, 528, 477.

[Co(L^{im})Br]PF_6. To a solution of L^{im} (51.0 mg, 0.131 mmol) in DCM (3 mL) was added $CoBr_2$ (28.5 mg, 0.130 mmol) as a solid. After stirring for 15 minutes, $TlPF_6$ (46.0 mg, 0.132 mmol) was added to the green suspension as a THF solution (3 mL). A white preciptate formed in the purple solution. After stirring for five hours, the mixture was filtered, and from it solvent was removed. Layering of diethyl ether onto a DCM solution of the product yielded dark green crystals (61.9 mg, 70.2%). ^{1}H NMR (δ, CD_2Cl_2, 400 MHz): 70.78, 40.05, 12.07, 7.35, 0.86, -5.50. μ_{eff} = 4.36 μ_B (Evans method, CD_3CN, 400 MHz). UV-vis (CH_2Cl_2): λ_{max}, nm (ε, M^{-1} cm^{-1}): 559 (56), 659 (75). FTIR (KBr, cm^{-1}): 3064, 1608, 1572, 1484, 1452, 1408, 1386, 1323, 1298, 1276, 1239, 1200, 1178, 1114, 1092, 1048, 1021, 1003, 984, 838, 765, 735, 688, 557, 528, 477.

[Zn(L^{im})$(Br)_2$]. To a solution of L^{im} (83.8 mg, 0.215 mmol) in THF (3 mL) was added $ZnBr_2$ (46.5 mg, 0.206 mmol) as a solid. After stirring for 1.25 hours, diethyl ether was added (10 mL) as the yellow solution was stirred vigorously. The crude powder was collected by filtration. Diffusion of diethyl ether into a MeOH: DCM solution yielded the crystalline, yellow product (88.3 mg, 70.1%). ^{1}H NMR (δ, CD_2Cl_2, 400 MHz): 8.70 (d, 2H, *J* = 9.2 Hz, ArH), 8.55 (dd, 2H, *J* = 8.0, 1.2 Hz, ArH), 7.70 (m, 1H, ArH), 6.62 (td, 2H, *J* = 6.4, 1.6 Hz, ArH), 7.53 (dd, 1H, *J* = 8.0, 1.2 Hz, =CH), 7.42 (m, 2H, ArH), 7.32 (dd, 1H, *J* = 7.6, 1.6, =CH), 7.25 (t, 2H, *J* = 7.6 Hz, ArH), 7.15 (m, 4H, ArH), 7.02 (m, 2H, ArH), 6.83

(dd, 2H, *J* = 8.0, 1.6 Hz, ArH), 3.12 (s, 3H, MeH). ^{13}C NMR (δ, CD_2Cl_2, 400 MHz): 169.78, 169.29, 145.95, 145.78, 144.20, 138.35, 134.96, 133.41, 132.13, 130.78, 129.84, 129.38, 129.06, 128.82, 127.89, 126.39, 124.27, 123.29, 122.18, 120.94. Positive mode ESI-MS (*m/z*) for $[ZnL^{im}(Br)]^+$ $(C_{27}H_{23}BrN_3Zn)^+$ calcd 532.0 and 534.0; found 532.0 and 534.0. FTIR (KBr, cm^{-1}): 3064, 2969, 2933, 2873, 1612, 1581, 1405, 1313, 1227, 1181, 1113, 1098, 1037, 887, 768, 725, 685, 477.

$[(CuL^{im})_2Cl]CuCl_2$. To a solution of L^{im} (160.5 mg, 0.412 mmol) in THF (5 mL), CuCl (41.1 mg, 0.415 mmol) was added as a solid, forming an orange solution. After stirring overnight, THF was removed *in vacuo* to yield a red solid. The product was recrystallized by the slow diffusion of diethyl ether into a THF/MeOH solution, yielding red needles of the desired product (103.8 mg, 70.2%). ^{1}H NMR (δ, CD_2Cl_2, 300 MHz): 8.33 (d, 4H, *J* = 7.2 Hz, ArH), 8.20 (s, 2H, =CH), 7.52 (m, 2H, ArH), 7.44 (t, 4H, *J* = 14.4, 7.5 Hz, ArH), 7.26 (m, 4H, ArH), 7.13 (td, 2H, *J* = 14.7, 7.8, 1.8 Hz, ArH), 6.91 (dd, 2H, *J* = 7.8, 0.6, ArH), 3.16 (s, 3H, MeH). ^{13}C NMR (δ, CD_2Cl_2, 300 MHz): 162.01, 146.62, 145.82, 134.64, 133.11, 130.25, 129.19, 128.11, 123.67, 120.68, 44.34. UV-vis (THF): λ_{max}, nm (ε, $M^{-1}\,cm^{-1}$): 456 (2282). Positive mode ESI-MS: $C_{54}H_{46}ClCu_2N_6$ *m/z* Calcd. 452.1 Found 452.3 $[CuL^{im}]^+$. FTIR (KBr, cm^{-1}): 3057, 2999, 2964, 2885, 1608, 1571, 1483, 1449, 1313, 1184, 1120, 1094, 973, 897, 873, 759, 685, 480.

$[Cu(NCCH_3)(L^{im})]PF_6$. To a solution of L^{im} (310.6 mg, 0.797 mmol) in THF (12

mL), $[Cu(NCCH_3)_4]PF_6$ (297.9 mg, 0.799 mmol) was added as a solid. After stirring for 3 hours, the volume of the solution was reduced to ~2 mL. Diethyl ether was added (10 mL) as the solution was stirred vigorously. The crude, yellow powder was collected by filtration (392.3 mg, 77.0%). Crystals suitable for X-ray diffraction were obtained by diffusion of diethyl ether into a THF solution of the product. ^{1}H NMR (δ, CD_2Cl_2, 400 MHz): 8.40 (s, 2H, =CH), 8.163 (d, 4H, J = 7.2 Hz, ArH), 7.58 (m, 6H, ArH), 7.361 (m, 4H, ArH), 7.27 (t, J = 13.2, 6.4 Hz, 2H, ArH), 7.06 (d, 2H, J = 7.6 Hz, ArH), 3.19 (s, 3H, MeH), 2.08 (s, 3H, $NCCH_3$). ^{13}C NMR (δ, CD_2Cl_2, 400 MHz): 163.93, 146.14, 145.41, 134.27, 134.02, 129.81, 129.57, 129.17, 127.59, 124.12, 120.87, 117.13, 45.65, 3.005. UV-vis (THF): λ_{max}, nm (ε, M^{-1} cm^{-1}): 455 (587). Positive mode ESI-MS (*m*/*z*) for $[CuL^{im}]^+$ ($C_{27}H_{23}CuN_3$) calcd 452.1; found 452.3. FTIR (KBr, cm^{-1}): 3061, 2937, 2878, 2253, 1610, 1572, 1451, 1389, 1298, 1260, 1214, 1180, 1115, 1097, 1052, 978, 840, 762, 691, 558, 482.

Crystallographic Data

For each complex, crystals were coated with Paratone N oil, and suitable crystals were suspended in small fiber loops. They were mounted in a cooled nitrogen gas stream at 173 K on a Bruker D8 APEX II CCD sealed tube diffractometer with graphite monochromated Mo Kα (0.71073 Å) radiation. Data was collected using a series of phi and omega scans with 10s frame exposures and 0.5° frame widths. The structures were solved using direct methods and difference Fourier techniques (Shelxtl, V6.12)[33]. Hydrogen atoms were added with the HFIX command. These were included in the final cycles of least squares

refinement, with isotropic Uij's that were determined by the riding model. All non-hydrogen atoms in the main residues were refined anisotropically. Residual solvent molecules in the unit cells were not refined anisotropically. Structure solution, refinement, and generation of publication materials were performed by using SHELX, V6.12 software.

$Co(L^{im})(Br)_2$, $Zn(L^{im})(Br)_2$, and $[Cu(NCCH_3)(L^{im})]PF_6$ crystallized in the space group $P2_1/c$, with R_1 = 0.0523, 0.0394, and 0.0718, respectively. $[(CuL^{im})_2Cl]CuCl_2$ crystallized in the spacegroup C2/c, with R_1 = 0.0432. $[Co(L^{im})(Br)]PF_6$ crystallized in the space group $P2_1/n$. Refinement yielded an R_1 = 0.0804. Residual diethyl ether solvent molecules were present in the unit cell of $[Co(L^{im})(Br)]PF_6$. These solvent molecules were disordered and did not refine suitably. Therefore, they were omitted from the structure using the SQUEEZE function in Platon.[34] This removed electron density peaks from four regions that held 48, 48, 48, and 47 electrons.

Table 4-6. Crystal data and structure refinement parameters for $Co(L^{im})(Br)_2$, $[Co(L^{im})(Br)]PF_6$, and $Zn(L^{im})(Br)_2$.

	$Co(L^{im})(Br)_2$	**$[Co(L^{im})(Br)]PF_6$**	**$Zn(L^{im})(Br)_2$**
Formula	$C_{27}H_{23}Br_2CoN_3$	$C_{27}H_{23}BrCoF_6N_3P$	$C_{27}H_{23}Br_2N_3Zn$
Crystal size (mm^3)	0.10 × 0.08 × 0.05	0.35 × 0.28 × 0.18	0.28 × 0.20 × 0.08
Form. wt. (g/mol)	608.23	673.29	614.67
Space group	$P2_1/c$	$P2_1/n$	$P2_1/c$
a (Å)	10.292(2)	8.074(2)	10.342(2)
b (Å)	24.373(5)	20.890(5)	24.325(6)
c (Å)	10.549(2)	17.839(4)	10.682(2)
α (deg)	90	90	90
β (deg)	113.409(3)	93.281(4)	113.111(3)
γ (deg)	90	90	90
V ($Å^3$)	2428.3(9)	3003.7(13)	2471.6(10)
Z	4	4	4
T (K)	173(2)	173(2)	173(2)
ϱ, calcd (g/cm)	1.664	1.489	1.652
Reflns collected	43409	51910	6647
Unique reflns	6275	7467	6647
Par/restr.	298/0	352/0	298/0
μ Kα (mm^{-1})	4.018	2.013	4.247
GOF[b]	1.024	1.003	0.841
Final *R* indices [$I > 2\sigma(I)$][b]	$R_1 = 0.0523$	$R_1 = 0.0804$	$R_1 = 0.0394$
All data	$wR_2 = 0.1069$	$wR_2 = 0.2270$	$wR_2 = 0.1279$

Table 4-7. Crystal data and structure refinement parameters for $[(CuL^{im})_2Cl]CuCl_2$ and $[Cu(NCCH_3)(L^{im})]PF_6$.

	$[(CuL^{im})_2Cl]CuCl_2$	**$[Cu(NCCH_3)(L^{im})]PF_6$**
Formula	$C_{54}H_{46}Cl_3Cu_3N_6$	$C_{29}H_{26}CuF_6N_4P$
Crystal size (mm^3)	0.26 × 0.16 × 0.14	0.45 × 0.33 × 0.16
Form. wt. (g/mol)	1075.94	639.05
Space group	C2/c	$P2_1/c$
a (Å)	17.214(5)	8.4932(3)
b (Å)	12.232(4)	20.6944(8)
c (Å)	23.232(7)	16.6030(7)
α (deg)	90	90
β (deg)	90.546(5)	103.015(2)
γ (deg)	90	90
V ($Å^3$)	4892(3)	2843.21(19)
Z	4	4
T (K)	173(2)	173(2)
ϱ, calcd (g/cm)	1.461	1.493
Reflns collected	48482	29076
Unique reflns	7462	5129
Par/restr.	300/0	365/30
μ Kα (mm^{-1})	1.500	2.202
GOF[b]	1.030	1.015
Final *R* indices [I > 2σ(*I*)][b]	R_1 = 0.0432	R_1 = 0.0718
All data	wR_2 = 0.1149	wR_2 = 0.2168

References

(1) Jenkins, D. M.; Betley, T. A.; Peters, J. C. *J. Am. Chem. Soc.* **2002**, *124*, 11238.

(2) Brown, S. D.; Betley, T. A.; Peters, J. C. *J. Am. Chem. Soc.* **2003**, *125*, 322.

(3) Scepaniak, J. J.; Fulton, M. D.; Bontchev, R. P.; Duesler, E. N.; Kirk, M. L.; Smith, J. M. *J. Am. Chem. Soc.* **2008**, *130*, 10515.

(4) Vogel, C.; Heinemann, F. W.; Sutter, J.; Anthon, C.; Meyer, K. *Angew. Chem., Int. Ed.* **2008**, *47*, 2681.

(5) Cowley, R. E.; Eckert, N. A.; Elhaïk, J.; Holland, P. L. *Chem. Commun.* **2009**, *2009*, 1760.

(6) Badiei, Y. M.; Krishnaswarny, A.; Melzer, M. M.; Warren, T. H. *J. Am. Chem. Soc.* **2006**, *128*, 15056.

(7) Mindiola, D. J.; Hillhouse, G. L. *J. Am. Chem. Soc.* **2002**, *124*, 9976.

(8) Seidel, W.; Müller, H.; Görls, H. *Angew. Chem., Int. Ed.* **1995**, *34*, 325.

(9) Wehmschulte, R. J.; Power, P. P. *Organometallics* **1995**, *14*, 3264.

(10) Power, P. P. *Chem. Rev.* **2012**, *112*, 3482.

(11) Ni, C.; Fettinger, J. C.; Long, G. J.; Power, P. P. *Dalton Trans.* **2010**, *39*, 10664.

(12) Ni, C.; Lei, H.; Power, P. P. *Organometallics* **2010**, *29*, 1988.

(13) Ni, C.; Power, P. P. *Chem. Commun.* **2009**, 5543.

(14) Holland, P. L. *Acc. Chem. Res.* **2008**, *41*, 905.

(15) Smith, A. L.; Hardcastle, K. I.; Soper, J. D. *J. Am. Chem. Soc.* **2010**, *132*, 14358.

(16) Chaudhuri, P.; Hess, M.; Müller, J.; Hildenbrand, K.; Bill, E.; Weyhermüller, T.; Wieghardt, K. *J. Am. Chem. Soc.* **1999**, *121*, 9599.

(17) Sharma, S. K.; May, P. S.; Jones, M. B.; Lense, S.; Hardcastle, K. I.; MacBeth, C. E. *Chem. Commun.* **2011**, *47*, 1827.

(18) Utz, D.; Kisslinger, S.; Heinemann, F. W.; Hampel, F.; Schindler, S. *Eur. J. Inorg. Chem.* **2011**, 255.

(19) Amirnasr, M.; Schenk, K. J.; Meghdadi, S.; Morshedi, M. *Polyhedron* **2006**, *25*, 671.

(20) Menif, R.; Martell, A. E.; Squattrito, P. J.; Clearfield, A. *Inorg. Chem.* **1990**, *29*, 4723.

(21) Hey, D. H.; Mulley, R. D. *J. Chem. Soc.* **1952**, 2276.

(22) Yang, L.; Powell, D. R.; Houser, R. P. *Dalton Trans.* **2007**, 955.

(23) Matyjaszewski, K.; Xia, J. *Chem. Rev.* **2001**, *101*, 2921.

(24) MacInnis, M. C.; McDonald, R.; Ferguson, M. J.; Tobisch, S.; Turculet, L. *J. Am. Chem. Soc.* **2011**, *133*, 13622.

(25) Suzuki, M. *Acc. Chem. Res.* **2007**, *40*, 610.

(26) Connelly, N. G.; Geiger, W. E. *Chem. Rev.* **1996**, *96*, 877.

(27) Peover, M. E.; White, B. S. *Chem. Commun.* **1965**, 183.

(28) Papish, E. T.; Donahue, T. M.; Wells, K. R.; Yap, G. P. A. *Dalton Trans.* **2008**, 2923.

(29) Kunishita, A.; Osako, T.; Tachi, Y.; Teraoka, J.; Itoh, S. *Bull. Chem. Soc. Jpn.* **2006**, *79*, 1729.

(30) Armarego, W. L. F.; Chai, C. L. L. *Purification of Laboratory Chemicals*; 5th ed.; Butterworth-Heinemann: New York, 2003.

(31) Evans, D. F. *J. Chem. Soc.* **1959**, 2003.

(32) Sur, S. K. *J. Magn. Reson.* **1989**, *82*.

(33) Sheldrick, G. M. *Acta Crystallogr., Sect. A: Found. Crystallogr.* **2008**, *A64*.

(34) Sluis, P. v. d.; Spek, A. L. *Acta Crystallogr., Sect. A: Found. Crystallogr.* **1990**, *A46*, 194.